Elucidating the basis of poorly understood floral traits associated with pollination biology

by

Brandi Zenchyzen

A thesis submitted in partial fulfillment of the requirements for the degree of

Doctor in Philosophy

in

Systematics and Evolution

Department of Biological Sciences
University of Alberta

ABSTRACT

Flowering plants have evolved a stunning array of floral colours, scents, and structures, which act synchronously as cues for pollinators. Comprehensive investigations of the extraordinarily diverse floral features involved in plant-pollinator interactions requires expansion of the comparative landscape beyond the traditional model organisms. Cleomaceae (Brassicales) is an ideal focal clade for such studies as it exhibits substantial floral variation. I explore floral features related to pollination biology in an evolutionary developmental context by integrating developmental morphology, chemical characterizations, and comparative transcriptomics of Cleomaceae. First, I describe and compare floral nectaries, the structures responsible for nectar secretion, within and among Cleomaceae genera. I reveal the substantive diversity in form with dramatic variation in floral nectary size and shape across Cleomaceae, and introduce a modified fast green and safranin O staining protocol to yield vibrant histological sections without highly hazardous chemicals. Second, I present the first *in vivo* colour images of ultraviolet-fluorescent nectar. Ultraviolet radiation induces vibrant blue fluorescence of Cleomaceae nectar, a crucial reward for pollinators. Next, I shift attention to *Gynandropsis gynandra* (Cleomaceae), an underutilized crop native to Africa and Asia. I characterize and compare the floral fragrance of African and Asian accessions of *G. gynandra* (Cleomaceae) and examine the floral morphology and gene expression patterns associated with scent production and emission. I discover drastically different floral scent profiles between the African and Asian accessions and identify the stalk-like floral structures as those putatively involved in olfactory signalling. Lastly, I focus on *G. gynandra*'s androgynophore, a stalk-like structure that elevates the reproductive organs of the flower, to provide a detailed description throughout development, examine global gene expression patterns, and identify candidate elongation genes. I show that the radially symmetric androgynophore of *G. gynandra* rapidly lengthens primarily via cell elongation and is

characterized by complex gene expression patterns including differential expression of floral organ identity genes and genes associated with organ development and growth in *Arabidopsis thaliana*. Overall, my research contributes to our understanding of floral features involved in plant-pollinator interactions by exploring the diversity of floral nectaries and exquisite nectar across Cleomaceae. It also provides a more holistic picture of *G. gynandra*'s flower from the unique floral structures (i.e., inconspicuous nectary and androgynophore) to the geographically variable floral scent.

PREFACE

Chapter 2 of this thesis has been published as "**Zenchyzen B, Weissner S, Martin J, Lopushinsky A, John I, Nahal I, Hall JC**. **2023**. Comparative Nectary Morphology across Cleomaceae (Brassicales). *Plants* **12**, 1263". JCH and I designed the experiments. All authors collected the data. I analyzed the data, prepared the figures, and wrote the manuscript. JCH and I reviewed and edited the manuscript.

Chapter 3 of this thesis is currently under review. I collaborated with John Acorn to capture the photographs. I prepared the figures and wrote the manuscript. JCH, JA, Rolf Vinebrooke, and I reviewed and edited the manuscript.

Chapter 4 of this thesis is in preparation for submission. I collected and analyzed the floral scent data. Kian Merkosky and I collected and analyzed the floral cell morphology data. Shane Carey and I processed tissue for sequencing and performed the transcriptome assembly and analyses. I prepared the figures and wrote the manuscript. JCH and I reviewed and edited the manuscript.

Chapter 5 of this thesis has been published as "**Zenchyzen B, Carey S, Antochi-Crihan G, Hall JC**. **2023**. Developmental and genetic basis of the androgynophore in *Gynandropsis gynandra*. *American Journal of Botany* e16193". JCH and I designed the study. I collected and analyzed floral and androgynophore growth measurements. JCH, GA-C, and I processed tissue for histology and scanning electron microscopy; I analyzed the data. SC and I processed tissue for sequencing and performed the transcriptome assembly and analyses. I prepared the figures and wrote the manuscript. JCH, SC, and I reviewed and edited the manuscript.

ACKNOWLEDGEMENTS

I would like to express my gratitude to Jocelyn Hall for her exceptional mentorship and unwavering support throughout my research. Her guidance has given me confidence in my abilities as a scientist. My sincere thanks to Shane Carey for his endless assistance with transcriptomics; his company made long days of cDNA preparations much more enjoyable. Thank you to the undergraduate students who contributed to my thesis, their assistance helped to propel my research forward. I would like to thank John Acorn for his invaluable support with UV-fluorescence photography and infectious enthusiasm about colour and vision. Thank you to my committee members, Maya Evenden and Glen Uhrig, their insight and feedback have greatly improved my research. Thanks to Kacie Norton, Arlene Oatway (Advanced Microscopy Facility, Department of Biological Sciences), and Nathan Gerein (Scanning Electron Microscopy Laboratory, Department of Earth and Atmospheric Sciences) for their aid with scanning electron microscopy. Thank you to Rolf Vinebrooke for the insightful research and writing advice. I would like to thank M. Eric Schranz for making much of my research possible by kindly providing *Gynandropsis gynandra* seeds. Finally, thank you to my family and friends for their constant support throughout my academic endeavours. My thesis research was funded by the Natural Sciences and Engineering Research Council of Canada (NSERC) [funding reference number 5014131].

TABLE OF CONTENTS

Chapter 1. Introduction **1**

1.1 Floral nectaries and nectar, a budding area of research **2**

1.2 Floral scent, an olfactory signal for pollinators **4**

1.3 The androgynophore, a novel floral structure with ties to pollinator interactions **5**

1.4 Cleomaceae, an ideal family for the study of floral traits related to pollination biology **7**

1.5 *Gynandropsis gynandra*, an up-and-coming model organism **9**

Chapter 2: Comparative Nectary Morphology across Cleomaceae (Brassicales) **11**

2.1 Introduction **11**

2.2 Results **13**

2.2.1 *Arivela viscosa* 13

2.2.2 *Cleome amblyocarpa* 14

2.2.3 *Cleome violacea* 14

2.2.4 *Gynandropsis gynandra* 15

2.2.5 *Melidiscus giganteus* 15

2.2.6 *Polanisia dodecandra* 16

2.2.7 *Sieruela hirta* 16

2.2.8 *Sieruela rutidosperma* 17

2.2.9 *Tarenaya houtteana* 17

2.3 Discussion **18**

2.3.1 Nectarostomata and vasculature are unifying features of Cleomaceae floral nectaries 19

2.3.2 Nectary parenchyma is variable throughout Cleomaceae 21

2.3.3 Evolutionary lability in floral nectary morphology across Cleomaceae 22

2.4 Materials and Methods **23**

2.4.1 Plant material 23

2.4.2 Scanning electron microscopy 24

2.4.3 Histological preparations 24

2.4.4 Fast green and safranin O staining 25

2.5 Conclusions **26**
2.6 Tables **27**
2.7 Figures **28**

Chapter 3: Fleur-escence: the visual phenomenon of ultraviolet-fluorescent nectar **49**
3.1 Main **49**
3.2 Materials and Methods **52**
3.3 Figures **53**

Chapter 4: Chemical, genetic, and morphological characterization of the floral scent and scent releasing structures of *Gynandropsis gynandra* (Cleomaceae, Brassicales) **56**
4.1. Introduction **56**
4.2. Results and Discussion **60**
4.2.1 Floral scent profiles differ between African and Asian accessions 60
4.2.2 Epidermal cell morphology is diverse across floral structures 62
4.2.3 Terpenoid biosynthetic pathway gene expression is highest in the stalk-like floral structures 64
4.3. Conclusions **67**
4.4. Experimental **67**
4.4.1. Plant material 67
4.4.2. Floral volatile collection 68
4.4.3. Floral volatile analyses 68
4.4.4. Identification of potential osmophores 69
4.4.5. RNA sequencing of floral structures 69
4.4.6. Transcriptome assembly and analyses 70
4.5 Tables **72**
4.6 Figures **75**

Chapter 5: Developmental and genetic basis of the androgynophore in *Gynandropsis gynandra* **83**
5.1 Introduction **83**
5.2 Materials and Methods **86**
5.2.1 Plant material 86

5.2.2 Floral growth measurements 86
5.2.3 Scanning electron microscopy and cell measurements 87
5.2.4 Histological preparations and imaging 88
5.2.5 RNA sequencing 89
5.2.6 Transcriptome assembly and analyses 90
5.3 Results 92
5.3.1 Androgynophore rapidly elongates 92
5.3.2 Androgynophore lengthens predominantly via cell elongation 93
5.3.3 Androgynophore internal anatomy is uniform 94
5.3.4 Androgynophore transcript expression is dynamic throughout development and is more similar to that of the gynophore than filaments 95
5.3.5 Floral organ identity genes and candidate elongation genes are expressed in the developing androgynophore 96
5.3.6 Plant hormones play a role in androgynophore development 97
5.4 Discussion 98
5.4.1 Androgynophore structure and elongation 99
5.4.2 Genetic mechanisms controlling androgynophore growth 100
5.4.3 What is the androgynophore? 102
5.5 Conclusions 103
5.6 Tables 103
5.7 Figures 105
Chapter 6: Conclusion 114
6.1 Floral nectary and nectar studies in Cleomaceae 114
6.2 *Gynandropsis gynandra*, a model organism for evo devo studies 118
Bibliography 121
Appendices 144

LIST OF TABLES

Table 2.1. Summary of floral nectary characteristics and pollination system for the nine Cleomaceae species. 27

Table 4.1. Percent composition and chemical class of the floral volatiles in the headspace of *Gynandropsis gynandra* African (TOT8917 from Malawi) and Asian (TOT7200 from Malaysia) accessions. 72

Table 4.2. Pollinators of *Gynandropsis gynandra* in Africa and Asia. 73

Table 4.3 *Arabidopsis thaliana* terpenoid biosynthetic pathway genes with homologs expressed in *Gynandropsis gynandra* (accession TOT8917 from Malawi) petals and/or stalk-like floral structures. 74

Table 5.1. Androgynophore epidermal cell dimensions at three developmental stages of *Gynandropsis gynandra*. 103

Table 5.2. Summary of the role of candidate *Gynandropsis gynandra* androgynophore elongation genes in *Arabidopsis thaliana* development. 104

LIST OF FIGURES

Figure 2.1. Anthetic flower with nectary inset of the nine Cleomaceae species. 28

Figure 2.2. *Arivela viscosa* nectary (A) photograph, (B–F) scanning electron micrographs, and (G–K) fast green and safranin O-stained sections. 29

Figure 2.3. *Cleome amblyocarpa* nectary (A) photograph, (B–F) scanning electron micrographs, and (G–L) fast green and safranin O-stained sections. 31

Figure 2.4. *Cleome violacea* nectary (A) photograph, (B–G) scanning electron micrographs, and (H–L) fast green and safranin O-stained sections. 33

Figure 2.5. *Gynandropsis gynandra* nectary (A) photograph, (B–H) scanning electron micrographs, and (I–L) fast green/safranin O-stained sections. 35

Figure 2.6. *Melidiscus giganteus* nectary (A) photograph, (B–F) scanning electron micrographs, and (G–L) fast green and safranin O-stained sections. 37

Figure 2.7. *Polanisia dodecandra* nectary (A) photograph, (B–F) scanning electron micrographs, and (G–L) fast green and safranin O-stained sections. 39

Figure 2.8. *Sieruela hirta* nectary (A) photograph, (B–F) scanning electron micrographs, and (G–K) fast green and safranin O-stained sections. 41

Figure 2.9. *Sieruela rutidosperma* nectary (A) photograph, (B–F) scanning electron micrographs, and (G–K) fast green and safranin O-stained sections. 43

Figure 2.10. *Tarenaya houtteana* nectary (A) photograph, (B–H) scanning electron micrographs, and (I–M) fast green and safranin O-stained sections. 45

Figure 2.11. Nectarostomata of the nine Cleomaceae species. 47

Figure 2.12. Cleomaceae phylogeny and floral nectaries of the nine species grouped by shape and position. 48

Figure 3.1. UV-fluorescent nectar of *Cleome violacea* and other Cleomaceae species. 53

Figure 3.2. UV-fluorescent nectar of *Polanisia dodecandra* and *Tarenaya hassleriana*. 54

Figure 3.3. UV-fluorescent nectar of *Sieruela hirta* and *Melidiscus giganteus*. 55

Figure 4.1. Illustration of *Gynandropsis gynandra* (accession TOT8917 from Malawi) flower. 75

Figure 4.2. Photographs of *Gynandropsis gynandra* inflorescences. 76

Figure 4.3. Proportions of floral volatiles captured from *Gynandropsis gynandra* categorized following Knudsen *et al.* (1993). 77

Figure 4.4. Scanning electron micrographs of *Gynandropsis gynandra* (accession TOT8917 from Malawi) perianth and floral nectary. 78

Figure 4.5. Scanning electron micrographs of *Gynandropsis gynandra* (accession TOT8917 from Malawi) stalk-like floral structures, anther, and pistil. 79

Figure 4.6. Principal component analysis of *Gynandropsis gynandra* (accession TOT8917 from Malawi) transcript counts. 80

Figure 4.7. Integrated heatmap and terpenoid biosynthetic pathway for *Gynandropsis gynandra* (accession TOT8917 from Malawi) representative transcripts expressed in $\log_2$(TPM). 81

Figure 5.1. *Gynandropsis gynandra* inflorescence. 105

Figure 5.2. Three developmental stages of *Gynandropsis gynandra*. 105

Figure 5.3. Growth curves of *Gynandropsis gynandra* flower and androgynophore length based on daily flower length measurements ($N = 50$) and corresponding calculated androgynophore lengths. 106

Figure 5.4. *Gynandropsis gynandra* floral development over 5 days. 107

Figure 5.5. Scanning electron micrographs of *Gynandropsis gynandra* androgynophore epidermal cells at three developmental stages. 107

Figure 5.6. Woven epidermal cells of *Gynandropsis gynandra* proximal androgynophore section at the anthetic stage. 108

Figure 5.7. Alcian blue/safranin O-stained sections of *Gynandropsis gynandra* androgynophore at the intermediate stage. 109

Figure 5.8. Principal component analysis of *Gynandropsis gynandra* transcript counts. 109

Figure 5.9. Heatmaps of significantly differentially expressed *Gynandropsis gynandra* transcripts expressed as *z*-scores. 110

Figure 5.10. Venn diagrams of *Gynandropsis gynandra* orthologous gene clusters. 111

Figure 5.11. Heatmaps of *Gynandropsis gynandra* representative transcripts expressed in $\log_2$(TPM). 112

Figure 5.12. Expression of *Gynandropsis gynandra* androgynophore transcripts in *Arabidopsis thaliana*-specific KEGG pathways. 113

ABBREVIATIONS

Genes:

AG	*AGAMOUS*
AN3	*ANGUSTIFOLIA3*
AP1-3	*APETALLA1-3*
BDX	*BIIDXI*
CRC	*CRABSCLAW*
DCR	*DEFECTIVE IN CUTICULAR RIDGES*
ER	*ERECTA*
FPPS1, 2	*FARNESYL DIPHOSPHATE SYNTHASE1, 2*
GASA4	*GIBBERELLIC ACID-STIMULATED ARABIDOPSIS4*
GGPPS2, 11, 12	*GERANYLGERANYL DIPHOSPHATE SYNATHASE2, 11, 12*
HTH	*HOTHEAD*
IAA19	*INDOLE-3-ACETIC ACID INDUCIBLE19*
IPPI2	*ISOPENTYL DIPHOSPHATE ISOMERASE2*
LNG1, 2	*LONGIFOLIA1, 2*
MYB21, 24	*MYELOBLASTOSIS21, 24*
PI	*PISTILLATA*
SEP1-4	*SEPALLATA*
SHP	*SHATTERPROOF*
TPS27	*TERPENE SYNTHASE27*

Other:

And	Androgynophore
Ant	Anthetic
BUSCO	Benchmarking Universal Single Copy Orthologs
DMAPP	Dimethylallyl diphosphate
FAA	Formalin-aceto-alcohol
FPP	Farnesyl diphosphate
Fil	Filaments
GGPP	Geranylgeranyl diphosphate

GPP	Geranyl diphosphate
Gyn	Gynophore
IAA	Indole-3-acetic acid (i.e., auxin)
Int	Intermediate
IPP	Isopentyl diphosphate
KEGG	Kyoto Encyclopedia of Genes and Genomes
MEP	Methylerythritol phosphate
MS	Mass spectrometry
MVA	Mevalonate
TOF	Time-of-flight
TPM	Transcripts per million
VIGS	Virus-induced gene silencing

Chapter 1. Introduction

The adaptive radiation of flowering plants brought forth an immense diversity of floral features and a vast species richness of roughly 300,000 (Willmer 2011; Soltis and Soltis 2014). Cross-pollination, in which pollen is moved from the anthers of one flower to the stigma of another conspecific flower, played an important role in this adaptive radiation because it leads to increased genetic variability (Willmer 2011). Since cross-pollination often occurs via animal vectors, plant-pollinator interactions are considered a key driving force behind the rapid evolution and diversification of floral form (Ollerton *et al.* 2011; Soltis and Soltis 2014). Most flowering plants rely on animal pollination for their reproductive success; as such, they exhibit suites of visual and olfactory cues to attract pollinators (Willmer 2011; Ollerton *et al.* 2011). For these reasons, plant-pollinator interactions have been investigated by a diversity of approaches, including but not limited to ecological studies of floral visitors and pollinator preferences, comparative phylogenetics of pollination systems, and evolutionary development of the mechanisms underlying floral form (Mitchell *et al.* 2009; Smith 2010; Specht and Howarth 2015).

Studies on the genetic basis of floral features have traditionally focused on model organisms such as *Arabidopsis thaliana* (Brassicaceae) and *Antirrhinum majus* (Plantaginaceae); however, attention is shifting from model organisms to flowering plant clades with greater floral diversity (Buzgo *et al.* 2004; Kramer 2007; Damerval and Becker 2017; Schrager-Lavelle *et al.* 2017). The rise in accessibility of genomic and transcriptomic resources allows for genetic exploration of taxa that possess characteristics absent in model organisms, ultimately providing a more complete picture of the evolution and diversification of floral features (Delaux *et al.* 2019). Morphological descriptions and chemical characterizations are essential for understanding flower diversity and are a prerequisite for elucidating the genetic basis of floral features (Buzgo *et al.* 2004; Specht and Howarth 2015). Like the uneven investigation of taxa, certain floral features have been more thoroughly examined than others (Kramer 2007, 2019). For instance, comparative morphological, chemical, and genetic investigations have led to significant contributions to our understanding of the mechanisms controlling floral symmetry and petal colour (Rausher 2008; Rosin and Kramer 2009; Sobel and Streisfeld 2013; Specht and Howarth 2015) while our understanding of other traits likely involved in pollinator interactions is lacking (e.g., floral nectaries, nectar, and novel organs) (Liao *et al.* 2021).

1.1 Floral nectaries and nectar, a budding area of research

Pollination often occurs via a mutualistic relationship between plants and animals, where the plant typically compensates the animal with a floral reward in exchange for pollen transfer (Nicolson *et al.* 2007; Willmer 2011). Nectar and pollen are the most common floral rewards; however, nectar is frequently the primary offering of the flower to protect the reproductively important pollen from consumption (Willmer 2011). As such, floral nectaries, the structures that secrete nectar, are widely distributed and have evolved multiple times throughout flowering plant diversification (Nicolson *et al.* 2007; Roy *et al.* 2017; Liao *et al.* 2021). Floral nectaries can be derived from any floral tissue, and thus vary significantly in size, shape, and position (Nicolson *et al.* 2007; Willmer 2011). Yet, they are often basally located to ensure the pollinator contacts the reproductive organs while feeding on the nectar (Willmer 2011). In addition to their diverse morphology, floral nectaries can secrete nectar through a variety of mechanisms including modified stomata (i.e., nectarostomata), trichomes, and cell rupture (Nicolson *et al.* 2007; Willmer 2011; Liao *et al.* 2021). Despite their prevalence and crucial role in pollinator interactions, floral nectaries have largely been neglected from morphological and phylogenetic studies but are of recent interest for more comprehensive investigation (Nicolson *et al.* 2007; Liao *et al.* 2021).

Like with floral nectaries, researchers are beginning to elucidate the complexities of nectar through interdisciplinary studies (Parachnowitsch *et al.* 2019; Liao *et al.* 2021). Though nectar is often simply described as a sugar solution, it not only includes carbohydrates but also a blend of amino acids, lipids, proteins, and secondary metabolites (e.g., pigments and scents) (Nicolson *et al.* 2007; Roy *et al.* 2017; Parachnowitsch *et al.* 2019). To add to its intricacy, microbial communities (i.e., bacteria and fungi) are found in nectar and can alter its composition (Roy *et al.* 2017; Liao *et al.* 2021). Nectar chemistry and volume vary greatly across taxa, reflecting the diversity of energetic and nutritional requirements of animal visitors (Nicolson *et al.* 2007; Liao *et al.* 2021). Further, the colour and scent of nectar contribute to pollinator attraction (Raguso 2004; Hansen *et al.* 2007; Willmer 2011). For example, the dark purple nectar of *Leucosceptrum canum* (Lamiaceae) and the red and yellow nectar of Mauritian flowering plant species function as visual signals for bird and lizard pollinators, respectively (Hansen *et al.* 2006; Zhang *et al.* 2012). Although coloured nectar is rare (Hansen *et al.* 2007), other types of visual signals related to nectar (e.g., ultraviolet (UV)-fluorescence and -reflectance) may play a

role in pollinator attraction (Thorp *et al.* 1975; Nicolson *et al.* 2007; Willmer 2011; Lunau *et al.* 2020).

UV-fluorescence is the phenomenon in which UV radiation is absorbed and lower energy light is emitted. This visual spectacle differs from UV nectar guides (i.e., patterns of UV-reflectance and -absorbance) in that UV nectar guides are only visible to animals capable of perceiving UV radiation (e.g., many insects and birds) (Willmer 2011); whereas, the lower energy light emitted via fluorescence can be in the spectral range visible to humans. Further, UV nectar guides have been much more thoroughly studied than UV-fluorescence (Willmer 2011; Koski and Ashman 2014; Lunau *et al.* 2020). However, UV-fluorescence is of growing interest with many recent discoveries of UV-fluorescence across the animal kingdom (e.g., flying squirrels, springhares, platypus, chameleons, salamanders) (Prötzel *et al.* 2018; Kohler *et al.* 2019; Lamb and Davis 2020; Anich *et al.* 2021; Olson *et al.* 2021). Behavioural studies within the animal kingdom have shown that UV-fluorescence may act as a visual cue (Arnold *et al.* 2002; Mazel *et al.* 2004; Lim *et al.* 2007). For example, female jumping spiders (*Cosmophasis umbratica*, Salticidae) have appendages that fluoresce bright green under UV radiation; in the absence of UV radiation, male jumping spiders do not perform typical courtship behaviour with non-fluorescing females (Lim *et al.* 2007). Similarly, budgerigars (*Melopsittacus undulatus*, Psittacidae) have UV-fluorescent yellow plumage on their crown and cheeks; both sexes prefer budgerigars of the opposite sex with fluorescent plumage over those with masked fluorescence (Arnold *et al.* 2002). In contrast, the prevalence and significance of UV-fluorescence across flowering plants has scarcely been investigated.

Nearly 50 years ago, Thorp *et al.* (1975) discovered UV-fluorescent nectar in several bee-pollinated flowering plant species and suggested that this phenomenon functions as a visual signal for bees. Apart from nectar fluorophore (i.e., fluorescent molecule) identification for one species (Scogin 1979a; b) and conceptual arguments about its ecological importance (Kevan 1976; Iriel and Lagorio 2010), our understanding of UV-fluorescent nectar has not progressed since its discovery. However, UV-fluorescence was recently discovered for the prey traps of several carnivorous plant species and the anthers and pollen of numerous species across flowering plants (Kurup *et al.* 2013; Mori *et al.* 2018). Similar to the UV-fluorescent animal studies, behavioural experiments with UV-fluorescent prey traps and anthers and pollen indicate that this phenomenon plays a role in animal attraction (Kurup *et al.* 2013; Mori *et al.* 2018).

Pitcher plants (*Nepenthes khasiana*, Nepenthaceae) with masked fluorescence catch significantly less insect prey (Kurup *et al.* 2013) and bees are attracted to filter paper containing a fluorescent compound identified from anthers and pollen (Mori *et al.* 2018). Though UV-fluorescence presumably contributes to the suite of visual cues involved in pollinator attraction, further exploration is needed to determine the prevalence of UV-fluorescence nectar across flowering plants and to establish a link to pollinator interactions.

1.2 Floral scent, an olfactory signal for pollinators

Along with the colours of floral structures and rewards, flowers emit aromas that predominantly function as olfactory signals for pollinator attraction (Dudareva and Pichersky 2006; Willmer 2011). Floral fragrances consist of blends of volatile organic compounds, chemicals of low molecular weight that can cross cell membranes and readily evaporate into the atmosphere (Dudareva and Pichersky 2006; Willmer 2011). Though floral scent was historically described using the human nose, analytical methods and instruments are now used to collect and characterize the complex mixtures of volatile organic compounds released by flowers (Dudareva and Pichersky 2006; Tholl *et al.* 2006). Over 1700 floral volatiles have been identified from approximately 990 taxa (Pichersky and Dudareva 2020). The most prevalent groups of floral volatiles are terpenoids, benzenoids, and aliphatics, while amino acid derivatives and nitrogen- and sulfur-containing compounds are less common (Farré-Armengol *et al.* 2020; Pichersky and Dudareva 2020). As with visual signals, floral fragrances can be associated with the attraction of specific pollinator classes (Dudareva and Pichersky 2006; Willmer 2011; Sheehan *et al.* 2012). For example, generalist flowering plant species (i.e., those that are pollinated by a variety of insects) commonly emit a blend of the three major floral volatile groups, with the terpenoids β-ocimene and pinene often dominant (Dudareva and Pichersky 2006; Willmer 2011). Whereas, the floral scent of bat pollinated species is frequently dominated by terpenoids, benzenoids, and nitrogen-containing compounds (Dudareva and Pichersky 2006; Willmer 2011).

Variation in floral scent not only occurs among different species but can also vary between populations or individuals of the same species and within a single flower (Dudareva and Pichersky 2006; Willmer 2011). Floral scent emission is commonly tissue specific, with petals often the main source of floral fragrance (Dudareva and Pichersky 2006; Willmer 2011). Though, different floral structures may release distinct volatile organic compounds (Dudareva

and Pichersky 2006; Willmer 2011). Floral volatiles are primarily synthesized in the tissue from which they are released and are immediately emitted into the atmosphere after production (Pichersky and Dudareva 2020). Like nectar secretion, floral fragrance is generally emitted via specialized cells (Dudareva and Pichersky 2006). While volatiles for herbivory defense are typically synthesized in and emitted from glandular trichomes on floral or vegetative structures, floral scent is often released by cells with a distinct epidermal surface (e.g., conical or papillate) (Dudareva and Pichersky 2006; Pichersky and Dudareva 2020). These regions of scent production and emission are sometimes referred to as osmophores (Dudareva and Pichersky 2006; Willmer 2011). Although osmophores can be challenging to identify, transcriptomic analysis of floral volatile biosynthetic pathway gene expression across the flower can provide insight into the scent-releasing structures.

1.3 The androgynophore, a novel floral structure with ties to pollinator interactions

Flowering plants exhibit immense variation in floral form, from the overall size and shape of the flower to the arrangement and elaboration of structures within the flower (Dafni *et al.* 1997; Endress 2006; Willmer 2011). As with flower colour and patterns, macro- and microstructure contributes to the suite of signals tied to pollinator interactions (Dafni *et al.* 1997; Willmer 2011). On a large scale, pollinators can be drawn to a specific arrangement of flowers within an inflorescence; flower orientation, size, and symmetry; petal shape; and position of reproductive organs and floral rewards (Dafni *et al.* 1997; Willmer 2011; Dellinger 2020). For instance, bat pollinated species tend to be large and conspicuous since bats are primarily nocturnal and commonly have poor vision, while butterfly pollinated species often have flat-topped flowers or inflorescences as butterflies land to feed (Willmer 2011). Whereas at the microscopic level, the shape and texture of floral cells may influence flower colour and the grip and foraging efficiency of pollinators (Whitney *et al.* 2011; Moyroud and Glover 2017).

Although extensive research on the floral structures of model organisms has significantly contributed our understanding of the development and genetics underlying floral form, it only provides insight on a glimpse of the variation in floral structure (Buzgo *et al.* 2004; Kramer 2007). Expanding investigations to other species produces a more comprehensive understanding of the conservation and diversification of floral form across flowering plants (Buzgo *et al.* 2004; Kramer 2007). Novel floral structures, such as atypical or modified organs, may contribute to the

wide variation in floral form (Endress and Matthews 2006; Litt and Kramer 2010; Kramer 2019). Well-studied novel floral structures include the staminodes (i.e., sterile stamens) and petal spurs (i.e., hollow extensions of the petal that secrete and hold nectar) of *Aquilegia* (Ranunculaceae) (Kramer 2009; Kramer and Hodges 2010; Sharma *et al.* 2014). These staminodes potentially provide protection during fruit development, while petals spurs are considered a key adaptation for pollination (Kramer and Hodges 2010; Meaders *et al.* 2020). Therefore, examination of novel floral structures not only provides insight into the diversity of flowering plants but also the evolution of functional innovations (Kramer 2007, 2019).

An understudied novel floral structure, likely related to pollinator interactions, is the androgynophore; a stalk-like structure elevating the reproductive organs of the flower. Though widely distributed across flowering plants, the androgynophore is often short and inconspicuous. However, a few of families, such as Passifloraceae and Cleomaceae, are known for housing species in which the androgynophore is a prominent component of the flower (Bernhard 1999; Bayat *et al.* 2018). Like the touch-stimulated leaf movement of sensitive plant (*Mimosa pudica*; Fabaceae) and Venus flytrap (*Dionaea muscipula*; Droseraceae) (Forterre *et al.* 2005; Volkov *et al.* 2010), several *Passiflora* (Passifloraceae) species have a conspicuous androgynophore that rapidly inclines in response to mechanical stimuli (Scorza and Dornelas 2014). It has been hypothesized that the touch-stimulated androgynophore is an adaptation to enhance cross pollination by increasing the likelihood of contact between the reproductive organs and pollinator (Scorza and Dornelas 2014). Similar in function, the stationary but curved androgynophore of *P. mucronata* is believed to provide easy access to the nectary while facilitating reproductive organ-pollinator contact (Rocha *et al.* 2015). In *Gynandropsis gynandra* (L.) Briq. (Cleomaceae), the elongated androgynophore presumably increases the chance of reproductive organ contact with short-tongued hawkmoths (Werth 1942; Oronje *et al.* 2012). Though the androgynophore is found throughout flowering plants and appears to be a structural innovation related to cross pollination, few studies have touched on its external morphology and internal anatomy (Raghavan 1939; Murty 1953; Dattagupta and Datta 1976; Rocha *et al.* 2015) and none have explored its genetic basis.

1.4 Cleomaceae, an ideal family for the study of floral traits related to pollination biology

Cleomaceae (Brassicales) is a small family of roughly 270 species with a cosmopolitan distribution, though primarily found in warm temperate, tropical, and arid climates (Iltis *et al.* 2011; Cardinal-McTeague *et al.* 2016; Bayat *et al.* 2018). Cleomaceae flowers are diverse in form; however, the general floral ground plan is as follows: four sepals, four petals, six to numerous stamens, bicarpellate pistil, and often with stalk-like structures subtending the reproductive organs (Iltis *et al.* 2011). The flowers tend to be monosymmetric (i.e., bilaterally symmetric), due to an upward curvature of the petals and reproductive organs (Patchell *et al.* 2011; Bayat *et al.* 2018). Shifts to monosymmetry appear to be associated with the evolution of specialized pollination syndromes (Hileman 2014); yet pollination studies reveal several Cleomaceae species are an exception to this trend (Bayat *et al.* 2018). Parallel with its diversity in floral form, Cleomaceae has a broad range of floral visitors and includes both generalist and specialist species (Bayat *et al.* 2018). For example, the pollinators of the generalist species *Arivela viscosa* (L.) Raf. and *Polanisia dodecandra* (L.) DC. include bees, flies, and butterflies (Higuera-Díaz *et al.* 2015; Raju and Rani 2016), whereas the specialist species *Melidiscus giganteus* (L.) Raf. and *Tarenaya houtteana* (Schltdl.) Soares Neto & Roalson are pollinated by bats (Machado *et al.* 2006; Fleming *et al.* 2009). *Gynandropsis gynandra* is unique in that its pollination system differs with geographic distribution (i.e., bee and butterfly pollination in Asia and hawkmoth pollination in Africa) (Werth 1942; Chandra *et al.* 2013; Martins and Johnson 2013; Raju and Rani 2016).

Cleomaceae is sister family to the large and well-known Brassicaceae (Brassicales) (Iltis *et al.* 2011; Bayat *et al.* 2018). As such, investigations on Cleomaceae are facilitated by the transfer of knowledge from the well-studied model species *A. thaliana* (Bayat *et al.* 2018) and our knowledge of trait evolution is elevated by robust phylogenetic hypotheses for Cleomaceae and its relationship to Brassicaceae (Iltis *et al.* 2011; Patchell *et al.* 2014). In addition, Cleomaceae research allows for advances in our understanding of floral evolution and diversity because it houses morphological variation not found in Brassicaceae (Bayat *et al.* 2018). Despite containing approximately 3700 species, the floral ground plan of Brassicaceae is surprisingly uniform with little disparity in organ number and arrangement (Patchell *et al.* 2014; Bayat *et al.* 2018); however, Nikolov (2019) argues Brassicaceae contains untapped floral variation for studies addressing the basis of morphological characteristics. Regardless, flowers from

Cleomaceae are diverse in organ number, colour, size, and elaboration (Iltis *et al.* 2011; Bayat *et al.* 2018). Much of the morphological variation of Cleomaceae flowers represents understudied components associated with pollinator attraction and rewards. Thus, Cleomaceae is an ideal family to explore the basis of such traits, while benefitting from *A. thaliana* data and strongly supported phylogenies, to address the gap in knowledge of floral features related to pollination biology.

Research on Cleomaceae ranges, but the most extensively studied aspects are C_4 photosynthesis and whole genome duplications (Bayat *et al.* 2018). C_4 *G. gynandra* provides an important juxtaposition to the C_3 species *A. thaliana* and *T. houtteana* (Cheng *et al.* 2013; Hoang *et al.* 2023). Further, Cleomaceae and Brassicaceae have undergone independent and shared whole genome duplications; such events drive flowering plant diversification (Edger *et al.* 2015; Cardinal-McTeague *et al.* 2016; van den Bergh *et al.* 2016). The focus of Cleomaceae flower investigations include symmetry (Patchell *et al.* 2011), pigmentation (Nozzolillo *et al.* 2010), stamen development (Koevenig 1973; Koevenig and Sillix 1973; Erbar and Leins 1997), and floral nectary genetics (Carey *et al.* 2023). Despite this body of work, there is much to be learned about Cleomaceae floral nectary diversity, nectar and scent chemistry, and organ elaboration (Bayat *et al.* 2018). Thus, the overarching goal of my thesis is to investigate floral features related to pollination biology in an evolutionary developmental context, by combining developmental morphology, chemical characterizations, and transcriptomics of Cleomaceae species. This was accomplished by: (1) investigating the morphological diversity of nectaries across Cleomaceae; (2) documenting the ultraviolet-fluorescent nectar of Cleomaceae taxa; (3) comparing floral scent profiles for African and Asian populations of *G. gynandra*; and (4) determining the developmental and genetic basis of the androgynophore in *G. gynandra*.

In **Chapters 2** and **3**, I examine the floral nectaries and nectar of morphologically diverse Cleomaceae species. The selected species comprise representatives for genera distributed across the Cleomaceae phylogeny, including the minor crop plants *G. gynandra* and *A. viscosa* and the ornamental *T. houtteana* (Onyango *et al.* 2013; Bayat *et al.* 2018; Sogbohossou *et al.* 2018; Pamarthi *et al.* 2022). Both the nectaries and nectar of Cleomaceae species are understudied components of the flower; previous studies briefly describe nectary shape (Iltis 1958; Karrer 1991; Lee, Baum, Oh, *et al.* 2005), focus on nectary development of one or two species (Erbar and Leins 1997; Carey *et al.* 2023), or include nectar volume and sugar concentration (Martins

and Johnson 2013; Higuera-Díaz *et al.* 2015; Raju and Rani 2016; Carey *et al.* 2023). In **Chapter 2**, I provide detailed descriptions and comparisons of floral nectary external morphology and internal anatomy for nine Cleomaceae species from seven genera. In **Chapter 3**, I shift attention from floral nectaries to the nectar they secrete, to document the striking UV-fluorescent nectar of five Cleomaceae species from different genera. In addition, I discuss the limited literature on UV-fluorescence in flowering plants and suggest directions for future nectar studies.

1.5 *Gynandropsis gynandra*, an up-and-coming model organism

With a rapidly changing climate and growing global population, food security is one of the main challenges facing society today (Sogbohossou *et al.* 2018; Mashamaite *et al.* 2022). Agricultural advancements have focused on increasing the yield of a few major crop plants, resulting in three species (i.e., maize, rice, and wheat) dominating much of the plant protein consumed by humans (Sogbohossou *et al.* 2018; Henkhaus *et al.* 2020; Mashamaite *et al.* 2022). However, expanding crop diversity and developing minor crop plants for domestication has been shown to improve ecosystem health and resilience amid a changing climate (Sogbohossou *et al.* 2018; Henkhaus *et al.* 2020; Achigan-Dako *et al.* 2021; Mashamaite *et al.* 2022). *Gynandropsis gynandra* is a leafy vegetable and medicinal plant native to Africa and Asia (Sogbohossou *et al.* 2018; Mashamaite *et al.* 2022; Hoang *et al.* 2023). This underutilized crop has been studied for its nutritional (Moyo *et al.* 2018; Sogbohossou *et al.* 2019), medicinal (Ghogare *et al.* 2009; Bala *et al.* 2010), and insecticidal properties (Lwande *et al.* 1999; Nyalala *et al.* 2013). Moreover, with the recently published genome of *G. gynandra* and the close relationship of Cleomaceae and Brassicaceae, C_4 *G. gynandra* and its C_3 relatives (i.e., *T. houtteana* and *A. thaliana*) are an excellent model system for evolutionary studies on the transition from C_3 to C_4 photosynthesis (Tronconi *et al.* 2020; Huang *et al.* 2021; Hoang *et al.* 2023). Although minor crop plants have untapped potential to improve food security and pollination is a crucial component of flowering plant reproduction, detailed characterizations of *G. gynandra* floral features and investigations of their genetic basis are lagging (Sogbohossou *et al.* 2018; Henkhaus *et al.* 2020; Achigan-Dako *et al.* 2021), with the exceptions of vascular anatomy and floral morph descriptions (Raghavan 1939; Murty 1953; Raju and Rani 2016; Zohoungbogbo *et al.* 2018).

Across its broad geographic distribution, *G. gynandra* varies in morphology and phytochemistry (Wu *et al.* 2018; Sogbohossou *et al.* 2019, 2020; Blalogoe *et al.* 2020; Houdegbe *et al.* 2022). For instance, characteristics such as plant height, leaf size, and leaf metabolites vary between West African, East African, and Asian accessions (Sogbohossou *et al.* 2019). Although the floral structures vary in size (Wu *et al.* 2018; Sogbohossou *et al.* 2019), *G. gynandra* flowers typically have four sepals, four white petals, six stamens, and a prominent androgynophore and gynophore (i.e., stalk-like structure subtending the pistil). Differences in floral features may contribute to the variation in pollinators between African and Asian populations of *G. gynandra*. To gain a more comprehensive understanding of the flower including features presumably involved in pollination (beyond the nectary; **Chapter 2**), I investigate the floral scent and androgynophore of *G. gynandra*. In **Chapter 4**, I compare the floral scent profiles of African and Asian accessions of *G. gynandra* and discuss the volatile organic compounds in the context of the reported pollination syndromes. Further, I explore cell morphology and gene expression patterns across the floral structures for the African accession to identify potential scent-releasing tissue and examine biosynthetic pathways related to floral scent. In **Chapter 5**, I investigate the morphological and genetic basis of the androgynophore throughout development in *G. gynandra*.

Chapter 2: Comparative Nectary Morphology across Cleomaceae (Brassicales)[1]

2.1 Introduction

Plant–animal interactions have played a crucial role in the rapid diversification of flowering plants (Willmer 2011). Most flowering plants have evolved a mutualistic relationship with animals in which floral rewards are exchanged for pollen transfer (Roy *et al.* 2017; Slavković *et al.* 2021). Consequently, flowering plants exhibit an array of morphological features and chemical signals to appeal to the visual and olfactory capabilities and preferences of animal visitors (Nicolson *et al.* 2007; Willmer 2011). Functioning as a floral reward and in reproduction, pollen has two mutually incompatible purposes and requires resource intensive excess production for animal-mediated pollination (Willmer 2011). As an alternative, nectar is easier for flowers to produce and animals to metabolize, deterring animals from exclusively consuming reproductively essential pollen (Willmer 2011). As such, floral nectaries have evolved independently several times throughout flowering plant diversification (Nicolson *et al.* 2007; Liao *et al.* 2021). Despite their prevalence and ecological significance, floral nectaries have been largely overlooked in morphological and systematic studies resulting in outstanding questions regarding their diversity and development as well as evolutionary patterns across flowering plants (Nicolson *et al.* 2007; Liao *et al.* 2021).

Although unified by their ability to secrete complex sugary solutions for animal-mediated pollination, floral nectaries exhibit substantial morphological diversity (Nicolson *et al.* 2007; Liao *et al.* 2021). Floral nectaries are diverse in size and shape but can be separated into two forms: structured and well-differentiated from adjacent tissue, or unstructured and inconspicuous but evident by the secretion of nectar (Nicolson *et al.* 2007; Liao *et al.* 2021). Structured floral nectaries typically consist of three components: vasculature that supplies phloem sap, nectary parenchyma that modifies phloem sap or stored starches to produce nectar, and the epidermis that secretes nectar (Willmer 2011; Roy *et al.* 2017). These components may originate from various floral structures; therefore, floral nectaries can be located anywhere in the flower but are often basally situated to ensure visitors contact the reproductive organs while accessing nectar (Nicolson *et al.* 2007; Willmer 2011). In addition, there are several means of nectar secretion

[1] A version of Chapter 2 has been published in *Plants* and is formatted accordingly. The published manuscript can be accessed through the following link: https://doi.org/10.3390/plants12061263

including: secretory trichomes; epidermal cell wall or cuticle rupture; and most commonly, modified stomata (nectarostomata) (Willmer 2011; Antoń and Kamińska 2015). Floral nectary location, structure, and secretory mechanisms vary substantively across flowering plants and their diversity and evolutionary patterns within families are largely unexplored (Nicolson *et al.* 2007). Further, the extent to which these structural variations are correlated to family and genera delimitations has been minimally addressed (Nicolson *et al.* 2007).

Cleomaceae is particularly well-suited for comparative developmental investigations. Sister to Brassicaceae, Cleomaceae is a relatively small family of approximately 270 species that houses significant floral diversity (Bayat *et al.* 2018). Cleomaceae has a cosmopolitan distribution but is most common in warmer environments such as arid deserts, grasslands, and humid forests (Iltis *et al.* 2011; Cardinal-McTeague *et al.* 2016; Bayat *et al.* 2018). Cleomaceae flowers vary in symmetry and organ colour, number, size, and elaboration (i.e., gynophores and androgynophores) (Iltis *et al.* 2011; Bayat *et al.* 2018). Much of the morphological variation in Cleomaceae flowers represent understudied components associated with pollinator attraction and rewards (Bayat *et al.* 2018). Floral nectaries are one such feature that remains relatively undocumented despite exhibiting diverse morphology across the family. Cleomaceae floral nectaries tend to develop from the receptacle tissue between the perianth and stamens (i.e., extrastaminal), after initiation and considerable growth of the perianth and reproductive structures (Erbar and Leins 1997; Patchell *et al.* 2011). Though most often located on the receptacle, the floral nectaries can also be derived from petal tissue and can vary in form from annular disks to elaborate adaxial protrusions (Stoudt 1941; Iltis 1958; Karrer 1991; Thulin and Roalson 2017). The morphologically diverse floral nectaries presumably influence the array of Cleomaceae pollinators. Although there is limited research on Cleomaceae pollination, studies suggest the family primarily consists of generalist species, pollinated by a variety of insects such as bees, flies, and butterflies (Cane 2008; Higuera-Díaz *et al.* 2015; Raju and Rani 2016). However, some species (*Melidiscus giganteus* and *Tarenaya houtteana*) may be specialists, exclusively pollinated by bats (Machado *et al.* 2006; Fleming *et al.* 2009). Regardless of the pollination syndrome, nectar plays a vital role in rewarding the array of pollinators (Machado *et al.* 2006; Cane 2008; Fleming *et al.* 2009; Higuera-Díaz *et al.* 2015; Raju and Rani 2016). Yet, Cleomaceae floral nectaries are scarcely mentioned in species descriptions (Tucker and

Vanderpool 2010) and their architecture and ultrastructure have not been characterized in detail across the family.

This work represents the first detailed comparative morphological investigation of floral nectaries across Cleomaceae and within genera, complementing brief comparisons of floral nectaries (Stoudt 1941; Iltis 1958; Karrer 1991) and more comprehensive developmental studies on floral symmetry and stamen number (Erbar and Leins 1997; Patchell *et al.* 2011). We studied nine species (Figure 2.1) including representatives scattered across seven of the 13 major clades in Cleomaceae (Patchell *et al.* 2014). For two of the clades (*Cleome* L. and *Sieruela* Raf.), we selected two species for within-genera comparisons. In addition to the phylogenetic distribution, this sampling of species reflects some of the floral diversity in Cleomaceae with taxa exhibiting a range of flower size, colour, and organ number and elaboration (Figure 2.1). We examined floral nectaries using visual observations, scanning electron microscopy, and a modified histological approach to (1) describe floral nectary position, structure, and internal anatomy; (2) characterize the mode of nectar secretion; and (3) evaluate patterns of floral nectary traits across and within genera.

2.2 Results

2.2.1 *Arivela viscosa*

Arivela viscosa (L.) Raf. has an inconspicuous adaxial extrastaminal nectary detectable by a small volume of nectar at the base of the adaxial petals and stamen filaments (hereafter referred to as filaments; Figure 2.2A). The nectary has three lobes, a medial lobe connected to two lateral lobes by narrow stretches of nectariferous tissue between the adaxial petals and filaments (Figure 2.2B,F). The nectary lobes are slightly convex while the base of the adaxial petals and filaments form a concavity for the narrow stretches of nectariferous tissue. Throughout development, the three nectary lobes increase in size. In the bud stage, the green nectary is challenging to distinguish from the surrounding green tissue. However, as the flower develops, maroon pigment accumulates at the base of the sepals, petals, and filaments, making the green nectary marginally less discreet (Figure 2.2A). Nectarostomata are primarily found on the medial lobe and the narrow stretches of nectariferous tissue, with few located on the lateral lobes (Figure 2.2C–E). In addition, nectarostomata are mainly situated on the distal half of the nectary, closer to the filaments. Small amounts of granular material can be found exuding from

the nectarostomata openings (Figure 2.2C,D). Nectary parenchyma (red-stained tissue) is present at the medial lobe, the concavities between the adaxial petals and filaments, and the lateral lobes, but does not occupy a large portion of the receptacle (Figure 2.2G–K). Vasculature diverges to supply the nectary and adjacent perianth and stamens (Figure 2.2G).

2.2.2 *Cleome amblyocarpa*

Cleome amblyocarpa Barratte and Murb. has a structured adaxial extrastaminal nectary with a complex form protruding from the receptacle (Figure 2.3A). The nectary has convex rims wrapping around the adaxial petals and filaments with concavities between these rims (Figure 2.3B,D). There are three nectary lobes, the medial lobe with an adaxial concavity between the adaxial petals, and two lateral lobes with apical concavities. During development, the nectary remains green while the convex rims and concavities become more pronounced. Nectarostomata are primarily scattered throughout the adaxial concavity of the medial lobe and the apical concavities of the lateral lobes and are often associated with the granular substance (Figure 2.3C,E,F). Nectar secretion corresponds to the location of nectarostomata. Nectary parenchyma is present at the apex of the nectary and spans down to the level of sepal attachment but is mainly absent from nectary tissue adjacent to the filaments (Figure 2.3G–L). Vasculature diverges from the perianth supply to feed the nectary (Figure 2.3G,I).

2.2.3 *Cleome violacea*

Cleome violacea L. has a structured adaxial extrastaminal nectary protruding from the receptacle (Figure 2.4A). The nectary has three prominent convex lobes, one medial lobe, and two lateral lobes (Figure 2.4B,D). From bud to flower, the nectary lobes become larger and more pronounced but remain green. Nectar droplets form on the apical, lateral, and abaxial surfaces of the nectary, corresponding to the location of nectarostomata. Nectarostomata are scattered about the apical and lateral surfaces (Figure 2.4C,E), including the apical crevices between lobes (Figure 2.4G), and are also positioned on the abaxial surface of the nectary, adjacent to the stamens (Figure 2.4F). The nectarostomata are often slightly sunken amongst the epidermal cells. The granular material can be found in nectarostomata openings (Figure 2.4G). Unlike the other eight species examined here, the nectary of *C. violacea* lacks prominent red-stained parenchyma. The nectary of pre-anthetic flowers tends to contain cells that are slightly stained red (Figure

2.4H) but this is not always the case (Figure 2.4J). Instead, the nectary contains vasculature which diverges from the perianth supply (Figure 2.4H) and extends from the receptacle to the apex of the nectary, along the abaxial half of the nectary lobes (Figure 2.4I,K,L).

2.2.4 *Gynandropsis gynandra*

Gynandropsis gynandra (L.) Briq. has an inconspicuous annular extrastaminal nectary detectable by the presence of 4–5 nectar droplets (Figure 2.5A). One nectar droplet is secreted opposite the four sepals, or rather than one adaxial nectar droplet, two nectar droplets are formed opposite the adaxial petals. During development, the nectary increases in size and transitions from a darker green to a lighter green. Occasionally, purple pigmentation accumulates at the sites of nectar secretion. The nectary is a convex ring covered in distinctive cells with finger-like projections (Figure 2.5B,C,G). Nectarostomata are primarily positioned at the base of these cells (Figure 2.5E) and are rarely found at their apex (Figure 2.5F). Due to the protruding cells, nectarostomata can be difficult to find but are easier to locate in the bud stage before the cellular extensions have developed (Figure 2.5D). Nectarostomata along with the granular residue are mainly located on the apical half of the nectary, opposite the sepals but can also be found opposite the petals (Figure 2.5B,D,H). Throughout most of the nectary, the nectary parenchyma is annular, forming a ring near the epidermis (Figure 2.5K). However, near the apex of the nectary, the nectary parenchyma is divided into four regions (Figure 2.5L). These four regions of nectary parenchyma are opposite the sepals and correspond to the positions of the four nectar droplets. The nectary is supplied by vasculature diverging from the perianth supply (Figure 2.5I,J).

2.2.5 *Melidiscus giganteus*

Melidiscus giganteus (L.) Raf. has a large and structured annular extrastaminal nectary (Figure 2.6A). The nectary has three main convex lobes, one medial lobe between the adaxial petals, and two lateral lobes between the adaxial and abaxial petals (Figure 2.6B,C). The distal half of the nectary is narrower than the proximal half. Typically, the abaxial side of the nectary does not have a prominent lobe. Most of the nectary remains light green throughout development. However, maroon pigment accumulates at the base of the nectary, above the sepal and petal bases. Nectar is secreted at the adaxial surface of the nectary and held in place by the

base of the petals. Nectarostomata and clusters of the granular substance are primarily located on the distal half of the nectary, exclusively on the adaxial side (Figure 2.6D–F). The nectary parenchyma occupies a large volume, extending from the nectary apex to the level of sepal attachment but is absent from the nectary tissue immediately adjacent to the epidermis (Figure 2.6G,I). Although nectar is only secreted on the adaxial surface of the nectary, the nectary parenchyma is annular, wrapping closely around the vasculature leading to the stamens (Figure 2.6J–L). Vasculature diverges from the perianth supply and is visible within the nectary parenchyma (Figure 2.6H) and along the inner boundary of nectary parenchyma near the staminal vascular supply (Figure 2.6G). The nectary varies substantially as the plant ages, becoming smaller with less defined lobes and fewer nectarostomata. In addition, nectary parenchyma is only found in the lateral nectary lobes and nectar production tends to cease in growth chamber conditions.

2.2.6 *Polanisia dodecandra*

Polanisia dodecandra (L.) DC. has a structured adaxial extrastaminal nectary protruding from the receptacle (Figure 2.7A). The nectary has a somewhat cordate-shaped concavity at its apex (Figure 2.7B–C) where nectar is secreted and held. The nectary is faintly coloured with purple pigment in the bud stage; however, as the flower develops, vibrant orange pigment accumulates. The apical surface of the nectary is relatively flat at the bud and intermediate stages (Figure 2.7D,G–H), but has an encompassing lip creating a cup-shape at the anthetic stage (Figure 2.7B,I). Nectarostomata are exclusively located on the apical surface of the nectary (Figure 2.7D–F). The granular deposit is often found in the apical concavity, near nectarostomata (Figure 7E,F). Nectary parenchyma is present throughout much of the nectary, excluding the exterior edges of the anthetic stage nectary (Figure 2.7K-L), and extending to the level of sepal attachment (Figure 2.7J). The nectary is supplied by vasculature which diverges from the perianth supply (Figure 2.7G–I), with vasculature sometimes visible within the nectary parenchyma (Figure 2.7H).

2.2.7 *Sieruela hirta*

Sieruela hirta (Klotzsch) Roalson and J. C. Hall has a structured adaxial extrastaminal nectary depressing into the receptacle (Figure 2.8A). The concavity spans from the lateral

nectary lobes between the adaxial petals and filaments, to the medial nectary lobe between the adaxial petals (Figure 2.8B,D). The adaxial filaments are basally fused, forming a wall along the nectary (Figure 2.8E). Nectar is held within the nectary concavity and basally fused adaxial filaments. During development, the nectary concavity becomes more pronounced and the adaxial filament wall extends while the nectary remains light green. Nectarostomata are congregated within the nectary concavity and are absent from the adaxial filament wall (Figure 2.8C). The granular substance is found along with the nectarostomata in the nectary concavity (Figure 2.8F). Nectary parenchyma is present in the nectary concavity and spans to the level of sepal attachment but is absent from the adaxial filament wall (Figure 2.8G–K). The vasculature diverges from the strands leading to the perianth to supply the nectary (Figure 2.8G).

2.2.8 *Sieruela rutidosperma*

Sieruela rutidosperma (DC.) Roalson and J. C. Hall has a structured adaxial extrastaminal nectary depressing into the receptacle (Figure 2.9A). The concavity extends from the lateral nectary lobes between the adaxial petals and filaments, to the medial nectary lobe between the adaxial petals (Figure 2.9B,D). The adaxial filaments are basally fused, forming a wall curved toward the adaxial sepal (Figure 2.9F). Nectar accumulates between the nectary concavity and the curved adaxial filament wall. Throughout development, the nectary concavity becomes more distinct and the adaxial filament wall extends, increasing in curvature. The nectary remains light green from bud to anthesis. Nectarostomata along with the granular deposit are located within the nectary concavity (Figure 2.9C,E). Nectarostomata are absent from the basally fused adaxial filaments. Nectary parenchyma is present within the nectary concavity but is shallow and does not occupy the adaxial filament wall (Figure 2.9G–K). The nectary is supplied by vasculature which diverges from the perianth supply (Figure 2.9G,H).

2.2.9 *Tarenaya houtteana*

Tarenaya houtteana (Schltdl.) Soares Neto & Roalson, comb. nov. (formerly *T. hassleriana*; see Neto *et al.* (2022) for recent taxonomic revision) has a structured extrastaminal annular nectary (Figure 2.10A). Nectar is secreted on the adaxial surface of the nectary and is held in place by the base of the petals. The nectary has three prominent lobes at its proximal half: a medial lobe between the adaxial petals, and two lateral lobes between the adaxial and abaxial

petals (Figure 2.10B,C). The abaxial side of the flower does not have a well-defined nectary lobe. The distal half of the nectary is narrower than the proximal half. The medial nectary lobe has convex rims wrapping around the adaxial petals, roughly forming a 'V' shaped depression pointed toward the adaxial sepal (Figure 2.10D,E). Wrinkles and folds are present along the 'V' shape (Figure 2.10B,D). The lateral nectary lobes are convex between the adaxial and abaxial petals but have a concave region near the base of the filaments (Figure 2.10B). The convex rims, wrinkles, and folds of the medial nectary lobe are absent in the bud stage but become apparent in the intermediate stage. Additionally, the nectary increases in size and remains light green during development. Nectarostomata are located on the medial lobe frequently within crevasses (Figure 2.10F–H). A large amount of the granular substance can often be found covering the wrinkles and folds of the medial nectary lobe (Figure 2.10E). The nectary parenchyma occupies a large volume, extending to the level of sepal attachment (Figure 2.10I,J). Although nectar is only secreted on the adaxial surface of the nectary, nectary parenchyma is found on all sides of the nectary. At the base of the nectary, the nectary parenchyma is present between the petal vasculature (Figure 2.10K). The nectary parenchyma is annular near the base of the petals, wrapping around the reproductive organ vascular supply (Figure 2.10L). At the distal half of the nectary, the nectary parenchyma separates into four main regions aligned with the four petals (Figure 2.10M). The nectary is fed by vasculature which diverges from the perianth supply (Figure 2.10I,J). For all nine species, the majority of nectarostomata are open at anthesis but can be found closed earlier in development, most often in the bud stage.

2.3 Discussion

Thorough analyses of the nine species revealed striking patterns in floral nectary morphology and anatomy across Cleomaceae (Figure 2.1). Each species has a nectary located either between the perianth and stamens or perianth and androgynophore; such is the case for *G. gynandra* which has a particularly prominent androgynophore elevating the reproductive organs (Figure 2.5). The nectaries range from structured protrusions or concavities to inconspicuous and challenging to discern from the receptacle. Nectar is secreted on the adaxial surface of the nectary, apart from *G. gynandra* which secretes one of four to five nectar droplets on the abaxial surface. Excluding the anthetic flowers of *C. violacea*, the nectaries contain nectary parenchyma, highly conspicuous bright red tissue in the fast green and safranin O-stained sections. The

volume of nectary parenchyma varies from a small portion in *A. viscosa* (Figure 2), to a large quantity in *M. giganteus* (Figure 2.6). Corresponding with the site of nectar secretion, the nectary parenchyma is primarily adaxially situated for *A. viscosa*, *C. amblyocarpa*, *C. violacea*, *P. dodecandra*, *S. hirta*, and *S. rutidosperma*; however, the nectary parenchyma is annular forming a ring around the vasculature supplying the reproductive organs for *G. gynandra*, *M. giganteus*, and *T. houtteana*. Regardless of the absence or presence and extent of nectary parenchyma, the nectary of each species is supplied by vasculature which diverges from the vasculature leading to the perianth. Scattered across the nectary epidermis of each species are nectarostomata (Figure 2.11). Nectarostomata may be closed or opened, most frequently in the bud and flowers stages, respectively. Though the abundance of nectarostomata varies from species to species, a granular substance is located near or extruding from nectarostomata in scanning electron micrographs.

2.3.1 Nectarostomata and vasculature are unifying features of Cleomaceae floral nectaries

Cleomaceae floral nectaries are united by nectarostomata as the mechanism for nectar secretion (Table 1.1). Nectarostomata are the most common secretory mechanism and have been extensively reported in eudicots and described in some Orchidaceae species (Nicolson *et al.* 2007; Roy *et al.* 2017). Erbar and Leins (1996) previously referred to the nectarostomata of *C. violacea* as nectar slits and, aside from the nine species in our study, nectarostomata have also been noted in *Cleomella sparsifolia* (Cleomaceae) (Erbar and Leins 1997; Lee, Baum, Oh, *et al.* 2005). Nectarostomata are often described as continuously open and unable to control nectar secretion (Nicolson *et al.* 2007). Yet, nectarostomatal aperture regulation has only been thoroughly studied in *Vicia faba* (Fabaceae) (Davis and Gunning 1992, 1993; Roy *et al.* 2017). In this taxon, nectarostomata development is asynchronous with most opening a few days prior to anthesis and rarely closing once mature (Davis and Gunning 1992). Consistent with Davis and Gunning (1992), we observed closed nectarostomata primarily in the bud stage when they are more likely to be immature. However, the possibility that these nectarostomata open later in development to initiate nectar secretion warrants further exploration.

A granular substance was found extruding from nectarostomata and spread across the nectary epidermis for all nine species. This substance has been previously described as “secretory material”, “spongy secretion”, or “granular structures” (Weryszko-Chmielewska and Sulborska 2011; Antoń and Kamińska 2015; Mercadante-Simões and Paiva 2016; Zhang and

Zhao 2018; Konarska 2020) and can often be observed in the scanning electron micrographs of nectary studies, even if not mentioned in text (Masierowska 2003; Almeida *et al.* 2013; Gotelli *et al.* 2017). It has been hypothesized that the occluding material could be crystallized nectar that may function as an alternative to guard cell movements to close the nectarostomata and perhaps prevent the entry of pathogens (Davis and Gunning 1992; Razem and Davis 1999; Nicolson *et al.* 2007). However, dissolved sugars in the nectar should be washed away during the fixation and dehydration processes and any crystalized sugars in the minute volume of nectar are likely to dissolve in FAA (Bouchard *et al.* 2007). Further, the granular material is distinct from the waxy cuticle and cellular debris, as observed by Davis and Gunning (1992). Alternatively, we propose the granular secretion is a remnant of the microbial community inhabiting the nectar. In congruence with our hypothesis, Carey *et al.* (2023) reported hits to bacteria and yeast-related rRNA in the *Cleome violacea* floral nectary transcriptome and material that looks like budding yeast cells in the nectarostomata openings. Bacteria and fungi, primarily yeast, reside in nectar and can alter its chemical composition, influencing pollinator attraction (Nicolson *et al.* 2007; Liao *et al.* 2021). The relationship between microbial communities in nectar and pollinator interactions is in the early stages of exploration with many intriguing questions remaining (Roy *et al.* 2017; Liao *et al.* 2021). Further research is needed to confirm the identity of the granular secretion.

In addition to nectarostomata, the floral nectaries of all nine Cleomaceae species are supplied by vasculature which diverges from the perianth vascular bundles (Table 1.1). Similar vasculature branching has been reported in *Cleomella serrulata* (Cleomaceae) (Stoudt 1941). Though challenging to observe with the densely stained nectary parenchyma of our specimens, Stoudt (1941) described the vasculature of Cleomaceae floral nectaries as unlignified and profusely branching in the base of the nectary parenchyma and suggested the nectary vascular supply was derived from a former staminal supply (Stoudt 1941). Although the branching patterns and sources vary, vasculature is a shared feature of floral nectaries across angiosperms (Pacini *et al.* 2003; Nicolson *et al.* 2007). Whether an evolutionary consequence of removing the excess sugars from phloem or hydrostatic pressure and weak expanding tissue causing “leaky phloem”, floral nectaries shifted from a physiological to an ecological function of secreting the main floral reward (De la Barrera and Nobel 2004; Nicolson *et al.* 2007; Willmer 2011).

2.3.2 Nectary parenchyma is variable throughout Cleomaceae

Nectary parenchyma varies substantially between Cleomaceae species, from presumably absent in *Cleome violacea* to annular and occupying a large volume in *M. giganteus* (Table 1.1). Secretion and accumulation of nectar on the adaxial side of the flower tends to correspond with adaxially positioned nectary parenchyma. Yet in *M. giganteus* and *T. houtteana*, nectary parenchyma is annular despite secretion of nectar exclusively on the adaxial surface. Abundance of nectary parenchyma may be one factor positively correlated to nectar volume (Pacini *et al.* 2003; Nicolson *et al.* 2007). The volume of nectar secreted is related to pollinator type, a balance between fulfilling the energy needs of the pollinator while encouraging visitation of other flowers (Willmer 2011). For example, flowers with high energy requirement pollinators, such as hawkmoths and bats, produce more nectar than those with lower energy requirement pollinators, including bees and butterflies (Cruden *et al.* 1983). Though some bees and wasps are endothermic (i.e., internally generate heat to regulate body temperature) and thus have higher energy needs, pollinators with larger body sizes such as hawkmoths and bats require more energy per individual (Willmer 2011; McCallum *et al.* 2013). The three species from our study that have annular nectary parenchyma also have high energy requirement pollinators (*G. gynandra*, *M. giganteus*, and *T. houtteana*; Table 1). Although nectar secretion exclusively occurs on the adaxial surface of the nectary for *M. giganteus* and *T. houtteana*, the extensive annular nectary parenchyma may allow the flower to produce enough nectar for bats. *Gynandropsis gynandra* is unique in that nectar secretion is not restricted to the adaxial surface of the nectary, yet the annular nectary parenchyma might permit enough nectar secretion to encourage hawkmoth visitation. Raju and Rani (2016) reported an average nectar volume of 0.26 ± 0.10 μL for *G. gynandra* and noted *A. viscosa* produces a trace amount of nectar, insufficient for nectar volume quantification. This finding is consistent with the hypothesis that the volume of nectary parenchyma is correlated to nectar production, as *A. viscosa* has a smaller amount of nectary parenchyma compared with *G. gynandra*. Though both *G. gynandra* and *P. dodecandra* have more extensive nectary parenchyma than *A. viscosa*, Higuera-Díaz *et al.* (2015) measured a higher average volume of nectar for the generalist species *P. dodecandra* (0.63 ± 0.32 μL), with lower energy requirement pollinators including bees, wasps, and flies. Additional pollination and nectar studies are required to confirm the relationship between the amount of nectary parenchyma, volume of nectar, and pollinator type.

Cleome violacea differs from the other eight species in that it does not have prominent nectary parenchyma at anthesis. However, the nectary tends to appear more red-stained earlier in development. Commonly, photosynthate is transported from elsewhere in the plant and stored as starch in the nectary parenchyma (Nicolson *et al.* 2007). Starch accumulation occurs in the nectary parenchyma of *Arabidopsis thaliana* (Brassicaceae; the sister family to Cleomaceae) (Ren *et al.* 2007). The degradation of starch acts a carbohydrate source for nectar, allowing for nectar production at any time of the day (Nicolson *et al.* 2007). In ornamental tobacco (Solanaceae), starch accumulates in the nectary parenchyma during development but is rapidly broken down one day before anthesis (Ren *et al.* 2007). Perhaps, the nectary of *Cleome violacea* may be more densely stained earlier in development due to the presence of starch which is subsequently broken down prior to anthesis in preparation for nectar secretion. Carey *et al.* (2023) reported a low average nectar volume (0.17 ± 0.07 μL) for *Cleome violacea* that decreased with daily collection. The small volume of secreted nectar does not cover the adaxial surface of the nectary lobes (Figure 2.4A). Like glistening nectar, the glossy exposed surface of the nectary may act as a cue for pollinators by reflecting incident light (Lunau *et al.* 2020). Additionally, as the nectary of *Cleome violacea* is a prominent component of the flower, its nectary size may play a role in pollinator attraction.

2.3.3 Evolutionary lability in floral nectary morphology across Cleomaceae

While unified by nectarostomata and vasculature, the diversity in floral nectary location, size, and shape has no clear evolutionary pattern across the family (Figure 2.12). The floral nectaries of the focal Cleomaceae species can be categorized by shape and position as follows: annular (*G. gynandra*, *T. houtteana*, *M. giganteus*; Figure 2.12B), protruding adaxial (*Cleome amblyocarpa*, *Cleome violacea*, *P. dodecandra*; Figure 2.12C), slightly convex adaxial (*A. viscosa*; Figure 2.12D), and concave adaxial (*S. hirta*, *S. rutidosperma*; Figure 2.12E). The annular and protruding adaxial nectaries are not confined to a specific clade or genus. Previous research fills in the gaps for some of the genera without representative species in our study; *Cleomella* species have an annular nectary protruding off the receptacle between the perianth and stamens (Stoudt 1941; Lee, Baum, Oh, *et al.* 2005; Higuera-Díaz *et al.* 2015) and *Rorida* species have petal appendages that act as nectaries (Thulin and Roalson 2017). Thus, Cleomaceae floral nectaries are not exclusively receptacular, but can also be derived from other organs. In addition,

the annular nectaries of *Cleomella*, *Gynandropsis*, *Melidiscus*, and *Tarenaya* are scattered across the phylogeny and Brassicaceae nectaries range from annular to two, four, or eight discrete sections (Nicolson *et al.* 2007). Although Iltis (1958) hypothesized that adaxial nectaries are derived from annular nectaries, this distribution in nectary shape and position does not clearly support that evolutionary pathway. That is, annular nectary parenchyma could be a derived character state associated with a shift to high energy requirement pollinators. Further, nectar secretion tends to occur exclusively on the adaxial side of the flower regardless of nectary parenchyma positioning. Adaxial nectar secretion could be selected for so that pollinators have easy access to nectar and are likely to contact the upward curving reproductive organs.

In addition, the degree of floral nectary similarity within genera can vary drastically. The nectaries of *S. hirta* and *S. rutidosperma* are similar in shape with a concavity extending from the lateral nectary lobes between the adaxial petals and basally fused adaxial filaments, to the medial nectary lobe between the adaxial petals. The primary difference being the angle of the basally fused adaxial filaments which function to hold the nectar in place. The wall of fused filaments is linear in *S. hirta* and curved toward the adaxial sepal in *S. rutidosperma*. Lunau *et al.* (2020) briefly describe *Sieruela monophylla* as having a glossy annular false floral nectary. As the flowers of all nine Cleomaceae species described here have nectar-secreting structures and species within the same genera (*S. hirta* and *S. rutidosperma*) have adaxial nectaries, verification of *S. monophylla*'s annular false nectary is needed. Although *Cleome amblyocarpa* and *Cleome violacea* both have nectaries that protrude off the receptacle, the shape of the nectaries is entirely different. *Cleome amblyocarpa* has a somewhat pelvis-shaped nectary, while *Cleome violacea* has a three-lobed nectary. Similarly, Iltis (1958) described considerable within-genera differences in nectary size and shape for *Polanisia*, with nectaries ranging from solid with a concave or truncate apex to tubular. Hence, floral nectary structure is diverse across Cleomaceae, and the drastic variation can also extend to within genera.

2.4 Materials and Methods

2.4.1 Plant material

Nine species from the Cleomaceae family were sampled: *Arivela viscosa* accession 815 from Hortus Botanicus; *Cleome amblyocarpa* accession 151485 from Royal Botanic Gardens Kew; *Cleome violacea* accession 813 from Hortus Botanicus; *Gynandropsis gynandra* accession

TOT8917 kindly provided by M. Eric Schranz, Wageningen University; *Melidiscus giganteus* accession 814 from Hortus Botanicus; *Polanisia dodecandra* accession 68456 from B & T World Seeds; *Sieruela hirta* accession 74520 from B & T World Seeds; *Sieruela rutidosperma* accession 512496 from B & T World Seeds; and *Tarenaya houtteana* accession FL2400 from West Coast Seeds. Seeds were grown in professional growing mix (Sun Gro Horticulture, Agawam, MA, USA) in University of Alberta Department of Biological Sciences growth chambers set to 28°C day/22°C night temperatures with a 12 h day/12 h night cycle. Voucher specimens were deposited at the University of Alberta Vascular Plant Herbarium (ALTA) (see Appendix 2.1 for ALTA accession numbers). Fresh flowers were photographed using a Pixel 5 (Google, Menlo Park, CA, USA) alone or attached to a SMZ1500 stereo microscope (Nikon, Tokyo, Japan) with a NexYZ 3-axis universal smartphone adaptor (Celestron, Torrance, CA, USA).

2.4.2 Scanning electron microscopy

For each species, flowers were binned into three developmental stages, (1) bud stage, (2) intermediate stage, and (3) anthetic stage (see Appendix 2.2 for stage descriptions). Flowers at the three developmental stages were fixed in FAA (50% ethanol, 10% formalin, and 5% glacial acetic acid) on ice under vacuum for 30 min and stored at 4°C. Fixed specimens were dehydrated in an ethanol series and critical point dried with carbon dioxide using a CPD 030 critical point dryer (Bal-Tec AG, Balzers, Liechtenstein). Dried specimens were dissected and mounted on scanning electron microscopy stubs with conductive carbon tabs, sputter coated with gold using a Hummer 6.2 sputter coater (Anatech USA, Sparks, NV, USA) and imaged using a ZEISS EVO 10 scanning electron microscope or a ZEISS Sigma 300 VP field emission scanning electron microscope (Carl Zeiss AG, Oberkochen, Germany). Contrast and brightness of the micrographs were adjusted using Adobe Photoshop but no other modifications were made.

2.4.3 Histological preparations

Flowers from the nine species at the three developmental stages were fixed in FAA and dehydrated in an ethanol series as previously mentioned. Samples were then cleared with CitriSolv (Decon Labs, King of Prussia, PA, USA), embedded in Paraplast Plus (SigmaAldrich, St. Louis, MI, USA), and stored at 4 ◦C. Samples were sectioned to 8 µm using a Microm HM

325 rotary microtome (Thermo Scientific, Waltham, MA, USA) and mounted on glass slides. Transverse and longitudinal sections were prepared for each species.

2.4.4 Fast green and safranin O staining

Johansen's fast green and safranin O protocol (1940) as adapted by Ruzin (1999) yields vibrantly stained plant tissues, yet it utilizes several hazardous chemicals. Because methyl cellosolve, xylene, and picric acid are toxic to humans and picric acid is highly explosive when dry and can react to form explosive substances (Sigma-Aldrich 2021a; b; c), we substituted these chemicals with less harmful alternatives. Historically, ethanol was used as a dehydrating agent but was replaced with methyl cellosolve, before the harmful properties of methyl cellosolve were known (Senior 1951). Therefore, we reverted to anhydrous ethanol and used CitriSolv and hydrochloric acid in place of xylene and picric acid, respectively. The detailed modified protocol is as follows.

Sectioned specimens were deparaffinized and rehydrated by placing slides in the following solutions: CitriSolv for 10 min, fresh CitriSolv for 10 min, 50% CitriSolv and 50% ethanol for 10 min, 100% ethanol for 5 min, 95% ethanol for 5 min, and 70% ethanol for 5 min. Slides were left overnight, approximately 16 h, in safranin O staining solution (1% w/v safranin O, 1% (w/v) sodium acetate, 2% (v/v) formalin, 3 volumes 100% ethanol, and 1 volume deionized water). Excess safranin O staining solution was washed away by submerging slides in deionized water then gently rinsing with deionized water in a squeezable wash bottle. To differentiate safranin O and dehydrate sectioned specimens, slides were placed in the following solutions: 95% ethanol and 0.5% hydrochloric acid for 10 s, 95% ethanol with 4 drops of ammonium hydroxide per 100 mL for 10 s, and 100% ethanol for 10 s. Sectioned specimens were counterstained in fast green staining solution (0.075% (w/v) fast green FCF, 2 volumes of 100% ethanol, and 1 volume methyl salicylate) for 10 s. To clear sectioned specimens, slides were placed in clearing solution (2 volumes methyl salicylate, 1 volume 100% ethanol, and 1 volume CitriSolv) for 10 s, CitriSolv with 3 drops of 100% ethanol for 3 s, CitriSolv for 5 s, and left in fresh CitriSolv until coverslips were mounted with Permount (Fisher Scientific, Waltham, MA, USA) to avoid drying out the sectioned specimens. Slides were imaged using a Pixel 5 attached to an Eclipse 80i light microscope (Nikon, Tokyo, Japan) with a NexYZ 3-axis universal smartphone adapter. Backgrounds were removed from photographs using the 'Magic

Eraser Tool' in Adobe Photoshop. The terms adaxial and abaxial refer to the position relative to the floral axis (unless otherwise noted), thus indicating the top and bottom halves of the flower, respectively. The terms frontal and sagittal are used to indicate the type of longitudinal section: (1) a frontal section through the middle of a Cleomaceae flower bisects the lateral sepals and (2) a sagittal section bisects the adaxial and abaxial sepals.

2.5 Conclusions

Though floral nectaries secrete a crucial reward for pollinators, description of nectary structure and development across and within families is lagging (Nicolson *et al.* 2007). As with other characteristics associated with pollinator interactions such as petal colour and patterns and floral organ number and elaboration, floral nectaries are a morphologically diverse feature across Cleomaceae. As such, detailed descriptions of floral nectaries would be a valuable addition to floras for the identification of Cleomaceae species. Although Cleomaceae floral nectaries vary in colour, size, and shape, they are most commonly receptacular features with nectary parenchyma often extending from the apex of the nectary to the level of perianth attachment. This variation is ideal for exploring outstanding questions regarding the genetic controls of floral nectary size, shape, and parenchyma position. With muddled boundaries of the nectary and receptacle, the receptacle does not always appear to be a well-defined floral organ. Although modifications of the receptacle such as nectaries and the androgynophore contribute to floral diversity in Cleomaceae and receptacular nectaries are common across flowering plants (Nicolson *et al.* 2007), the receptacle is often overlooked in floral evo-devo studies. Thus, the involvement of the receptacle in floral diversification and pollinator interactions necessitates further investigation.

2.6 Tables

Table 2.1. Summary of floral nectary characteristics and pollination system for the nine Cleomaceae species.

Species	Nectary type	Nectary location	Nectary parenchyma	Nectary vasculature	Nectar secretion mechanism	Pollination system
Arivela viscosa	Slightly convex adaxial	Between perianth and stamens	Present	Present	Nectarostomata	Generalist (Chandra *et al.* 2013; Raju and Rani 2016; Saroop and Kaul 2019)
Cleome amblyocarpa	Protruding adaxial	Between perianth and stamens	Present	Present	Nectarostomata	Unknown
Cleome violacea	Protruding adaxial	Between perianth and stamens	Absent/not prominent	Present	Nectarostomata	Unknown
Gynandropsis gynandra	Annular	Between perianth and androgynophore	Present	Present	Nectarostomata	Generalist/hawkmoth (Werth 1942; Chandra *et al.* 2013; Martins and Johnson 2013; Raju and Rani 2016)
Melidiscus giganteus	Annular	Between perianth and stamens	Present	Present	Nectarostomata	Bat (Fleming *et al.* 2009)
Polanisia dodecandra	Protruding adaxial	Between perianth and stamens	Present	Present	Nectarostomata	Generalist (Higuera-Díaz *et al.* 2015)
Sieruela hirta	Concave adaxial	Between perianth and stamens	Present	Present	Nectarostomata	Unknown
Sieruela rutidosperma	Concave adaxial	Between perianth and stamens	Present	Present	Nectarostomata	Generalist (Widhiono and Sudiana 2015)
Tarenaya houtteana	Annular	Between perianth and stamens	Present	Present	Nectarostomata	Bat (Machado *et al.* 2006)

2.7 Figures

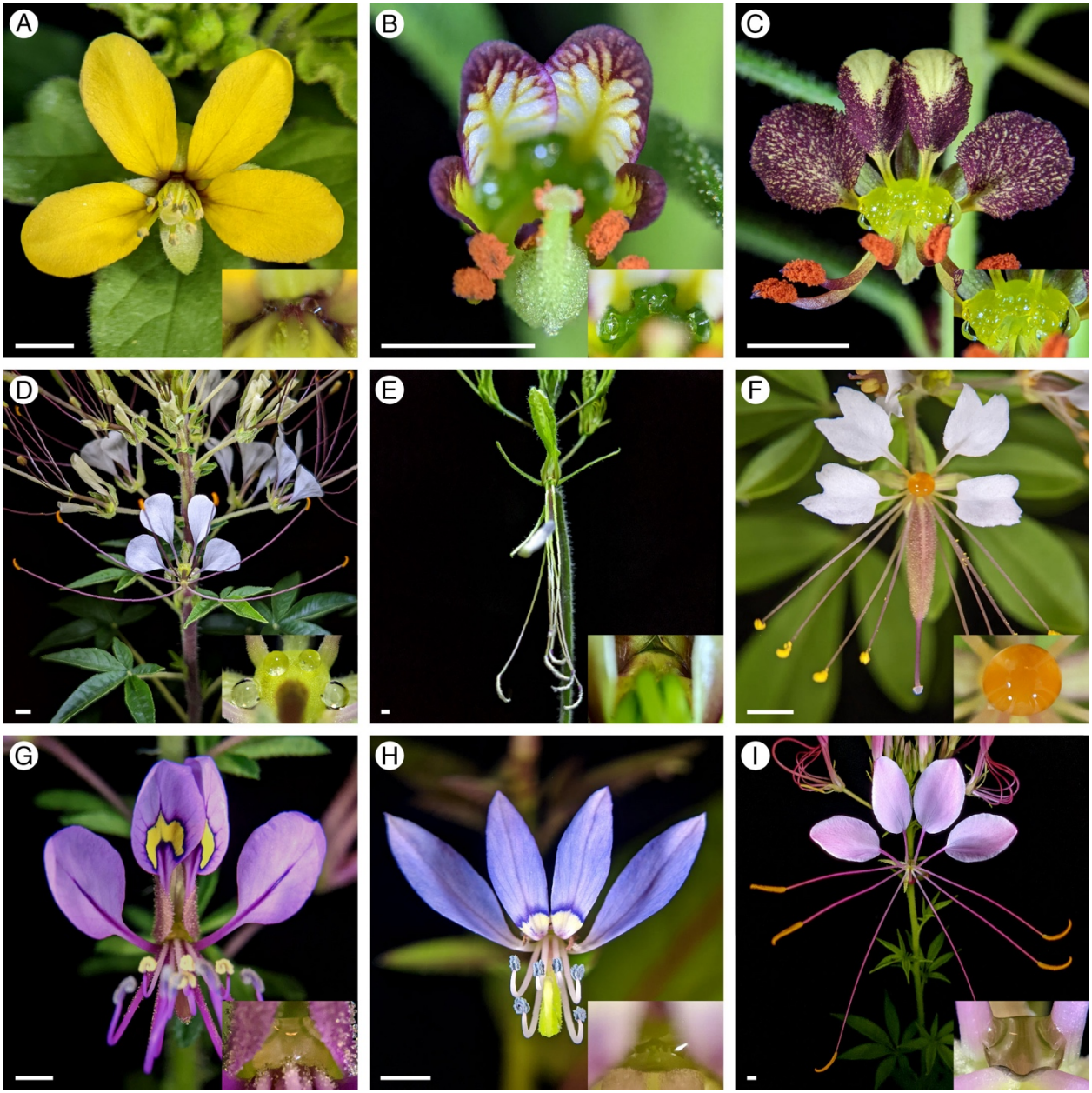

Figure 2.1. Anthetic flower with nectary inset of the nine Cleomaceae species. (A) *Arivela viscosa*. (B) *Cleome amblyocarpa*. (C) *Cleome violacea*. (D) *Gynandropsis gynandra*. (E) *Melidiscus giganteus*. (F) *Polanisia dodecandra*. (G) *Sieruela hirta*. (H) *Sieruela rutidosperma*. (I) *Tarenaya houtteana*. The scale bar represents 0.25 cm in all images to illustrate the drastic variation in flower size.

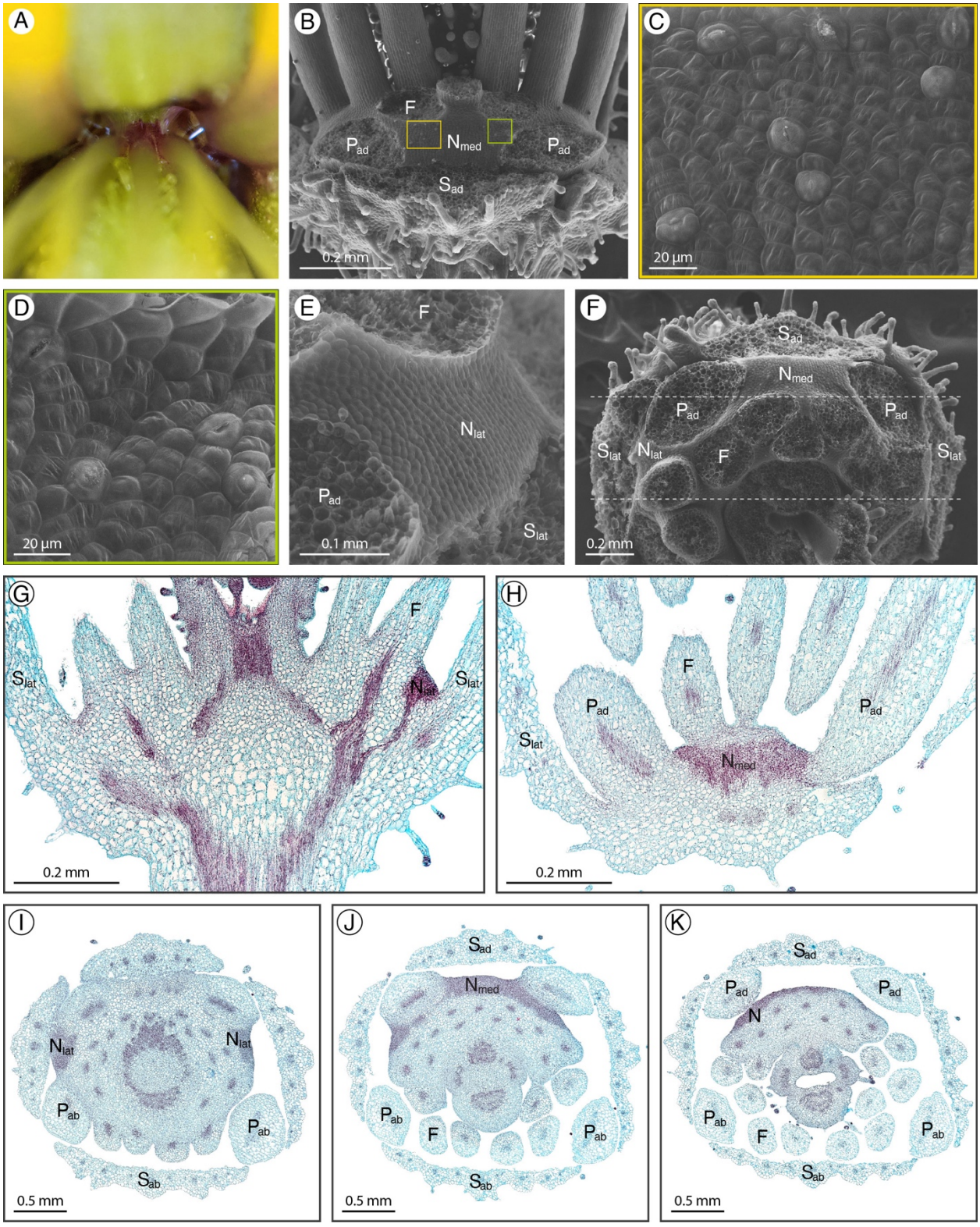

Figure 2.2. *Arivela viscosa* nectary (A) photograph, (B–F) scanning electron micrographs, and (G–K) fast green and safranin O-stained sections. (A) Apical view of the nectary. (B) Adaxial

view of the nectary. (C–E) Adaxial view close-ups: (C,D) medial nectary lobe, corresponding to the left and right boxes in (B), respectively, and (E) lateral nectary lobe. (F) Apical view of the nectary. (G,H) Longitudinal sections (frontal plane), corresponding to the bottom and top dashed lines in (F), respectively. (I–K) Transverse sections of the nectary from proximal to distal positioning. All images are of anthetic stage specimens. F: filament; Nlat: lateral nectary lobe; Nmed: medial nectary lobe; Pab: abaxial petal; Pad: adaxial petal; Sab: abaxial sepal; Sad: adaxial sepal; Slat: lateral sepal.

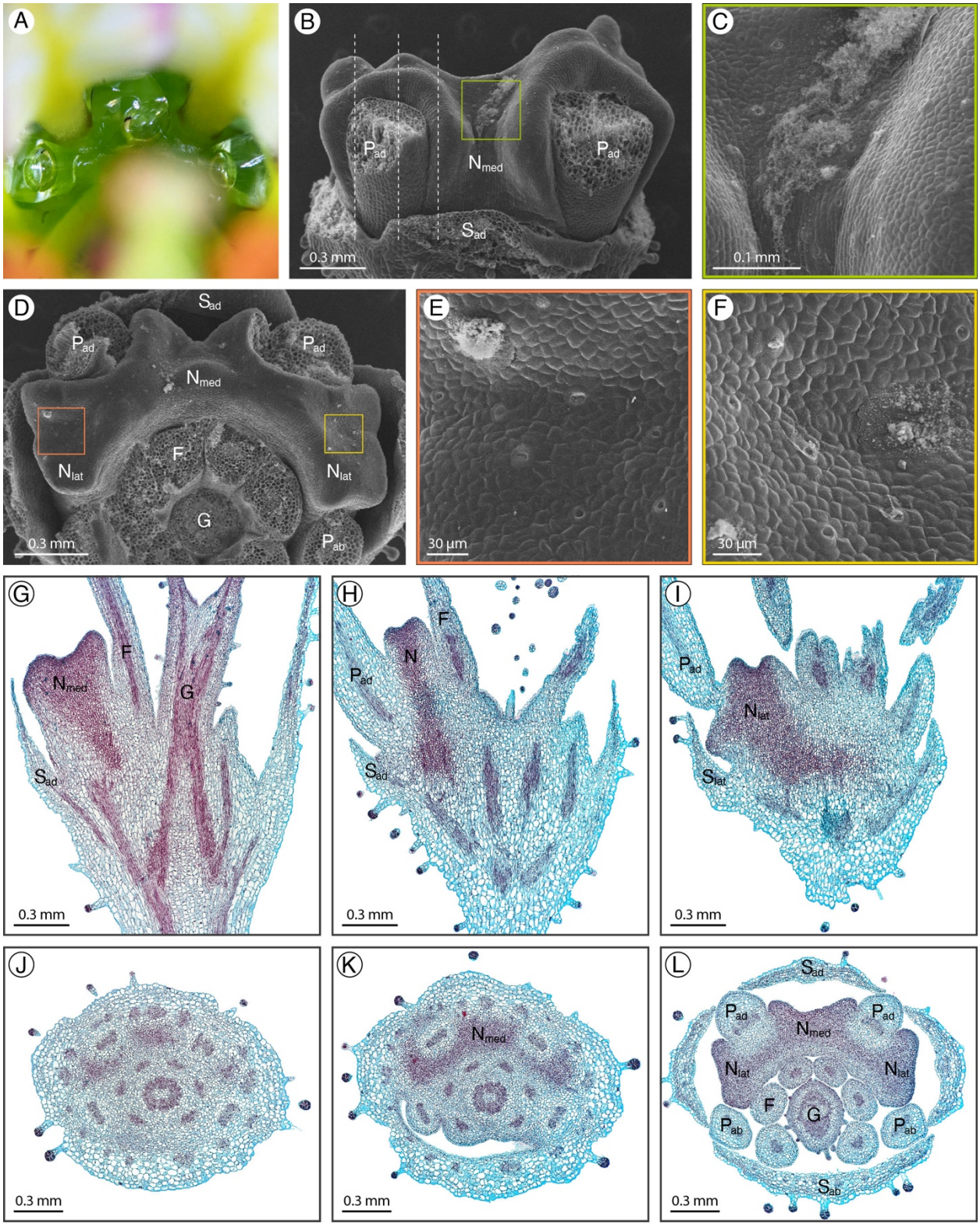

Figure 2.3. *Cleome amblyocarpa* nectary (A) photograph, (B–F) scanning electron micrographs, and (G–L) fast green and safranin O-stained sections. (A) Apical view of the nectary. (B)

Adaxial view of the nectary. (C) Adaxial view close-up of the medial nectary lobe, corresponding to the box in (B). (D) Apical view of the nectary. (E,F) Apical view close-ups of the lateral nectary lobes, corresponding to the left and right boxes in (D), respectively. (G–I) Longitudinal sections (sagittal plane) of the nectary, corresponding to the dashed lines in (B) from right to left, respectively. (J–L) Transverse sections of the intermediate stage nectary from proximal to distal positioning. All images are of anthetic stage specimens unless indicated otherwise. F: filament; G: gynophore; Nlat: lateral nectary lobe; Nmed: medial nectary lobe; Pab: abaxial petal; Pad: adaxial petal; Sab: abaxial sepal; Sad: adaxial sepal.

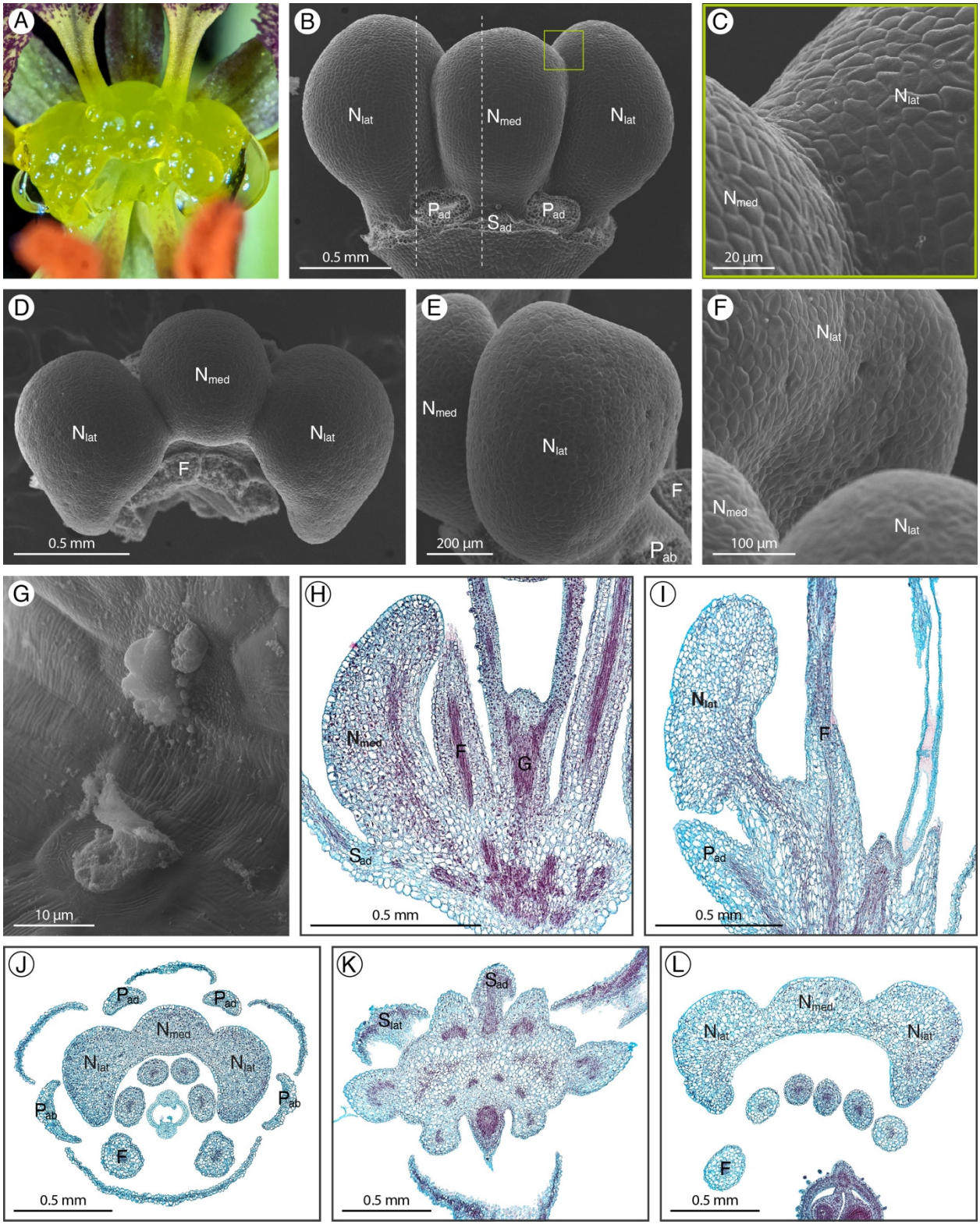

Figure 2.4. *Cleome violacea* nectary (A) photograph, (B–G) scanning electron micrographs, and (H–L) fast green and safranin O-stained sections. (A) Apical view of the nectary. (B) Adaxial

view of the nectary. (C) Adaxial view close-up of the medial and lateral nectary lobes, corresponding to the box in (B). (D) Apical view of the nectary. (E) Lateral view of the nectary. (F) Lateral view close-up of the nectary. (G) Close-up of nectarostomata. (H,I) Longitudinal sections (sagittal plane) of the nectary, corresponding to the right and left dashed lines in (B), respectively: (H) intermediate stage nectary, and (I) anthetic stage nectary. (J–L) Transverse sections: (J) intermediate stage nectary, (K,L) anthetic stage nectary from proximal to distal positioning. All images are of anthetic stage specimens unless indicated otherwise. F: filament; G: gynophore; Nlat: lateral nectary lobe; Nmed: medial nectary lobe; Pab: abaxial petal; Pad: adaxial petal; Sad: adaxial sepal; Slat: lateral sepal.

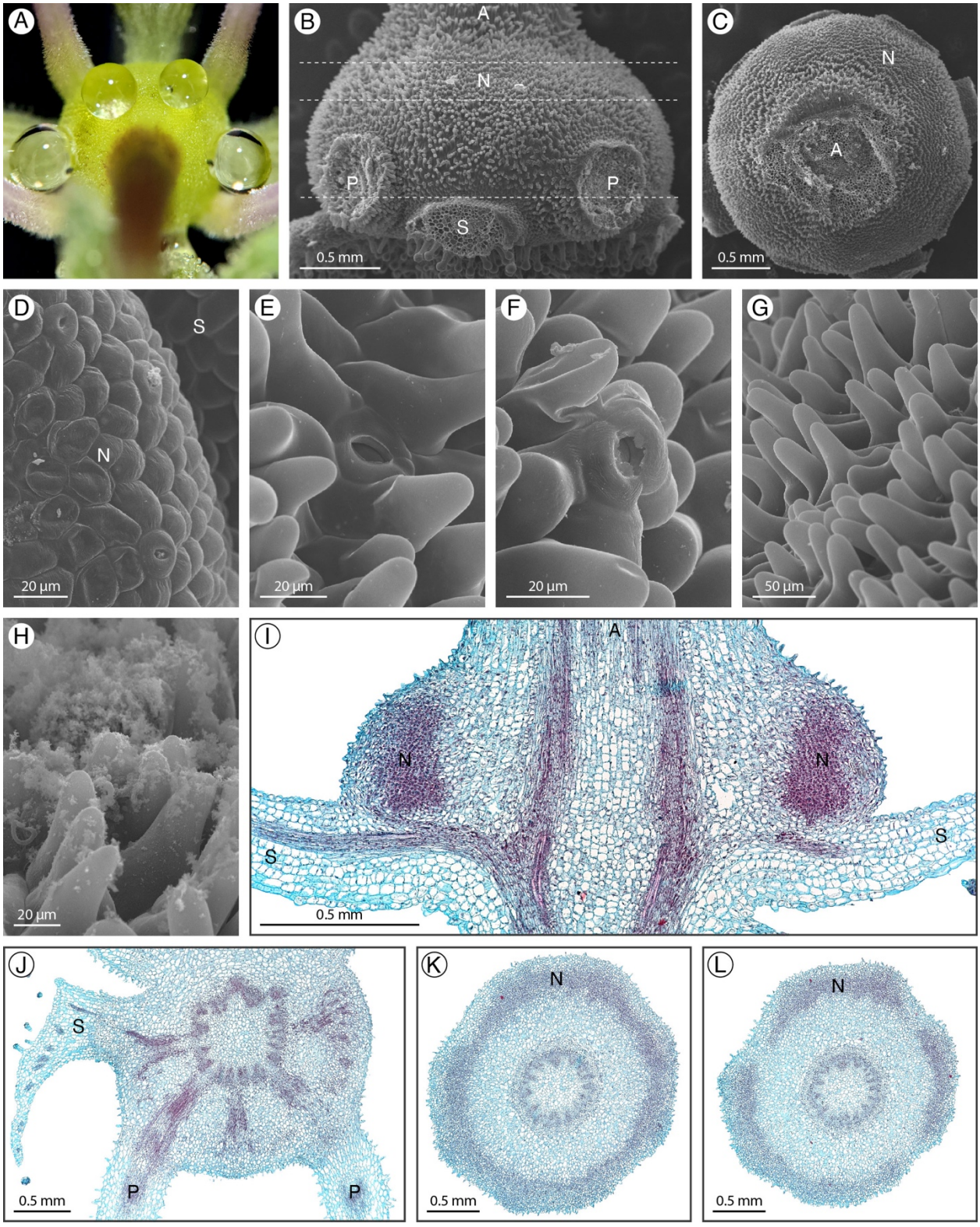

Figure 2.5. *Gynandropsis gynandra* nectary (A) photograph, (B–H) scanning electron micrographs, and (I–L) fast green/safranin O-stained sections. (A) Apical view of the nectary.

(B) Side view of the nectary. (C) Apical view of the nectary. (D) Apical view close-up of the bud stage nectary. (E,F) Closeup of nectarostomata. (G,H) Close-up of the nectary. (I) Longitudinal section of the intermediate stage nectary. (J–L) Transverse sections of the nectary, corresponding to the dashed lines in (B) from proximal to distal, respectively. All images are of anthetic stage specimens unless indicated otherwise. A: androgynophore; F: filament; N: nectary; P: petal; S: sepal.

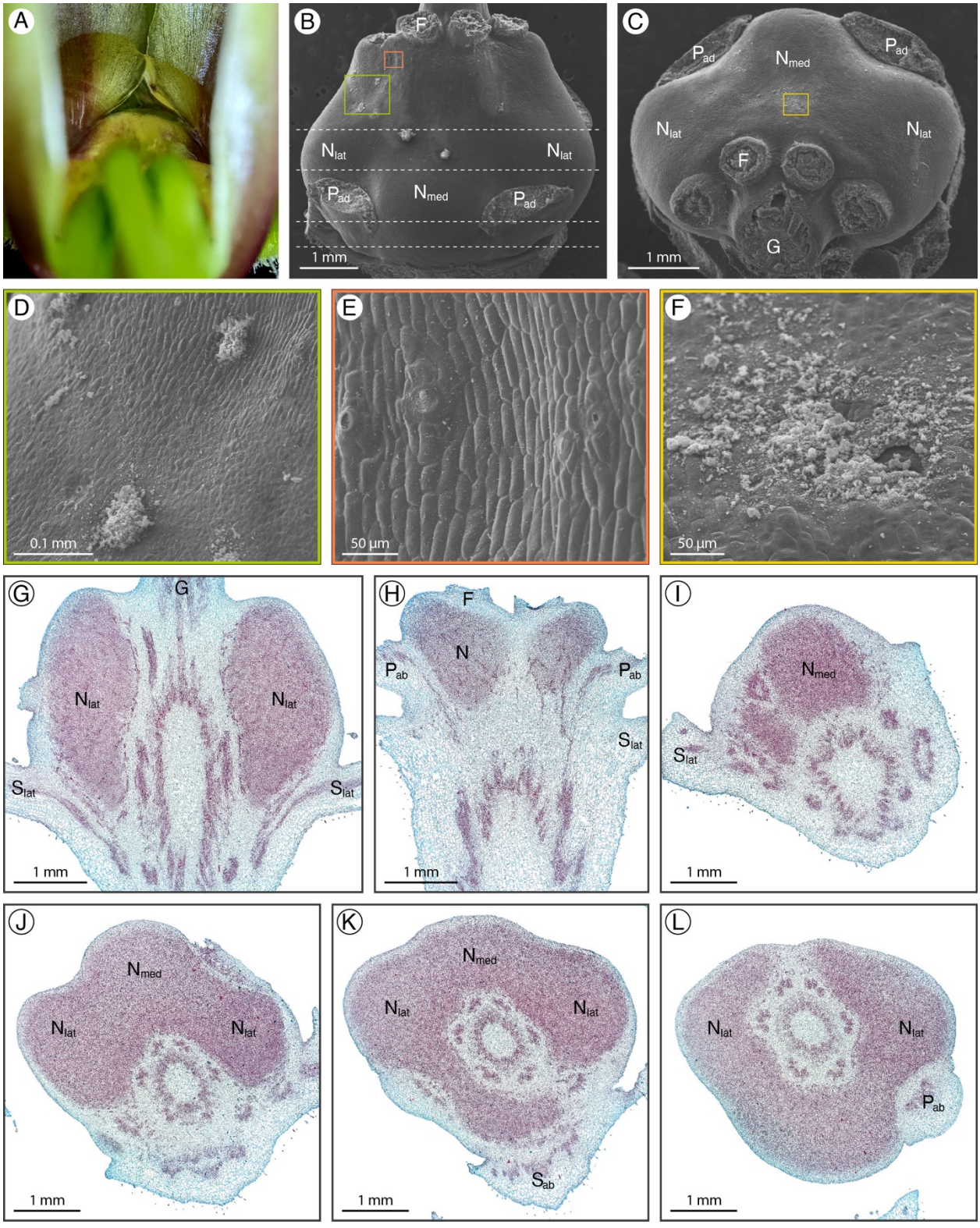

Figure 2.6. *Melidiscus giganteus* nectary (A) photograph, (B–F) scanning electron micrographs, and (G–L) fast green and safranin O-stained sections. (A) Apical view of the nectary. (B)

Adaxial view of the nectary. (C) Apical view of the nectary. (D,E) Adaxial view close-ups, corresponding to the bottom and top boxes in (B), respectively. (F) Apical view close-up, corresponding to the box in (C). (G,H) Longitudinal sections (frontal plane): (G) lateral nectary lobes and (H) abaxial side of nectary. (I–L) Transverse sections of the nectary, corresponding to the dashed lines in (B) from proximal to distal, respectively. All images are of anthetic stage specimens. F: filament; G: gynophore; Nlat: lateral nectary lobe; Nmed: medial nectary lobe; Pab: abaxial petal; Pad: adaxial petal; Sab: abaxial sepal; Sab: abaxial sepal; Slat: lateral sepal.

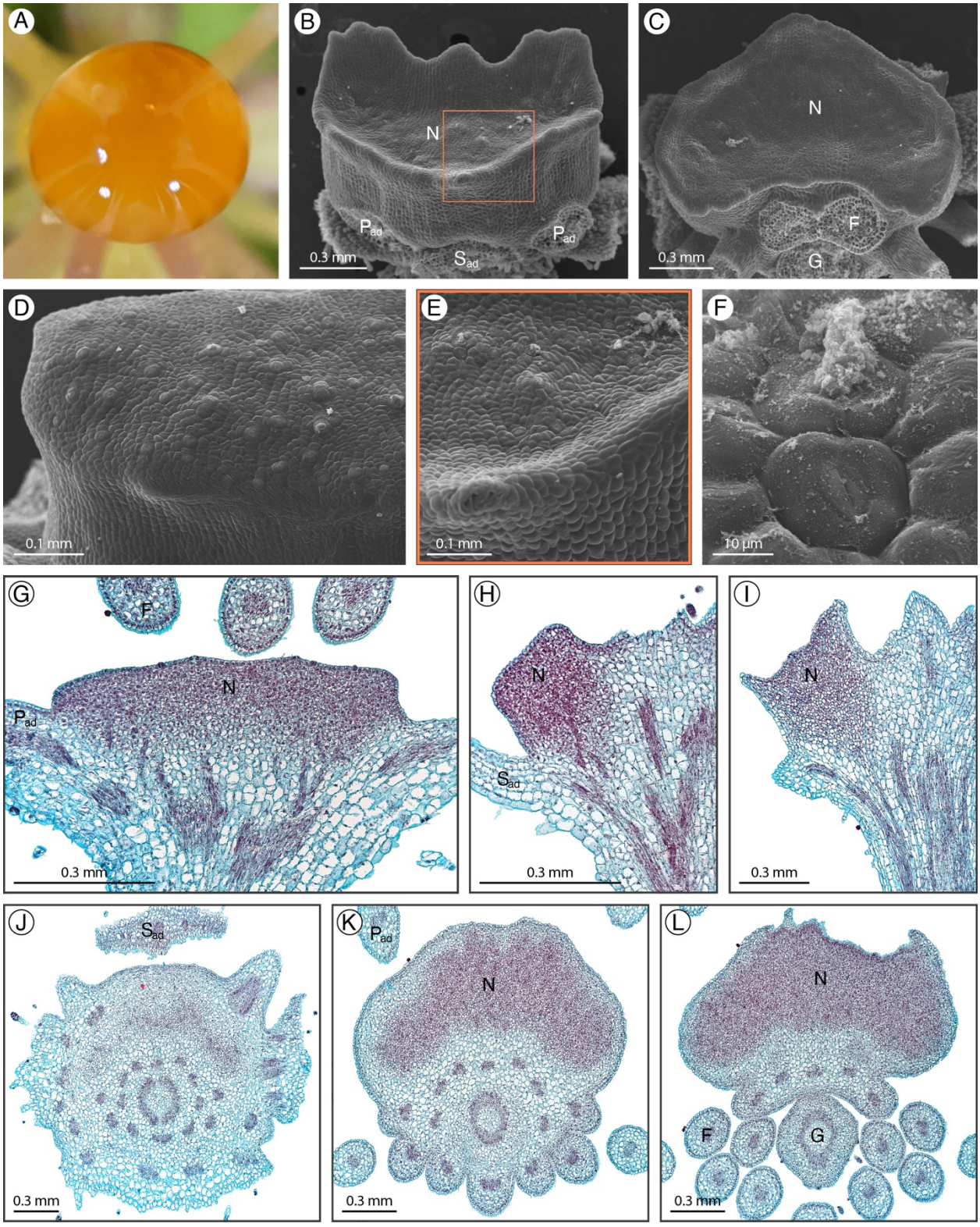

Figure 2.7. *Polanisia dodecandra* nectary (A) photograph, (B–F) scanning electron micrographs, and (G–L) fast green and safranin O-stained sections. (A) Apical view of the nectary. (B)

Adaxial view of the nectary. (C) Apical view of the nectary. (D–F) Adaxial view close-ups: (D) bud stage nectary, (E) anthetic stage nectary, corresponding to the box in (B), and (F) anthetic stage nectarostomata. (G) Longitudinal section (frontal plane) of the intermediate stage nectary. (H,I) Longitudinal section (sagittal plane): (H) intermediate stage nectary and (I) anthetic stage nectary. (J–L) Transverse sections of the nectary from proximal to distal positioning. All images are of anthetic stage specimens unless indicated otherwise. F: filament; G: gynophore; N: nectary; Pad: adaxial petal; Sad: adaxial sepal.

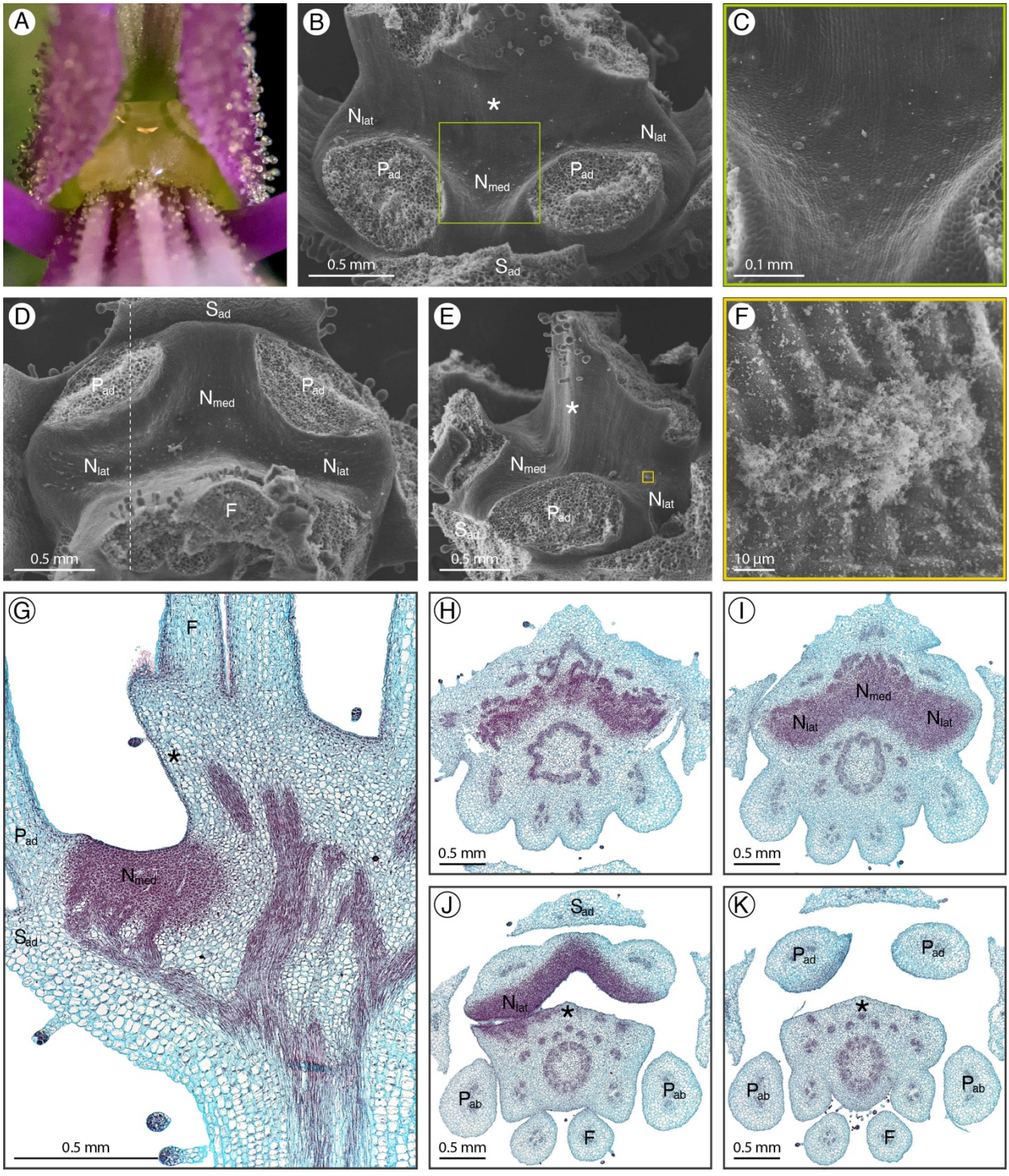

Figure 2.8. *Sieruela hirta* nectary (A) photograph, (B–F) scanning electron micrographs, and (G–K) fast green and safranin O-stained sections. (A) Apical view of the nectary. (B) Adaxial view of the nectary. (C) Adaxial view close-up of the nectary, corresponding to the box in (B). (D) Apical view of the nectary. (E) Lateral view of the nectary. (F) Lateral view close-up of the nectary, corresponding to the box in (E). (G) Longitudinal section (sagittal plane) of the

intermediate stage nectary, corresponding to the dashed line in (D). (H–K) Transverse sections of the nectary from proximal to distal orientation. All images are of anthetic stage specimens unless indicated otherwise. Basal fusion of adaxial filaments is indicated with an asterisk. F: filament; Nlat: lateral nectary lobe; Nmed: medial nectary lobe; Pab: abaxial petal; Pad: adaxial petal; Sad: adaxial sepal.

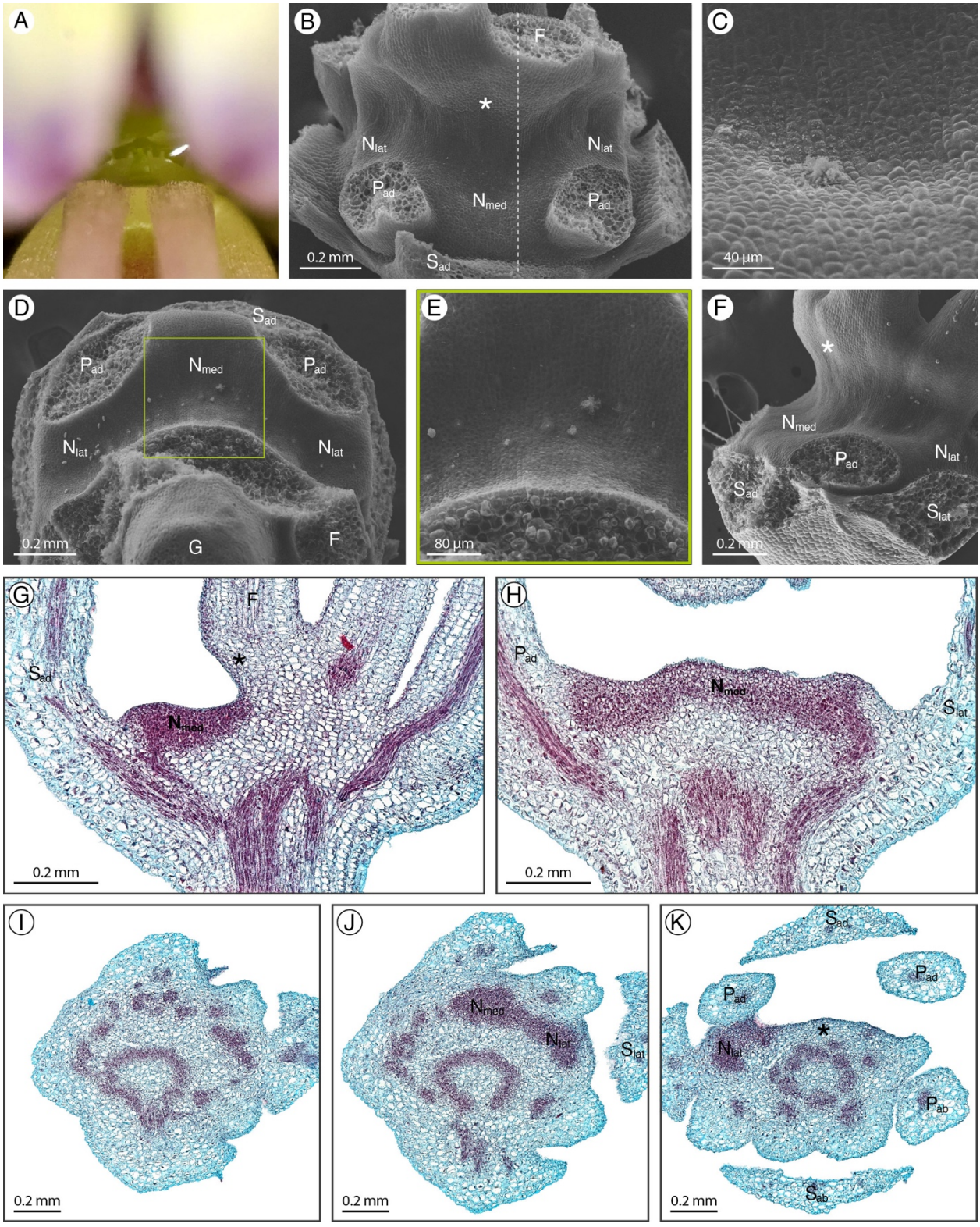

Figure 2.9. *Sieruela rutidosperma* nectary (A) photograph, (B–F) scanning electron micrographs, and (G–K) fast green and safranin O-stained sections. (A) Apical view of the

nectary. (B) Adaxial view of the nectary. (C) Adaxial view close-up of the medial nectary lobe. (D) Apical view of the nectary. (E) Apical view close-up of the nectary, corresponding to the box in (D). (F) Lateral view of the nectary. (G) Longitudinal section (sagittal plane) of the intermediate stage nectary, corresponding to the dashed line in (B). (H) Longitudinal section (frontal plane) of the nectary. (I–K) Transverse section of the nectary from proximal to distal positioning. All images are of anthetic stage specimens unless indicated otherwise. Basal fusion of adaxial filaments is indicated with an asterisk. F: filament; G: gynophore; Nlat: lateral nectary lobe; Nmed: medial nectary lobe; Pab: abaxial petal; Pad: adaxial petal; Sab: abaxial sepal; Sad: adaxial sepal; Slat: lateral sepal.

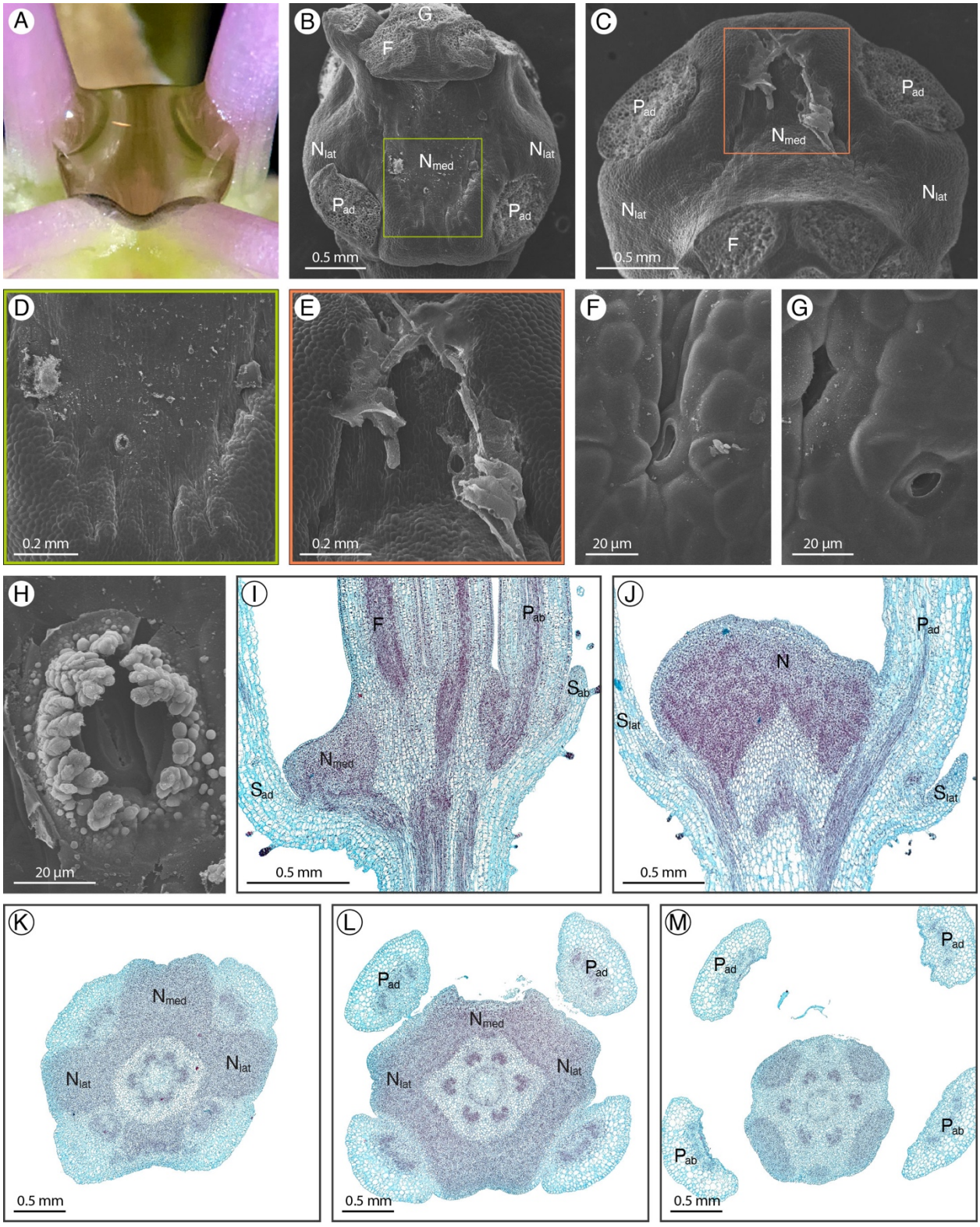

Figure 2.10. *Tarenaya houtteana* nectary (A) photograph, (B–H) scanning electron micrographs, and (I–M) fast green and safranin O-stained sections. (A) Apical view of the nectary. (B)

Adaxial view of the nectary. (C) Apical view of the nectary. (D) Adaxial view close-up of the nectary, corresponding to the box in (B). (E) Apical view close-up of the nectary, corresponding to the box in (C). (F–H) Close-up of nectarostomata. (I) Longitudinal section (sagittal plane) of the bud stage nectary. (J) Longitudinal section (frontal-oblique plane) of the intermediate stage nectary. (K–M) Transverse sections of the nectary from proximal to distal positioning. All images are of anthetic stage specimens unless indicated otherwise. F: filament; G: gynophore; Nlat: lateral nectary lobe; Nmed: medial nectary lobe; Pab: abaxial petal; Pad: adaxial petal; Sab: abaxial sepal; Sad: adaxial sepal; Slat: lateral sepal.

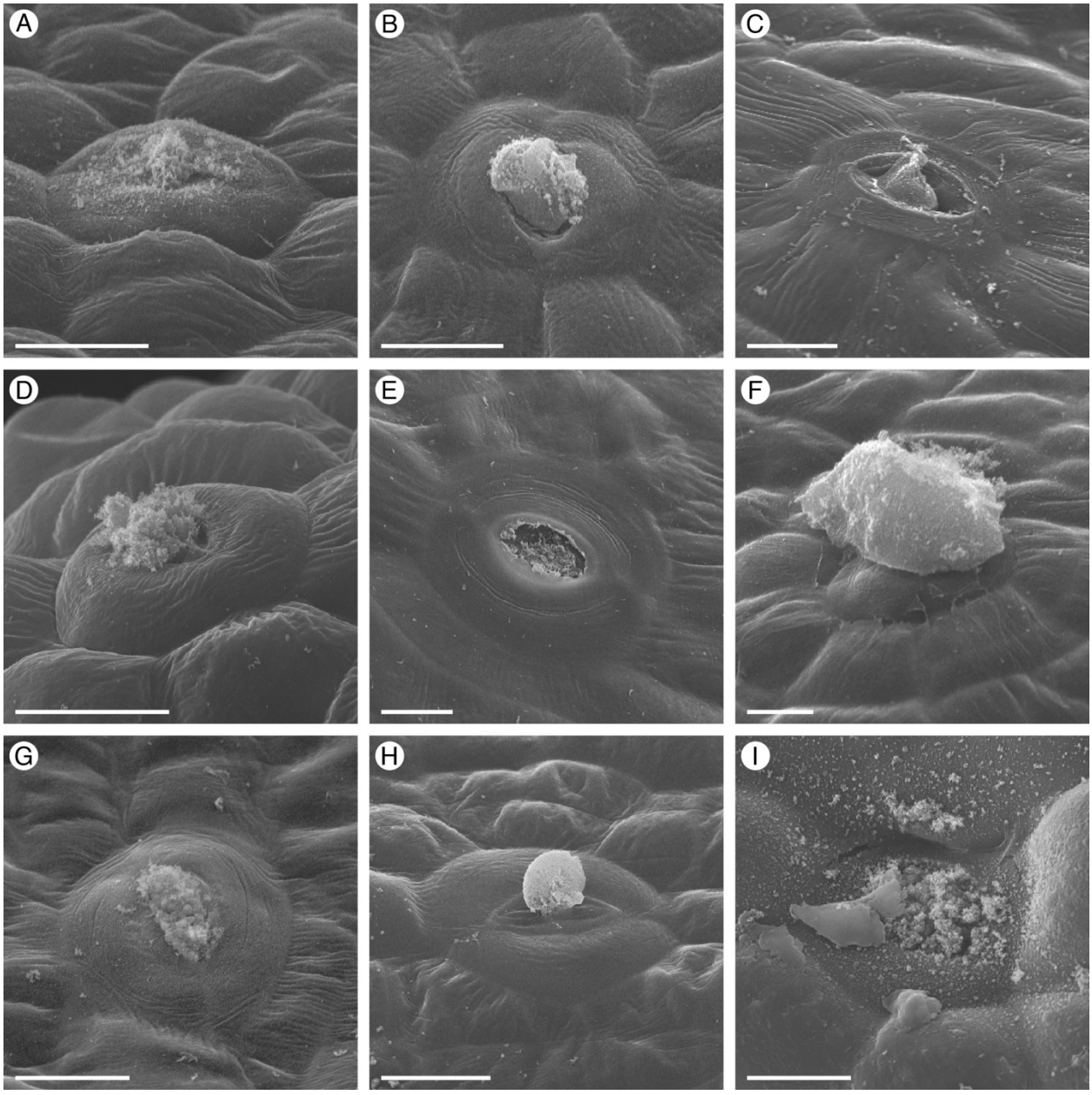

Figure 2.11. Nectarostomata of the nine Cleomaceae species. (A) *Arivela viscosa*. (B) *Cleome amblyocarpa*. (C) *Cleome violacea*. (D) *Gynandropsis gynandra*. (E) *Melidiscus giganteus*. (F) *Polanisia dodecandra*. (G) *Sieruela hirta*. (H) *Sieruela rutidosperma*. (I) *Tarenaya houtteana*. All images are of anthetic stage specimens, except *C. amblyocarpa* (intermediate stage) and *G. gynandra* (bud stage). Scale bar represents 10 μm.

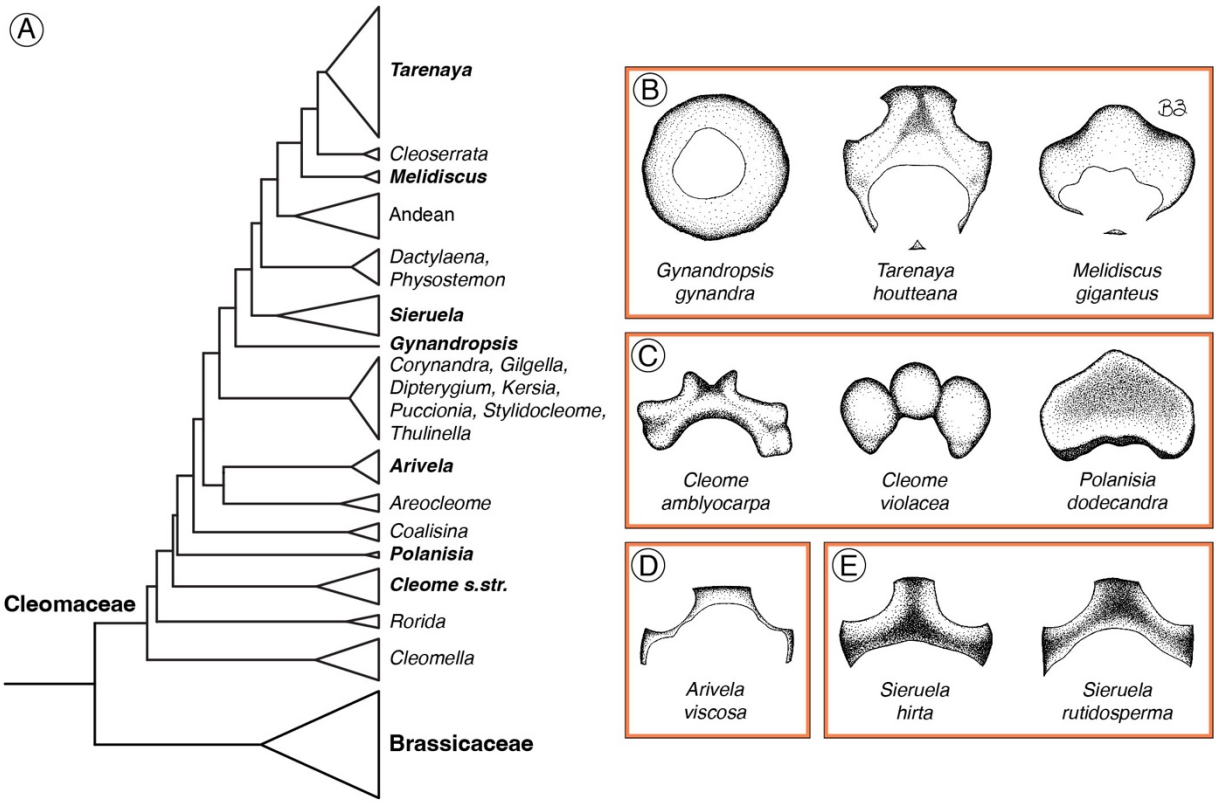

Figure 2.12. Cleomaceae phylogeny and floral nectaries of the nine species grouped by shape and position. (A) Cleomaceae phylogenetic tree derived from that of Patchell *et al*. (2014) and Bayat *et al*. (2018) with clades sampled here bolded. (B) Annular nectaries. (C) Protruding adaxial nectaries. (D) Slightly convex adaxial nectary. (E) Concave adaxial nectaries. Illustrations depict the apical view of the nectary with stippling to represent more basal or concave regions. Nectary size varies between species; illustrations are not to the same scale.

Chapter 3: Fleur-escence: the visual phenomenon of ultraviolet-fluorescent nectar[2]

3.1 Main

From colours and patterns to fragrances and novel structures, flowering plants have evolved an astonishing array of floral characteristics, which act as visual and olfactory signals for pollinator attraction (Willmer 2011). The innate and learned preferences of pollinators to these suites of floral cues encourage visitation (Giurfa *et al.* 1995; Riffell *et al.* 2013), with flowering plants often offering rewards such as nectar and pollen in exchange for pollen transfer. One such floral feature, which may play a role in pollinator interactions, is ultraviolet (UV)-fluorescence; a type of luminescence in which UV radiation is absorbed and longer wavelength light is emitted. Thorp *et al.* (1975) were among the first to report the brilliant UV-fluorescence of nectar in flowering plants. Out of the 102 species examined, 24 species had nectar that fluoresced yellow to blue with varying degrees of intensity and the majority pollinated by bees (Thorp *et al.* 1975). Since this intriguing discovery in 1975, UV-fluorescent nectar is only seldom addressed in the scientific literature and has not been scrutinized in an ecological or phylogenetic context.

Occurrences of UV biofluorescence have been discovered across animals and studies suggest this phenomenon can be more than a coincidental by-product of chemical structure. For instance, the UV-fluorescent plumage of budgerigar parrots (*Melopsittacus undulatus*) and palps of jumping spiders (*Cosmophasis umbritica*) function as sexual signals (Arnold *et al.* 2002; Lim *et al.* 2007) and the UV-fluorescent markings of mantis shrimp (*Lysisquillina glabriuscula*) contribute to their underwater visibility (Mazel *et al.* 2004). Despite captivating examples and behavioural assays in animals, the prevalence of UV-fluorescence in flowers and its relationship to pollinator attraction is not well understood.

Here, we present the first *in vivo* colour images of UV-fluorescent nectar in flowering plants. The nectar of several Cleomaceae species is colourless under visible light but exhibits vibrant, blue-coloured fluorescence when illuminated by UV-A radiation with peak intensity at 365 nm. Under visible light, the nectar of *Cleome violacea* is challenging to discern from the green three-lobed nectary (Fig. 3.1a). Yet, when excited with UV-A radiation, the vividly fluorescent nectar droplets are easily distinguished from the nectary and contrast the less intense

[2] A version of Chapter 3 is currently under review and is formatted according to journal specifications.

red fluorescence of chlorophyll (Marshall and Johnsen 2017) (Fig. 3.1b,c). Similarly, the nectar of *Polanisia dodecandra* and *Tarenaya hassleriana* intensely fluoresces under UV-A radiation (Fig. 3.1d, 3.2). In addition, the vasculature within the petals of *P. dodecandra* fluoresces blue and the petals of *T. hassleriana* fluoresce bright pink. *Sieruela hirta* and *Melidiscus giganteus* also secrete UV-fluorescent nectar, however the nectaries are partially obscured by the perianth and the nectar does not appear as vibrant against the strong fluorescence of other floral structures (Fig. 3.1d, 3.3). Of note, the pollen fluorescence can also be rather vivid though the nectar fluorescence often steals the show (i.e., *P. dodecandra*) (Fig. 3.2b). This seemingly prevalent phenomenon in Cleomaceae raises the question: does UV-fluorescent nectar act as a visual cue for the array of Cleomaceae pollinators?

The significance of UV-fluorescence for pollinator attraction has been debated. Thorp *et al.* (1975) posited that UV-fluorescent nectar functions as a visual signal for foraging bees. However, this hypothesis has been criticized because the emitted fluorescence may be imperceptible to insects amid the reflected light (Kevan 1976; Iriel and Lagorio 2010). Yet, behavioural assays have shown that honeybees make fine colour discriminations and are attracted to compounds that fluoresce blue under UV light (Dyer and Neumeyer 2005; Mori *et al.* 2018). Likewise, masking of the UV-fluorescent blue rim of the pitcher plant *Nepenthes khasiana* significantly reduced the capture of insect prey (Kurup *et al.* 2013). Also, prey capture of unmasked pitcher plants primarily occurred at night suggesting UV-fluorescence may play a role in insect attraction in low light settings (Kurup *et al.* 2013).

Cleomaceae consists of both generalist species pollinated by a variety of insects (e.g., *Arivela viscosa*, *Cleomella serrulata*, and *P. dodecandra*) (Higuera-Díaz *et al.* 2015; Saroop and Kaul 2019) and specialist species solely pollinated by bats (e.g., *M. giganteus* and *T. hassleriana*) (Machado *et al.* 2006; Fleming *et al.* 2009). Though orientation by bats is mainly achieved through echolocation, all bat species have functional eyes (Winter *et al.* 2003). For example, one of the bat pollinators (*Glossophaga soricina*) of *T. hassleriana* is colour-blind but able to perceive UV radiation as well as human-visible light (Winter *et al.* 2003). With evidence from the behavioral assays suggesting fluorescence aids in the attraction of diurnal and nocturnal pollinators, it is possible that fluorescent nectar in Cleomaceae not only acts as a visual signal for daytime pollinators but may also assist in the attraction of bats during twilight.

As with the relevance of UV-fluorescence for pollinator attraction, there is much to be learned about the components responsible for UV-fluorescence (i.e., fluorophores) in flowering plants. Though often perceived as a simple sugar solution, nectar consists of a complex array of biomolecules and microorganisms (Nicolson *et al.* 2007; Carey *et al.* 2023). Major constituents such as water, carbohydrates, amino acids, and ions reward pollinators; proteins can tailor nectar chemistry for pollinators and prevent microbial infections; and scented compounds such as terpenoids aid in pollinator attraction (Nicolson *et al.* 2007). Since biomolecules, including large macromolecules such as proteins, can act as fluorophores and microorganisms can contain fluorophores (Marshall and Johnsen 2017), the complexity of nectar represents a challenge for the identification of UV-fluorescent components. Yet, in response to the fascinating finding of Thorp *et al.* (1975), Scogin (1979a; b) identified an isoflavone and its glucoside as the UV-fluorescent compounds in the nectar of two Malvaceae species (*Fremontodendron californicum* and *F. mexicanum*). However, since this discovery no further progress has been made in identifying nectar fluorophores in other taxa.

Though there is limited evidence about its prevalence, the apparently scattered distribution of UV-fluorescent nectar suggests this phenomenon arose multiple times across flowering plants. Thus, bringing forth the question: are different fluorophores responsible for nectar fluorescence throughout the flowering plant phylogeny? Like nectar, species with anthers and pollen that emit blue fluorescence under UV radiation are dispersed across flowering plants. Mori *et al.* (2018) identified the anther and pollen fluorophores of five species in four different eudicot families as caffeoyl and feruloyl esters and suggested a widespread distribution of these compounds in fluorescent blue anthers and pollen. Alternatively, UV-fluorescent compounds can be unique to specific clades and thus act as taxonomically informative characters. For example, ester-linked ferulic acid occurs in the cell walls of the monophyletic clades, commelinid monocots and core Caryophyllales (Harris and Trethewey 2010). When observed with UV-fluorescence microscopy, cell walls with ester-linked ferulic acid fluoresce blue when in water and green when in acid (Harris and Trethewey 2010). Further analyses are required to determine whether unique or shared compounds act as nectar fluorophores in Cleomaceae and other taxa.

Studies on the visual cues of flowers have predominately focused on pigmentation that is reflective in the visible range, or UV absorptive or reflective, while neglecting UV-fluorescence as a potential signal for pollinators. Yet, with the recent wave of UV-fluorescence discoveries in

animals from the secretions of salamander skin and dermal tubercles of chameleons to the fur of flying squirrels (Prötzel *et al.* 2018; Kohler *et al.* 2019; Lamb and Davis 2020), UV-fluorescence is a budding area of research with many outstanding questions. Whether tied to pollinator interactions or merely a chemical by-product, we hope the visually striking UV-fluorescence of Cleomaceae nectar raises interest in the UV-fluorescence of flowering plants as an area that warrants further ecological and systematic investigations.

3.2 Materials and Methods

The following five Cleomaceae species were grown from seed in professional growing mix (Sun Gro Horticulture): *Cleome violacea* L. accession 813 from Hortus Botanicus, *Polanisia dodecandra* (L.) DC. accession 68456 from B & T World Seeds, *Tarenaya hassleriana* (Chodat) Iltis accession FL2400 from West Coast Seeds, *Sieruela hirta* (Klotzsch) Roalson & J. C. Hall accession 74520 from B & T World Seeds, and *Melidiscus giganteus* (L.) Raf. accession 814 from Hortus Botanicus. CMP3244 growth chambers (Environmental Growth Chambers) were set to a 28°C 12 h light and 22°C 12 h dark regime. Voucher specimens were deposited in the University of Alberta Vascular Plant Herbarium (ALTA) (Appendix 2.1). Flowering plants and nectar in capillary tubes were photographed while illuminated with an iLED gooseneck illuminator (Laxco) or C8 Convoy 365 nm UV flashlights (Yooperlites) using a D80 DLSR camera (Nikon) with an AF Micro-NIKKOR 60 mm f/2.8 D or AF Micro-NIKKOR 105 mm f/2.8 AI-S lens (Nikon) or a D500 DLSR camera (Nikon) with AF-S Teleconverter TC-14 III and AF-S Micro-NIKKOR 105 mm f/2.8 IF-ED lenses (Nikon). All methods were performed in accordance with the relevant guidelines and regulations.

3.3 Figures

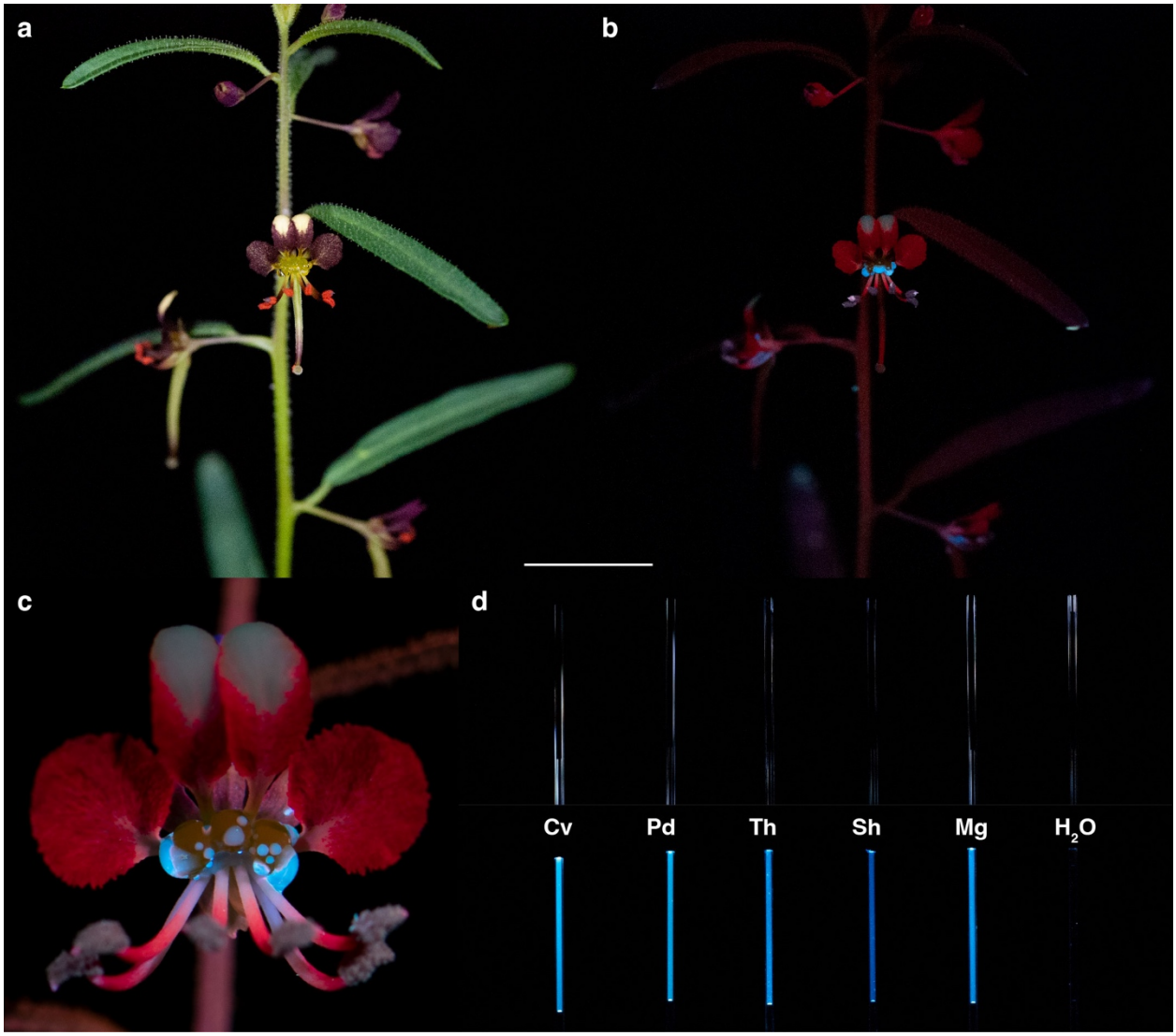

Figure 3.1. UV-fluorescent nectar of *Cleome violacea* and other Cleomaceae species. **a**, **b**, *Cleome violacea* under visible light (**a**) and UV-A radiation (**b**) (scale bar, 1 cm). **c**, Close up of *C. violacea* flower under UV-A radiation. **d**, Nectar of five Cleomaceae species and water in microcapillary tubes under visible light (top) and UV-A radiation (bottom). Cv, *Cleome violacea*; Pd, *Polanisia dodecandra*; Th, *Tarenaya houtteana*; Sh, *Sieruela hirta*; Mg, *Melidiscus giganteus*.

Figure 3.2. UV-fluorescent nectar of *Polanisia dodecandra* and *Tarenaya houtteana*. **a**, **b**, *Polanisia dodecandra* under visible light (**a**) and UV-A radiation (**b**) (scale bar, 1 cm). **c**, **d**, *Tarenaya houtteana* under visible light (**c**) and UV-A radiation (**d**) (scale bar, 1 cm).

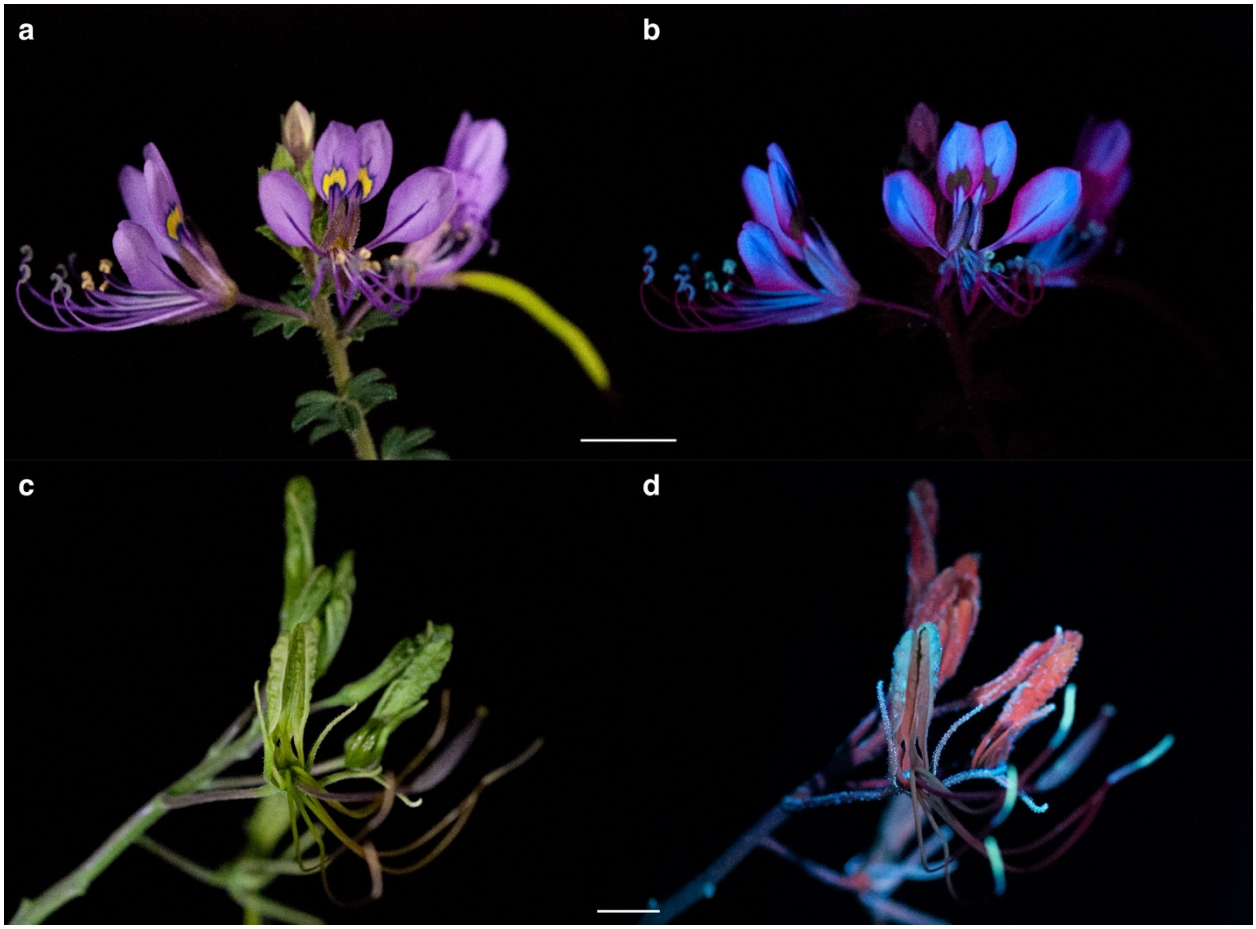

Figure 3.3. UV-fluorescent nectar of *Sieruela hirta* and *Melidiscus giganteus*. **a**, **b**, *Sieruela hirta* under visible light (**a**) and UV-A radiation (**b**) (scale bar, 1 cm). **c**, **d**, *Melidiscus giganteus* under visible light (**c**) and UV-A radiation (**d**) (scale bar, 1 cm).

Chapter 4: Chemical, genetic, and morphological characterization of the floral scent and scent releasing structures of *Gynandropsis gynandra* (Cleomaceae, Brassicales)[3]

4.1. Introduction

Approximately 85% of flowering plants are pollinated by animals (Ollerton *et al.* 2011). In turn, most flowering plants exhibit an array of features that act synergistically as signals for pollinator attraction (Dudareva and Pichersky 2006; Willmer 2011; Junker and Parachnowitsch 2015). In conjunction with visual displays, flowers present limitless possibilities of fragrance blends consisting of different volatile compounds and ratios, which can be learned and recognized by pollinators (Dudareva and Pichersky 2006; Willmer 2011). The diversity of floral scent is shaped by biotic and abiotic factors such as pollinator interactions and environmental conditions (Raguso 2008; Keefover-Ring 2022). As a result, floral volatile profiles tend to vary widely within genera and may differ between populations or individuals of a single species (Willmer 2011; Pichersky and Dudareva 2020). For example, Chess *et al.* (2008) reported differences in the floral volatile ratios of *Linanthus dichotomus* (Polemoniaceae) subspecies. The two subspecies are morphologically similar but can be distinguished by geography, flowering time, and pollinators (Chess *et al.* 2008). Similarly, populations of *Chiloglottis valida* s.l. (Orchidaceae) had two differing floral scent morphs that were later described as two morphologically similar species with fragrances attracting different wasp pollinators (Bower 2006). As such, divergence of floral scent profiles can be a key isolating mechanism for speciation, with each fragrance blend attracting different pollinators (Willmer 2011).

Though floral fragrance is often released from the entire flower, variation in the composition and emission of volatile compounds may occur across floral structures (Willmer 2011; Pichersky and Dudareva 2020; García *et al.* 2021). For instance, García *et al.* (2021) reported that tissue involved in visual signaling (e.g., petals) tends to emit greater proportions of volatile compounds associated with pollinator attraction and can emit unique attractive compounds compared to non-visual signaling tissue. Alternatively, floral scent can be exclusively emitted from a particular structure or localized to specific regions of tissue (Willmer 2011; Pichersky and Dudareva 2020). Regions of specialized scent-emitting tissue are often referred to as osmophores and commonly display unique cell types compared to neighboring

[3] Chapter 4 is in preparation for submission and is formatted according to journal specifications.

areas (Vogel and Renner 1990; Dudareva and Pichersky 2006; Willmer 2011). Regardless of the secretion location, floral volatiles are predominantly produced in epidermal cells and released into the atmosphere immediately after synthesis (Dudareva and Pichersky, 2006; Pichersky and Dudareva, 2020). Therefore, the highest expression of genes involved in floral volatile biosynthesis occurs in the scent-emitting tissue of the flower (Pichersky and Dudareva 2020).

Floral scent compounds are united by their low molecular weight (< 300 g/mol) and sufficient vapour pressure for release into the atmosphere from epidermal cells (Willmer 2011; Pichersky and Dudareva 2020). There are several chemical classes of floral volatiles that are widely distributed across flowering plants, likely due to conserved biosynthetic pathways (Pichersky and Dudareva 2020). Terpenoids, the most common class, are derived from the five-carbon building blocks, isopentyl diphosphate (IPP) and dimethylallyl diphosphate (DMAPP) (Farré-Armengol *et al.* 2020; Pichersky and Dudareva 2020). These chemicals are products of the mevalonate (MVA) pathway that produces IPP, and the methylerythritol phosphate (MEP) pathway that produces IPP and DMAPP (Dudareva *et al.* 2013; Pichersky and Dudareva 2020). Terpene synthases are the enzymes that catalyze the formation of terpenoids from IPP and DMAPP derivatives, with many capable of forming multiple terpenoids from a single precursor (Tholl 2006; Degenhardt *et al.* 2009; Pichersky and Dudareva 2020). The second and third most common classes are: benzenoids, derived from phenylalanine through complex branched biosynthetic pathways; and aliphatics (also referred to as fatty acid derivatives), synthesized from the fatty acids, linolenic acid and linoleic acid (Dudareva and Pichersky 2006; Dudareva *et al.* 2013; Farré-Armengol *et al.* 2020; Pichersky and Dudareva 2020). A less abundant class is amino acid derivatives, which includes nitrogen- and sulfur-containing compounds (Dudareva *et al.* 2013; Farré-Armengol *et al.* 2020; Pichersky and Dudareva 2020).

Gynandropsis gynandra (L.) Briq. (Cleomaceae) is a minor crop plant native to Africa and Asia (Sogbohossou *et al.* 2018; Achigan-Dako *et al.* 2021). With its extensive geographical distribution, *G. gynandra* exhibits intra- and inter-continental variation in morphology, phenology, and foliar phytochemistry (Wu *et al.* 2018; Sogbohossou *et al.* 2019, 2020; Blalogoe *et al.* 2020; Houdegbe *et al.* 2022). African accessions are taller with greater biomass and larger seeds, have a lower germination rate, and take longer to reach seed maturation than Asian accessions (Wu *et al.* 2018; Sogbohossou *et al.* 2019; Blalogoe *et al.* 2020; Houdegbe *et al.* 2022). For some traits there are distinctions between Western African and Southeastern African

accessions, with Western African accessions more similar to Asian accessions than Southeastern African accessions (Sogbohossou *et al.* 2019, 2020). For instance, the leaves of Western African and Asian accessions are lower in carotenoids and chlorophylls, higher in tocopherols, and overall have greater similarity in semi-polar metabolite profiles than Southeastern African accessions (Sogbohossou *et al.* 2019, 2020). Despite the differences in non-volatile metabolites, variation in leaf volatile profiles does not correlate with geographic regions (Sogbohossou *et al.* 2020).

The flowers of *G. gynandra* are arranged in bracteate racemes (Raju and Rani 2016; Zohoungbogbo *et al.* 2018; Das *et al.* 2022). Though differing floral morphs (i.e., staminate and hermaphroditic) and abnormal flowers (e.g., atypical fusion or number of floral parts) are not uncommon (Raghavan 1939; Murty 1953; Zohoungbogbo *et al.* 2018), *G. gynandra* flowers tend to have four sepals, four white or lightly coloured petals (pale pink, purple, or yellow), an annular nectary, an elongated androgynophore and gynophore (i.e., stalk-like structures subtending the reproductive organs and pistil, respectively), six stamens, and a bicarpellate pistil (Raju and Rani 2016; Das *et al.* 2022; Zenchyzen *et al.* 2023) (Fig. 4.1). Like most Cleomaceae taxa, *G. gynandra* flowers are monosymmetric due to an upward curvature of the floral structures (Patchell *et al.* 2011; Bayat *et al.* 2018). Monosymmetry is often considered an adaptive innovation connected to specialized pollination syndromes (Armbruster 2017; Bayat *et al.* 2018). Further, the androgynophore and gynophore may play a role in pollination by providing optimal reproductive organ positioning for pollinator contact (Rocha *et al.* 2015). Geographic differences in the flowers include floral structure length, with Western African and Asian accessions having shorter stamen filaments and gynophore than Southeastern African accessions (Sogbohossou *et al.* 2019).

In addition to the variation in vegetative and floral traits, the reported insect visitors of *G. gynandra* differ between continents. In Asia (India), floral visitors include bees (*Amegilla cingulata*, *Apis cerana*, *Apis florea*, *Tetragonula iridipennis*, and *Xylocopa latipes*), butterflies (*Catopsilia pomona*, *Danaus chrysippus*, *Pachliopta aristolochiae*, and *Papilio polytes*), an ant (*Crematogaster* sp.; Formicidae), and a fly (unknown sp.) (Burkill 1916; Chandra *et al.* 2013; Raju and Rani 2016). Raju and Rani (2016) noted only bees and butterflies are effective pollinators, while the ant and fly species act as nectar robbers. The bees forage for *G. gynandra* pollen and nectar but only contribute to pollination while collecting pollen as they do not

distinguish between the anthers and stigma, whereas the butterflies contact the reproductive organs while feeding on nectar (Raju and Rani 2016). Like in Asia, *G. gynandra* floral visitors in Southeast Africa (Kenya and Tanzania) include bees (*Amegilla* spp. and *Lasioglossum* sp.), an ant (unknown sp.), and a fly (Syrphidae sp.) (Werth 1942; Oronje *et al.* 2012). However, Oronje *et al.* (2012) and Werth (1942) stated that these species are nectar and pollen thieves and do not contribute to pollination. Rather, hawkmoths (Sphingidae) are responsible for *G. gynandra* pollination in Southeast Africa with short-tongued hawkmoth visitors (*Basiothia medea*, *Daphnis nerii*, *Hippotion celerio*, *H. eson*, *H. osiris*, *Hyles* sp., *Nephele aequivalens*, *N. comma*, and *Temnora* sp.) more effective in pollination than long-tongued hawkmoth visitors (*Agrius convolvuli*, *Coelonia* sp., and *Xanthopan morganii*) as they are more likely to contact the reproductive organs while consuming nectar (Monteiro 1875; Werth 1942; Oronje *et al.* 2012; Martins and Johnson 2013).

Like the trends of visual cues, there are seemingly convergent floral scents associated with the attraction of specific pollinator groups (Dudareva and Pichersky 2006; Willmer 2011). For instance, generalist plant taxa that are pollinated by a diversity of animals emit a blend of floral volatiles from the three major groups: aliphatics, terpenoids, and benzenoids (Dudareva and Pichersky 2006; Willmer 2011). Whereas, hawkmoth pollinated taxa have floral scents dominated by oxygenated terpenoids, benzenoid esters, and nitrogen-containing compounds (Willmer 2011; Pichersky and Dudareva 2020). Despite the continental distinctions in vegetative and floral traits and observed pollinators, the floral scent of *G. gynandra* populations has yet to be characterized.

As *G. gynandra* is an important vegetable in some African countries and food security is a global concern (Onyango *et al.* 2013; Sogbohossou *et al.* 2018; Achigan-Dako *et al.* 2021), understanding the floral morphology and genetics associated with pollinator interactions is an important component for ensuring its reproductive success. The abovementioned differences suggest the possibility of distinct, geographically separated *G. gynandra* morphs, which could be further supported with floral fragrance profiles. Therefore, our overarching goal was to characterize the floral scent blends of African (Malawi, Southeastern Africa) and Asian (Malaysia, Asia) *G. gynandra* accessions to compare volatile compound composition between geographical regions and to pollination syndromes (Fig. 4.2). To identify possible scent releasing structures and integrate emitted floral scent compounds with volatile biosynthetic pathway

expression profiles, we also described the floral cell morphology and explored gene expression patterns across floral organs for the African accession.

4.2. Results and Discussion

4.2.1 Floral scent profiles differ between African and Asian accessions

The dynamic headspace technique and gas chromatography/mass spectrometry (GC/MS) were used to collect and characterize the floral scent profiles of *G. gynandra* African (TOT8917 from Malawi) and Asian (TOT7200 from Malaysia) accessions. In addition to the geographic variation in morphology, phenology, and foliar phytochemistry (Wu *et al.* 2018; Sogbohossou *et al.* 2019, 2020; Blalogoe *et al.* 2020), the African and Asian accessions have distinct floral scent profiles. Nineteen and 11 floral volatiles were captured from the headspace of the African and Asian accessions, respectively (Table 4.1). The floral fragrance of both accessions consists of aliphatics, benzenoids, terpenoids, and nitrogen-containing compounds. However, the proportions of these chemical classes vary drastically between accessions, with the majority of the floral scent profile comprised of nitrogen-containing compounds for the African accession (50.4%; Fig. 4.3A) and benzenoids for the Asian accession (88.8%; Fig. 4.3B). Further, the floral scent of each accession is dominated by two compounds, the nitrogen-containing compound (*Z*)-methyl-2-butanal oxime (38.3%) and terpenoid (*Z*)-β-ocimene (30.7%) for the African accession, and the benzenoids benzyl alcohol (66.1%) and benzaldehyde (22.3%) for the Asian accession (Table 4.1). Three of these dominant compounds (i.e., (*Z*)-β-ocimene, benzyl alcohol, and benzaldehyde) are unique to the floral fragrance of their respective accession.

In Asia, generalist pollination of *G. gynandra* was reported, with bees and butterflies as the effective pollinators (Burkill 1916; Chandra *et al.* 2013; Raju and Rani 2016) (Table 4.2). Generalist flowering plants do not have unifying patterns of floral fragrance, except that they typically consist of the three major floral scent chemical classes (i.e., aliphatics, terpenoids, and benzenoids) and usually have one chemical class dominating the others (Dudareva and Pichersky 2006; Willmer 2011). Further, floral scent profiles of bee pollinated species are frequently dominated by terpenoids but may also be dominated by benzenoids (Dudareva and Pichersky 2006). Benzenoids, including benzyl alcohol and benzaldehyde, are common and abundant in the floral fragrance of butterfly pollinated taxa (Andersson *et al.* 2002; Dudareva and Pichersky 2006). With the three major chemical classes present and benzenoids dominating, the floral scent

profile of the *G. gynandra* Asian accession is comparable to other generalist, bee, and butterfly pollinated flowering plants. The floral scent of the Asian accession also includes a small proportion of one nitrogen-containing compound (*Z*)-2-methylbutanal oxime (2.3%); nitrogen-containing compounds may be secreted in low quantities by butterfly pollinated flowers (Andersson *et al.* 2002; Dudareva and Pichersky 2006).

In contrast, hawkmoths were described as the effective pollinators of *G. gynandra* in Africa (Monteiro 1875; Werth 1942; Oronje *et al.* 2012; Martins and Johnson 2013) (Table 4.2). Hawkmoth pollinated flowers typically emit a strong sweet odor consisting of oxygenated terpenoids, benzenoid esters, and nitrogen-containing compounds (Dudareva and Pichersky 2006; Willmer 2011; Stöckl and Kelber 2019). However, non-oxygenated terpenoids such as (*E*)-β-ocimene, myrcene, and limonene are also common (Knudsen and Tollsten 1993). Though the floral scent profile of the *G. gynandra* African accession does not contain oxygenated terpenoids or benzenoid esters, it includes an abundance of (*Z*)-β-ocimene, the less common stereoisomer (i.e., mirror image) of (*E*)-β-ocimene (Farré-Armengol *et al.* 2017), and nitrogen-containing compounds. Of the nitrogen-containing compounds, the stereoisomers (*Z*)- and (E)-2-methylbutanal oxime are most abundant. Similarly, the floral fragrance of noctuid moth (Noctuidae) pollinated *Oenothera xenogaura* (Onagraceae) and a hawkmoth pollinated *Datura* sp. (Solanaceae) are dominated by methylbutanal oximes (Teranishi *et al.* 1991; Knudsen and Tollsten 1993; Shaver *et al.* 1997; Krakos and Fabricant 2014). Methylbutanal oximes are also prevalent in hawkmoth pollinated *Nicotiana* spp. (Solanaceae) (Raguso *et al.* 2003). In summary, the floral scent profiles of the African and Asian accessions of *G. gynandra* are distinct and comparable to that of other hawkmoth and generalist pollinated taxa, respectively.

Although the mass spectra for many of the detected floral volatiles had a high similarity match to a compound in the NIST Mass Spectral Library, further verification of the chemical identities is required (Dudareva and Pichersky 2006). Conclusive identification can be achieved by comparing the retention indices and mass spectra of the floral volatiles to an authentic standard or using other instrumentation (Dudareva and Pichersky 2006; Pichersky and Dudareva 2020). For example, two-dimensional gas chromatography (GC x GC) coupled with time-of-flight mass spectrometry (TOF-MS) provides higher resolution and accuracy for enhanced chemical identification (Dimandja 2020; Pichersky and Dudareva 2020). Further, additional replicates with consistent conditions (i.e., sampling time and GC/MS settings) are required for

thorough chemical characterization of within accession variation and to verify the differences between accessions. Of note, some of the volatile compounds from the inflorescence headspace may have been emitted by the small leaf-like bracts along the axis of the inflorescence. However, even if scent-releasing, these bracts would likely contribute to the overall aroma detected by pollinators.

4.2.2 Epidermal cell morphology is diverse across floral structures

As volatile biosynthesis and emission can spatially vary within a flower and scent emitting regions tend to display distinct cell types, we used scanning electron microscopy to characterize the epidermal cell morphology across the flower of *G. gynandra* (accession TOT8917). Epidermal cell morphology varies drastically between floral structures and within the sepals, petals, and pistil. The sepal epidermis primarily consists of elongate jigsaw-shaped cells (Fig. 4.4A,B); however, near the base of the sepal, cells are circular to rectangular without complex jigsaw-shapes. Scattered among these cells on the abaxial surface and near the margin of the sepal are stomata and multicellular capitate-stalked glandular trichomes (Fig. 4.4A). There are no differences in epidermal cell morphology between the four sepals. The epidermal cells of the petal blades are jigsaw-shaped with random spaghetti-like surface striations (Fig. 4.4C). On the adaxial surface near the middle of the petal blade, there are gaps between the jigsaw-shaped cells forming circular cavities (Fig. 4.4D). The gaps are less prominent on the abaxial surface of the petals blades. Near the apex of the petal claw, the epidermal cells are elongate with linear surface striations (Fig. 4.4E). At the midsection of the petal claw, the elongate epidermal cells have smooth surfaces and some have spherical papillae at their centers (Fig. 4.4F). Near the base of the claw, all elongate epidermal cells have extended papillae at their centers; although the papillae are unicellular, they often have a distinct head (Fig. 4.4G). There are no distinctions in epidermal cell morphology between the four petals (i.e., no adaxial/abaxial petal differences). The epidermal cells of the receptacular nectary have finger-like papillae (Zenchyzen *et al.* 2023); unlike the papillae at the base of the petal claw, these do not have distinct heads (Fig. 4.4H). Mainly scattered throughout the apical half of the receptacular nectary are stomata modified for nectar secretion (i.e., nectarostomata) (Zenchyzen *et al.* 2023).

Gynandropsis gynandra flowers have three stalk-like structures: an androgynophore (Fig. 5A,B), stamen filaments (Fig. 4.5D,E), and a gynophore (Fig. 4.5G,H; Fig. 4.1). All three

structures have elongated epidermal cells. The elongated cells are woven near the base of the androgynophore and filaments (i.e., cells weave below adjacent cells; Fig. 4.5A,D). Stomata are scattered throughout the elongated cells of the gynophore but are rarely found on the androgynophore and filaments. The filaments are unique in that they are the only stalk-like structure with linear surface striations; these striations are absent from the proximal section of the filaments (Fig. 4.5D,E). At the junction of the stalk-like structures (i.e., the point at which the androgynophore, filaments, and gynophore diverge), cells are circular to oblong with some having finger-like papillae similar to the receptacular nectary (Fig. 4.5C). Stomata are located throughout the junction. The filaments and gynophore subtend the anthers and pistil, respectively. The epidermal cells of the anthers and pistil differ from those of the stalk-like structures. The anthers have an assortment of cell shapes, all having spaghetti-like surface striations (Fig. 4.5F). Stomata are located between the two thecae. The pistil has square to rectangular epidermal cells with stomata scattered throughout (Fig. 4.5I). Multicellular capitate-stalked glandular trichomes are located on the valves of the pistil but not the replum. Altogether, cell morphology varies from circular to rectangular shaped to more complex jig-saw shapes (sepals and petals), unicellular papillae (petals and nectary), multicellular trichomes (sepals and pistil), and stomata (nectary, sepals, gynophore, and pistil). Additionally, cell surfaces range from smooth to adorned with intricate striations (petals, filaments, and anthers).

Multicellular capitate-stalked glandular trichomes, like those on the abaxial surface of the sepals and valves of the pistil of *G. gynandra* flowers, contain cells that synthesize and store specialized metabolites (Pichersky and Dudareva 2020; Schuurink and Tissier 2020). These specialized metabolites, which can include volatile compounds, presumably act as chemical weapons against herbivory or pathogens rather than pollinator attractants (Muhlemann *et al.* 2014; Pichersky and Dudareva 2020; Schuurink and Tissier 2020). With the sepals and valves of the pistil safeguarding the developing flower and seeds, respectively (Willmer 2011), the presence of glandular trichomes on these structures provides an extra layer of protection. Unlike pollinator-attracting floral volatiles that are primarily emitted into the atmosphere immediately after synthesis, glandular trichomes often hold and only release the specialized metabolites upon damage (e.g., consumption by a herbivore) (Dudareva and Pichersky 2006; Pichersky and Dudareva 2020; Schuurink and Tissier 2020).

Alternatively, epidermal tissue involved in pollinator-attracting floral volatile production and emission typically possess unique cell shapes (e.g., conical, papillate) (Dudareva and Pichersky 2006). Papillae are commonly abundant on the surface of osmophoric regions (Endress 1984; Vogel and Hadacek 2004; Gonçalves-Souza *et al.* 2017; Kettler *et al.* 2019; Gotelli *et al.* 2020); Gonçalves-Souza *et al.* (2017) suggest that papillae serve as an indicator of osmophores. In *G. gynandra* flowers, papillae are located on the surface of the petal claws, nectary, and occasionally the junction of the androgynophore, filaments, and gynophore.

Floral volatiles are likely released directly from the osmophore cells via a combination of passive diffusion and active transport through the cell membrane, cell wall, and cuticle (Dudareva and Pichersky 2006; Widhalm *et al.* 2015). However, modified stomata may also be involved in floral scent emission (Maiti and Mitra 2017). For example, in *Agave amica* (Asparagaceae), the petaloid tepals serve as the primary source of floral fragrance; stomata are predominately present on the adaxial surface of the petaloid tepals and respond positively to histological tests associated with scent emission (Maiti and Mitra 2017). In *G. gynandra*, stomata are located on the abaxial surface of the sepals, apical half of the nectary, gynophore, and pistil. Further, there is no evidence that epidermal surface striations, such as those located on the epidermal cells of the petals, filaments, and anthers of *G. gynandra* flowers, are involved in scent emission (Dudareva and Pichersky 2006). Rather, these nanostructures seemingly contribute to the suite of visual cues for pollinators via structural colouration, i.e., cells with disordered ridges scatter blue light and ultraviolet radiation, producing a blue halo visible to insects (Moyroud *et al.* 2017).

4.2.3 Terpenoid biosynthetic pathway gene expression is highest in the stalk-like floral structures

Unlike the long-distance transport of many plant hormones, floral volatiles are primarily synthesized in epidermal cells and immediately emitted into the atmosphere (Dudareva and Pichersky 2006; Pichersky and Dudareva 2020). Therefore, to explore the spatial variation in floral volatile biosynthesis and emission, we performed RNA-sequencing across the following *G. gynandra* (accession TOT8917) floral structures: adaxial and abaxial petals, androgynophore, filaments, and gynophore. The read depth, averaged across replicates, ranges from 18.6 million (filaments) to 35.4 million (abaxial petals). A minimum of 10 million reads is sufficient for

differential expression analyses (Liu *et al.* 2014). Across all structures, median Phred quality scores are no lower than 32 for each base position; a Phred quality score of 30 represents a base call accuracy of 99.9% (Shi *et al.* 2016). The assembled transcriptome has 221985 transcripts and a completeness of 93.6%, indicating the percentage of highly conserved single-copy Brassicales genes present in our assembly (Appendix 4.1, 4.2). In the principal component analysis (PCA) of transcript reads, replicates cluster by floral structure with little variance between the adaxial and abaxial petals (Fig. 4.6); though the petals differ in position, they are morphologically identical (i.e., colour, size, shape). PC1 and PC2 explain 46.28% and 12.69% of the variance, respectively.

As terpenoid biosynthesis is the most thoroughly studied of the floral volatile biosynthetic pathways (Dudareva and Pichersky 2006; Vranová *et al.* 2013; Muhlemann *et al.* 2014; Pichersky and Dudareva 2020), and the floral scent profile of the *G. gynandra* African accession contains several terpenoids, including (*Z*)-β-ocimene as a dominant component, the expression of genes involved in terpenoid biosynthesis were examined in detail (Fig. 4.7; Table 4.3). The MVA and MEP pathways, which are conserved across flowering plants, produce the essential building blocks for terpenoids (Tholl and Lee 2011; Vranová *et al.* 2013; Pichersky and Dudareva 2020). The MVA pathway results in IPP alone, whereas the MEP pathway yields a 6:1 ratio of IPP and DMAPP; both IPP and DMAPP are required for terpenoid synthesis (Tholl and Lee 2011; Pichersky and Dudareva 2020). In the petals and stalk-like floral structures of *G. gynandra*, most genes involved in the MVA and MEP pathways are expressed, apart from *GgAACT2* and *GgPMK* in the petals (MVA pathway) and *GgMCT* and *GgCMK* in the petals and filaments (MEP pathway), which have < 5 TPM (transcripts per million; averaged between replicates). Of note, *Arabidopsis thaliana* has two functionally redundant *MDD* and *DXS* genes (Vranová *et al.* 2013; de Luna-Valdez *et al.* 2021), while only one copy of each is expressed in *G. gynandra* petals and stalk-like structures.

IPP isomerases balance the equilibrium of IPP and DMAPP by converting IPP to DMAPP (Tholl and Lee 2011; Vranová *et al.* 2013). In *A. thaliana*, there are two IPP isomerases, IPPI1 and IPPI2; however, they are only partially redundant as IPPI2 is also involved in perianth development (Phillips *et al.* 2008; Tholl and Lee 2011). In the petals and stalk-like structures of *G. gynandra*, only *GgIPPI2* is expressed. Geranyl diphosphate (GPP), farnesyl diphosphate (FPP), and geranylgeranyl diphosphate (GGPP) synthases catalyse the

formation of GPP, FPP, and GGPP using DMAPP and IPP (Tholl and Lee 2011; Vranová *et al.* 2013). GPP is a precursor for monoterpenes, while FPP and GGPP are used for the synthesis of larger molecules including terpenoids (diterpenes, triterpenes, and sesquiterpenes), plant hormones (abscisic acid, brassinosteroids, and gibberellins), and pigments (carotenoids and chlorophyll) (Tholl and Lee 2011; Vranová *et al.* 2013). Only monoterpenes were detected in the floral headspace of *G. gynandra*, although pigments and hormones are likely present in these structures. In *A. thaliana*, a heterodimer of GGPP11 and GGPP12 is the only enzyme presumed to synthesize GPP (Wang and Dixon 2009; Vranová *et al.* 2013). Three out of the 12 *A. thaliana* GGPP synthase genes, including *GgGGPP11 and GgGGPP12*, and both *A. thaliana* FPP synthase genes are expressed in *G. gynandra*, however *GgFPPS2* expression is just below 5 TPM in the petals.

Functional investigations have been conducted on approximately 12 out of the 30 terpene synthase genes (*TPS1-30*) in *A. thaliana* (Aubourg *et al.* 2002; Tholl and Lee 2011). However, none of these studies have demonstrated that any of the investigated genes primarily produce (*Z*)-β-ocimene (Tholl and Lee 2011; Farré-Armengol *et al.* 2017). In *G. gynandra*, only one of the *A. thaliana* terpene synthase genes (*GgTPS27*) is expressed in the stalk-like structures and none are expressed in the petals. The protein encoded by *AtTPS27* converts GPP into ten monoterpenes with 1,8-cineole as the major product (52%) (Chen *et al.* 2004). 1,8-cineole was not identified in the floral headspace of *G. gynandra*, implying *GgTPS27* is involved in the synthesis of other monoterpenes, though functional studies are required for confirmation.

Although the petal claws of *G. gynandra* contain papillae which are commonly associated with osmophores (Gonçalves-Souza *et al.* 2017), the < 5 TPM expression of *GgPMK* in the MVA pathway and *GgMCT* and *GgCMK* in the MEP pathway, and absence of terpene synthase gene expression suggest that the petals are not predominately involved in terpenoid production and emission. However, floral structures can emit different volatile compounds and compositions (Dudareva and Pichersky 2006; Willmer 2011), i.e., floral structures that are not involved in terpenoid emission may release other volatiles (e.g., nitrogen-containing compounds). The filaments of *G. gynandra* have < 5 TPM expression of *GgCMK* in the MEP pathway, yet with the expression of genes throughout the MVA pathway and *IPPI2*, some of the IPP produced could be converted to DMAPP resulting in the required precursors for terpenoid synthesis. The expression of genes throughout the MVA and MEP pathways for the

androgynophore and gynophore of *G. gynandra*, indicate these structures may be involved in terpenoid synthesis and secretion. As the stalk-like floral structures are united by elongated cells, this cell morphology could be important for olfactory signalling. Further, the stalk-like structures may not act alone in terpenoid synthesis and emission as floral rewards (i.e., nectar and pollen) can also emit odors (Dobson and Bergström 2000; Raguso 2004).

4.3. Conclusions

Flowering plants present suites of floral signals to appeal to the visual and olfactory capabilities of pollinators (Willmer 2011). For instance, generalist flowering plants exhibit an enormous diversity in floral form; however, the flowers tend to be open and have floral rewards that are easily accessible to a range of pollinators (Willmer 2011). Whereas hawkmoth pollinated flowers typically have white or pale tubular or spurred petals with abundant nectar at their base, and a strong fragrance (Willmer 2011; Stöckl and Kelber 2019). Martins and Johnson (2013) noted that *G. gynandra* differs from other hawkmoth pollinated flowers in Africa in that it has an open flower (i.e., the petals are not tubular or spurred) and a weak fragrance. Though these observations alone are atypical for hawkmoth pollinated flowers, our study highlights the importance of examining the array of floral features in detail. We revealed drastically different floral scent profiles between geographically distinct *G. gynandra* accessions, with the floral fragrance of the Asian and African accessions comparable to that of other generalist and hawkmoth pollinated flowers, respectively. Though faint to the human nose, these data suggest floral aroma plays an important role in pollinator attraction for *G. gynandra*. Further, the differing floral scent profiles combined with the variation in morphology, phenology, foliar phytochemistry, and pollinators (Wu *et al.* 2018; Sogbohossou *et al.* 2019, 2020; Blalogoe *et al.* 2020; Houdegbe *et al.* 2022), suggest there may be geographically separated subspecies of *G. gynandra*.

4.4. Experimental

4.4.1. Plant material

Gynandropsis gynandra accessions TOT8917 from Malawi and TOT7200 from Malaysia (Sogbohossou *et al.* 2020) were grown from seed in professional growing mix (Sun Gro Horticulture, Agawam, Massachusetts, USA). Plants of each accession was grown in separate

CMP3244 growth chambers (Environmental Growth Chambers, Chagrin Falls, Ohio, USA) set to identical regimes of 28°C 12 h light and 22°C 12 h dark. Voucher specimens were deposited at the University of Alberta Vascular Plant Herbarium (ALTA) with the following accession numbers: 143368 and 143369 (TOT8917), 144831 (TOT7200). Plants were photographed using an EOS Rebel T7i DSLR camera with an EF-S 18-55 mm STM lens (Canon, Tokyo, Japan).

4.4.2. Floral volatile collection

Floral volatiles were collected *in vivo* from the first inflorescence of four plants for each accession using the dynamic headspace technique (Raguso and Pellmyr 1998; Tholl *et al.* 2006) as follows. The inflorescence was enclosed within a LOOK oven bag (McCormick & Co., Inc., Baltimore, Maryland, USA). The oven bag was affixed to a tomato cage with tape to prevent the bag from collapsing onto the inflorescence and sealed around the base of the raceme and a charcoal trap with a plastic tie. The charcoal trap consisted of a glass Pasteur pipette (Fisher Scientific, Pittsburgh, Pennsylvania, USA) containing 100 mg of ground activated charcoal (Sigma-Aldrich, St. Louis, Missouri, USA) between two pieces of loosely packed glass wool. A small hole was cut into a corner of the oven bag and sealed around a Porapak Q sorbent tube (part number 226-59-03; SKC, Eighty Four, Pennsylvania, USA) with tape. The sorbent tube was attached to a Pocket Pump TOUCH (SKC) with Tygon S3 tubing (Saint-Gobain, Courbevoie, France). To determine the optimal sampling time, floral volatiles were collected for 24, 48, and 72 h with a pump flowrate of 500 mL/min. Floral volatile collection was conducted in the aforementioned growth chambers. Sorbent tubes were sealed and stored at 4°C until extraction. The front and back sections of the Porapak Q sorbent tube were each extracted with 500 µL of analytical grade hexane (EMD Millipore, Burlington, Massachusetts, USA) in separate vials and placed on a shaker for 1 h. Extracts were stored at -20°C for a maximum of 1 week from the date of sampling.

4.4.3. Floral volatile analyses

Volatile organic compounds were analyzed for hexane solvent blanks and the aforementioned floral volatile extracts with a 7890 GC/5975C MSD system (Agilent Technologies, Santa Clara, California, USA) using a 1:10 split injection of 1 µL extract at 230°C with helium as the carrier gas at a split flow rate of 10 mL/min. The gas chromatograph was

equipped with a HP-5 column (30 m length, 250 μL inner diameter, 0.25 μL film thickness; Agilent). The oven temperature was held at 50°C for 2 min, increased by 10°C/min to 250°C, held at 250°C for 5 min, and increased by 40°C/min to 290°C; however, there was some slight variation in these settings across samples. Volatiles were ionized by electron ionization, mass scanned from 40 to 350 m/z with 2.0 scans/s, and putatively identified using ChemStation (version E.01.00 MSD; Agilent) with the NIST 17 Mass Spectral Library. The extracts from the sampling time that yielded the greatest peak intensity (72 h; 1 biological replicate for each accession) were used for subsequent analyses. The floral volatiles were categorized into chemical classes and subclasses according to Knudsen *et al.* (1993). Percent composition for each floral volatile and chemical class was calculated by dividing the respective peak area by the total peak area.

4.4.4. Identification of potential osmophores

Anthetic flowers from four *G. gynandra* (accession TOT8917) plants were fixed in FAA solution (50% ethanol, 10% formalin, 5% acetic acid), vacuum infiltrated for 30 min while on ice, and stored at 4°C overnight. Specimens were dehydrated in an ethanol series and critical point dried with carbon dioxide using a CPD 030 critical point dryer (Bal-Tec AG, Balzers, Liechtenstein). Sepals, petals, nectary, androgynophore, stamens, gynophore, and pistil were dissected from the dried specimens. The floral structures were mounted onto scanning electron microscopy stubs with conductive carbon tabs and sputter coated with gold using a Hummer 6.2 Sputter Coater (Anatech USA, Sparks, Nevada, USA). Mounted structures were imaged using a ZEISS Sigma 300 VP Scanning Electron Microscope (Carl Zeiss AG, Oberkochen, Germany). Photoshop (Adobe, Mountain View, California, USA) was used to adjust contrast and brightness of the scanning electron micrographs.

4.4.5. RNA sequencing of floral structures

Adaxial and abaxial petals, androgynophore, filaments, and gynophore were excised from anthetic flowers between 14:00 and 16:00, flash frozen in liquid nitrogen, and stored at -80°C. As both floral and vegetative glandular trichomes are suspected to exclusively produce defensive compounds (Effmert *et al.* 2005; Dudareva and Pichersky 2006), we excluded the floral structures with glandular trichomes (i.e., sepals and pistil) from our RNA-seq analyses. Floral

structures were pooled from four (androgynophore, filaments, gynophore) or five (adaxial and abaxial petals) flowers on the same plant from a total of four plants (i.e., four biological replicates per floral structure). Pooled structures were manually ground while submerged in liquid nitrogen. RNA was extracted from the ground structures using a RNeasy Micro Kit (Qiagen, Hilden, Germany) using the manufacturer protocol with the following modifications: (1) following the initial vortexing, ground structures were incubated in buffer RTL for 5 mins to enhance lysis; (2) after adding RNase-free water, the RNeasy MinElute spin column was incubated for 5 mins before centrifugation and the resulting eluate was dispensed into the same spin column and centrifuged again to maximize RNA yield. A NanoDrop 2000 spectrophotometer (Thermo Fisher Scientific, Waltham, Massachusetts, USA) and 2100 Bioanalyzer (Agilent, Santa Clara, California, USA) were used for RNA quantification and qualification. A cDNA library was generated for each sample using a TruSeq Stranded mRNA Library Prep Kit (cat. no. RS-122-2101; Illumina, San Diego, California, USA) following the manufacturer low sample protocol with NucleoMag NGS Clean-up and Size Select magnetic beads (Macherey-Nagel, Düren, Germany) instead of AMPure XP magnetic beads (Agencourt, Beverly, Massachusetts, USA). Adaxial and abaxial petals and androgynophore libraries were normalized, pooled, and sequenced with a HiSeq 2500 System (Illumina, San Diego, California, USA) by The Centre for Applied Genomics (TCAG) at the Hospital for Sick Children (Toronto, Canada). Filaments and gynophore libraries were normalized, pooled, and sequenced with a HiSeq X System (Illumina, San Diego, California, USA) by Canada's Michael Smith Genome Sciences Centre at BC Cancer (British Colombia, Canada). Variation in error rate is typically greater between samples than sequencing platforms; however, samples that are prepared by the same lab group tend to have consistent error rates (Stoler and Nekrutenko 2021).

4.4.6. Transcriptome assembly and analyses

Raw reads were trimmed with Trim Galore! (version 0.6.6) and quality checked with FastQC (version 0.11.9), then assembled *de novo* using Trinity (version 2.12.0) (Grabherr *et al.* 2011). To confirm no batch effects were introduced by the sequencing platforms, a principal component analysis was performed on transcript counts using the Trinity 'PtR' script. The transcriptome assembly completeness was evaluated using Benchmarking Universal Single Copy Orthologs (BUSCO) (version 5.1.2) with the 'brassicales_odb10' dataset (Manni *et al.* 2021).

The transcriptome was annotated using BLASTn (version 2.13.0) (Altschul *et al.* 1990) with default parameters and the Araport 11 database (Cheng *et al.* 2017). Transcripts with the highest bit-score were selected as representatives for the genes of interest; except when there was another transcript with a similar bit-score and length but higher expression than the transcript with the highest bit-score, in which case it was selected instead. Further, transcripts with expression below 5 TPM, in at least three replicates, for all structures were excluded. A heatmap was generated using the 'gplots' R package with representative transcripts for the *A. thaliana* genes from the KEGG (Kyoto Encyclopedia of Genes and Genomes) terpenoid backbone biosynthesis pathway (ath00900) (Kanehisa *et al.* 2023) and *A. thaliana* terpenoid synthase genes summarized in Aubourg *et al.* (2002) and Tholl and Lee (2011).

4.5 Tables

Table 4.1. Percent composition and chemical class of the floral volatiles in the headspace of *Gynandropsis gynandra* African (TOT8917 from Malawi) and Asian (TOT7200 from Malaysia) accessions, arranged by ascending retention time.

	Percent composition			
Chemical ID	African	Asian	Chemical class	Chemical subclass
4-Methyl-2-pentanone oxime*	0.3		Nitrogen-containing	
(*Z*)-2-methylbutanal oxime	38.3	2.3	Nitrogen-containing	
(*E*)-2-methylbutanal oxime	9.7		Nitrogen-containing	
(*E*)-3-methylbutanal oxime	1.1		Nitrogen-containing	
Isoamyl acetate	4.4		Aliphatic	Ester
2-Methylbutyl acetate	1.4		Aliphatic	Ester
2-Heptanone		1.9	Aliphatic	Ketone
2-Nitropentane*	0.9		Nitrogen-containing	
Orthodene or Sabinene*	0.5	0.4	Aliphatic	Alkene
Benzaldehyde		22.3	Benzenoid	Aldehyde
Unknown floral volatile	0.4		Undetermined	
Unknown floral volatile	0.5		Undetermined	
2-Methylpentyl acetate	2.2		Aliphatic	Ester
4-Hexen-1-ol acetate*	3.9		Aliphatic	Ester
3-Carene*	0.7	2.1	Terpenoid	Monoterpene
Limonene*	0.6	0.3	Terpenoid	Monoterpene
Benzyl alcohol		66.1	Benzenoid	Alcohol
(*E*)-β-Ocimene*	1.2		Terpenoid	Monoterpene
(*Z*)-β-Ocimene*	30.7		Terpenoid	Monoterpene
1,1-Dimethylpropyl ester pentanoic acid*		0.6	Aliphatic	Ester
Linalool*		1.7	Terpenoid	Monoterpene
Nonanal	1.9		Aliphatic	Aldehyde
(*E*)-4,8-Dimethylnona-1,3,7-triene	0.7	2.0	Terpenoid	Irregular terpene
2,6-Bis(1,1-dimethylethyl)-4-(1-oxopropyl)phenol	0.5	0.4	Benzenoid	Alcohol

* Highest similarity match to the NIST 17 Mass Spectral Library but with less than 50% match probability

Table 4.2. Pollinators of *Gynandropsis gynandra* in Africa and Asia.

Continent	Country	Pollinator Order	Pollinator Family	Pollinator Species	References
Africa	Kenya	Lepidoptera	Sphingidae	*Agrius convolvuli**	Werth 1942; Oronje *et al.* 2012; Martins and Johnson 2013
				Coelonia sp.*	
				Daphnis nerii	
				Hippotion celerio	
				Hippotion eson	
				Hyles sp.	
				Nephele aequivalens	
				Nephele comma	
				Temnora sp.	
				*Xanthopan morganii**	
	Tanzania			*Basiothia medea*	
	Kenya, Tanzania			*Hippotion osiris*	
Asia	India	Hymenoptera	Apidae	*Amegilla cingulata*	Burkill 1916; Chandra *et al.* 2013; Raju and Rani 2016
				Apis cerana	
				Apis florea	
				Tetragonula iridipennis	
				Xylocopa latipes	
		Lepidoptera	Pieridae	*Catopsilia pomona*	
			Nymphalidae	*Danaus chrysippus*	
			Papilionidae	*Pachliopta aristolochiae*	
				Papilio polytes	

* Less effective pollinators; long-tongued hawkmoths

Table 4.3. *Arabidopsis thaliana* terpenoid biosynthetic pathway genes with homologs expressed in *Gynandropsis gynandra* (accession TOT8917 from Malawi) petals and/or stalk-like floral structures.

Locus	Abbreviation	Gene
AT5G47720	*AACT1*	*ACETOACETYL-COA THIOLASE21*
AT5G48230	*AACT2*	*ACETOACETYL-COA THIOLASE21*
AT4G11820	*HMGS*	*3-HYDROXY-3-METHYLGLUTARYL-COA SYNTHASE*
AT1G76490	*HMG1*	*3-HYDROXY-3-METHYLGLUTARYL COA REDUCTASE1*
AT2G17370	*HMG2*	*3-HYDROXY-3-METHYLGLUTARYL COA REDUCTASE2*
AT5G27450	*MK*	*MEVALONATE KINASE*
AT1G31910	*PMK*	*PHOSPHOMEVALONATE KINASE*
AT3G54250	*MDD2*	*MEVALONATE DIPHOSPHATE DECARBOXYLASE2*
AT4G15560	*DXS1*	1-*DEOXY-D-XYLULOSE 5-PHOSPHATE SYNTHASE*
AT5G62790	*DXR*	*1-DEOXY-D-XYLULOSE 5-PHOSPHATE REDUCTOISOMERASE*
AT2G02500	*MCT*	*2-C-METHYL-D-ERYTHRITOL 4-PHOSPHATE CYTIDYLTRANSFERASE*
AT2G26930	*CMK*	*4-(CYTIDINE 5'-DIPHOSPHO)-2-C-METHYL-D-ERYTHRITOL KINASE*
AT1G63970	*MDS*	*2-C-METHYL-D-ERYTHRITOL 2,4-CYCLODIPHOSPHATE SYNTHASE*
AT5G60600	*HDS*	*4-HYDROXY-3-METHYLBUT-2-ENYL DIPHOSPHATE SYNTHASE*
AT4G34350	*HDR*	*4-HYDROXY-3-METHYLBUT-2-ENYL DIPHOSPHATE REDUCTASE*
AT3G02780	*IPP2*	*ISOPENTENYL DIPHOSPHATE ISOMERASE2*
AT2G18620	*GGPPS2*	*GERANYLGERANYL PYROPHOSPHATE SYNTHASE2*
AT4G36810	*GGPPS11*	*GERANYL(GERANYL) PYROPHOSPHATE SYNTHASE11*
AT4G38460	*GGPPS12*	*GERANYL(GERANYL) PYROPHOSPHATE SYNTHASE12*
AT5G47770	*FPS1*	*FARNESYL DIPHOSPHATE SYNTHASE1*
AT4G17190	*FPS2*	*FARNESYL DIPHOSPHATE SYNTHASE2*
AT3G25820	*TPS27*	*TERPENE SYNTHASE27*

4.6 Figures

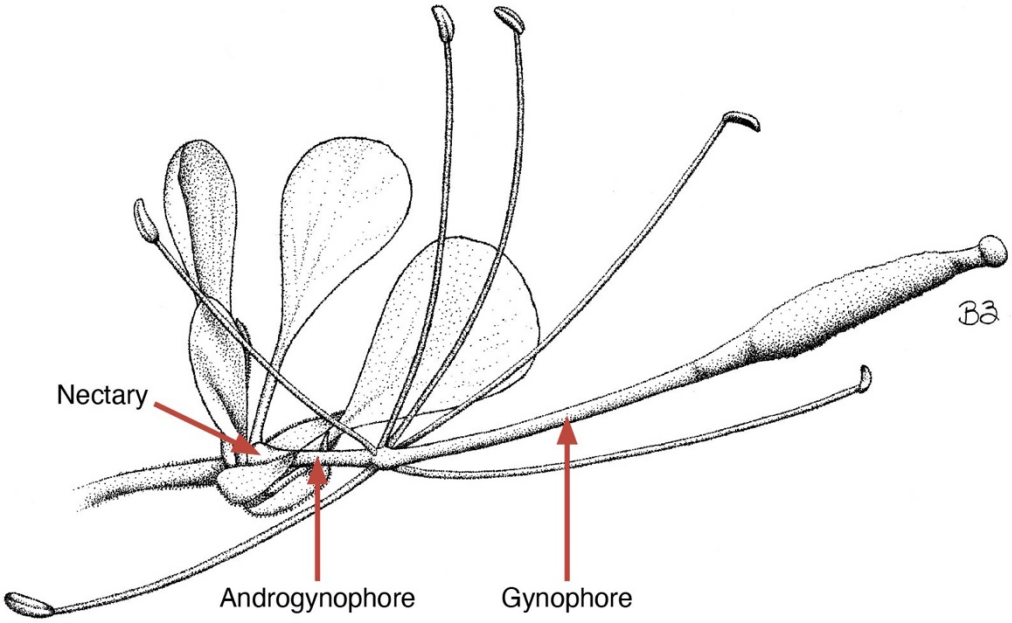

Figure 4.1. Illustration of *Gynandropsis gynandra* (accession TOT8917 from Malawi) flower.

Figure 4.2. Photographs of *Gynandropsis gynandra* inflorescences: **(a)** accession TOT8917 from Malawi; **(b)** accession TOT7200 from Malaysia.

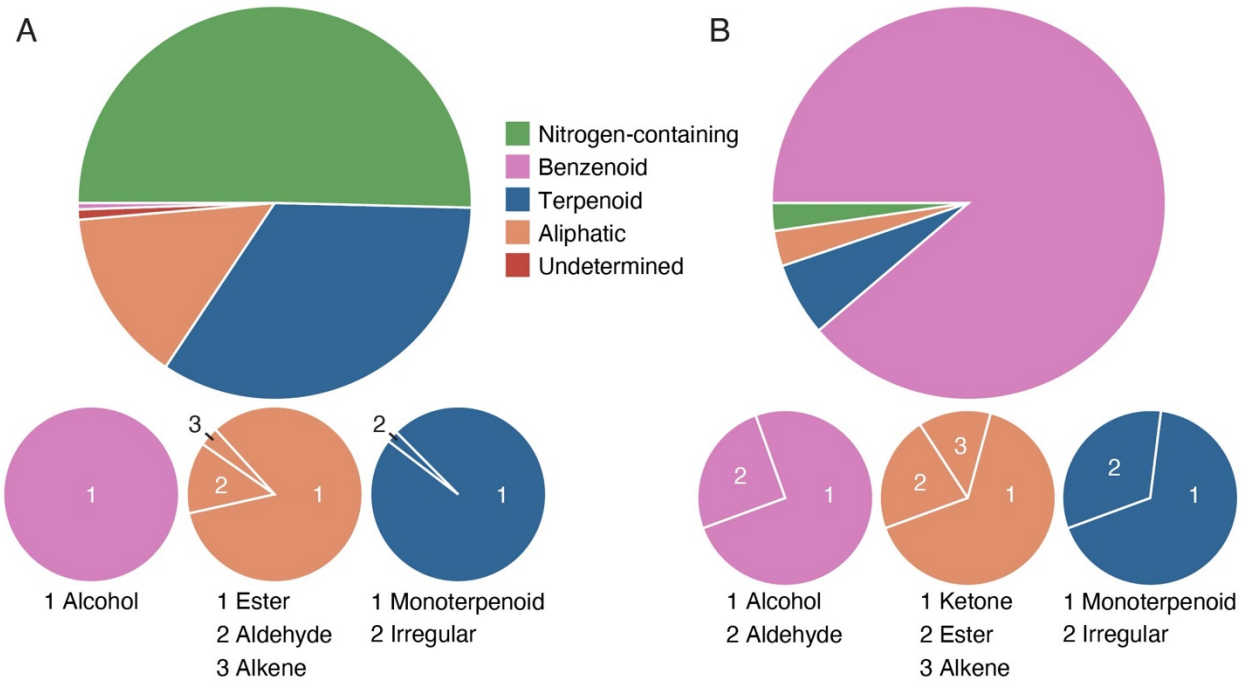

Figure 4.3. Proportions of floral volatiles captured from *Gynandropsis gynandra* categorized following Knudsen *et al.* (1993): **(a)** accession TOT8917 from Malawi; **(b)** accession TOT7200 from Malaysia. The upper and lower pie charts depict the proportions of the main chemical classes and the benzenoid, aliphatic, and terpenoid chemical subclasses, respectively.

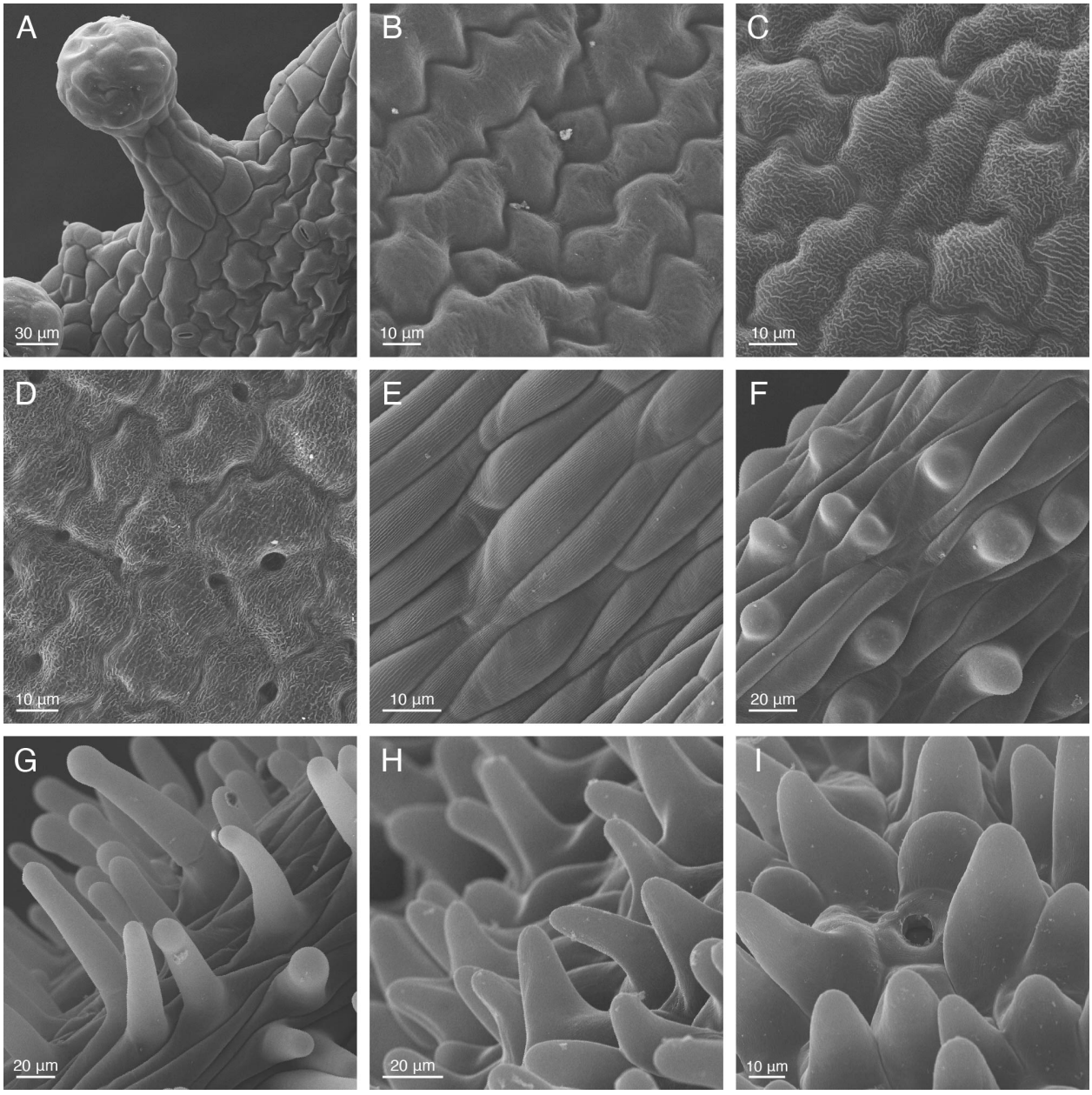

Figure 4.4. Scanning electron micrographs of *Gynandropsis gynandra* (accession TOT8917 from Malawi) perianth and floral nectary: **(a, b)** distal section and adaxial surface of the sepal; **(c)** distal section and adaxial surface of the petal blade; **(d)** middle section and adaxial surface of the petal blade; **(e)** distal section and abaxial surface of the petal claw; **(f)** middle section and adaxial surface of the petal claw; **(g)** proximal section and adaxial surface of the petal claw; **(h, i)** nectary.

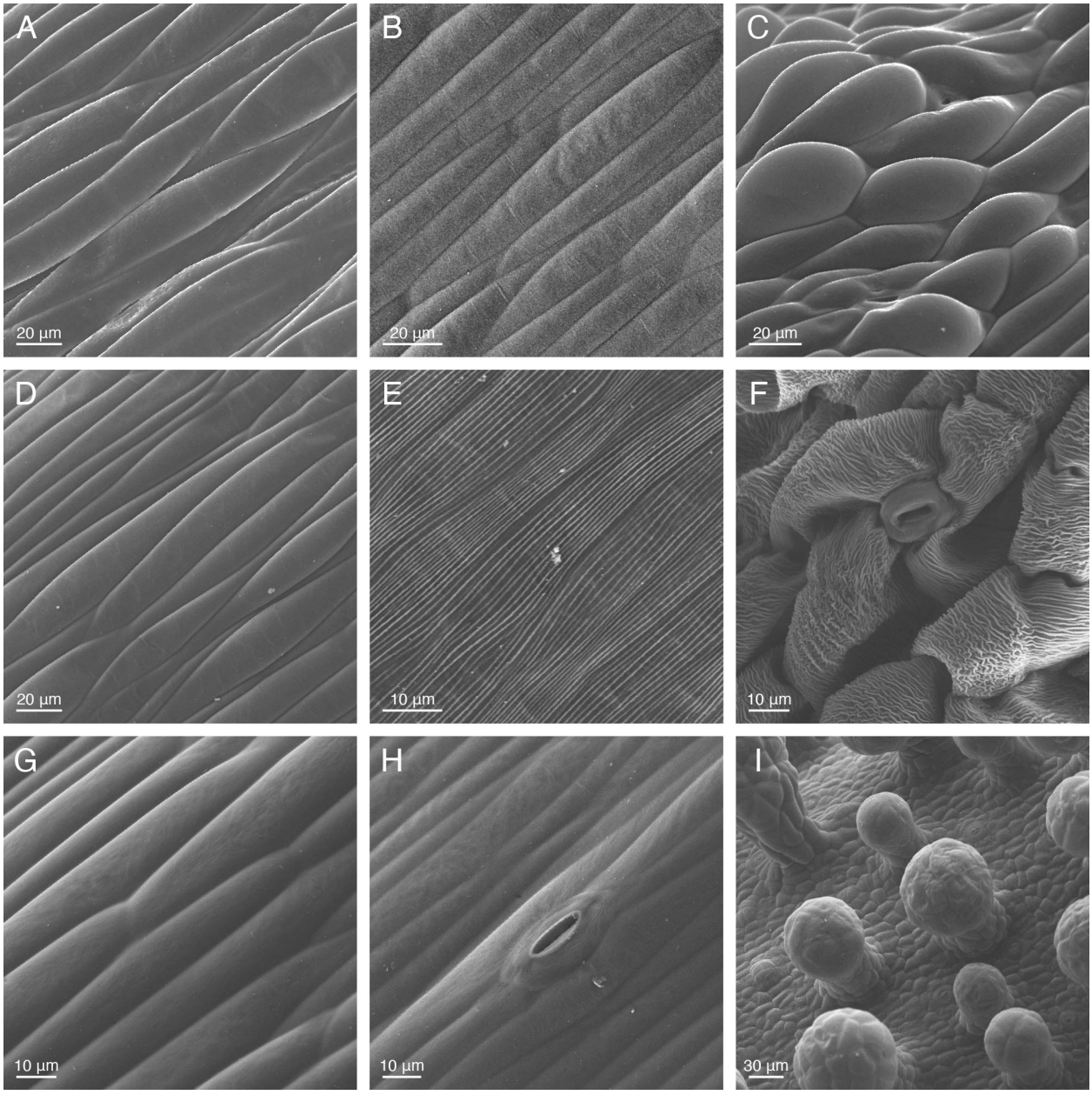

Figure 4.5. Scanning electron micrographs of *Gynandropsis gynandra* (accession TOT8917 from Malawi) stalk-like floral structures, anther, and pistil: **(a)** proximal section of the androgynophore; **(b)** distal section of the androgynophore; **(c)** filament and gynophore junction; **(d)** proximal section of the filament; **(e)** distal section of the filament; **(f)** anther; **(g)** proximal section of the gynophore; **(h)** middle section of the gynophore; **(i)** proximal section of the pistil.

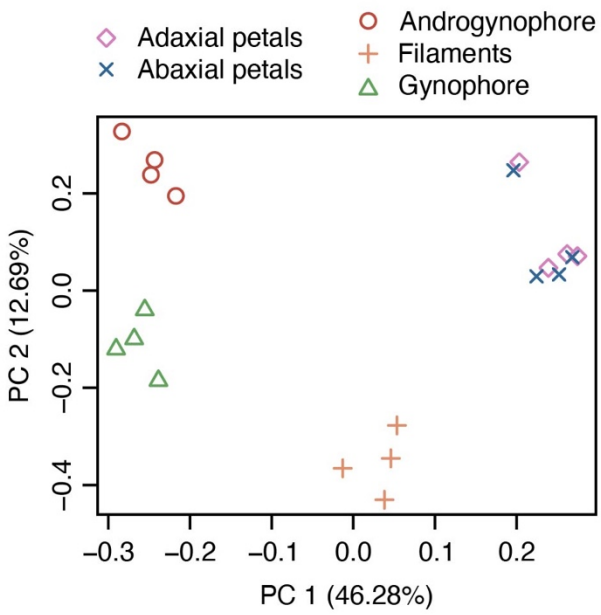

Figure 4.6. Principal component analysis of *Gynandropsis gynandra* (accession TOT8917 from Malawi) transcript counts.

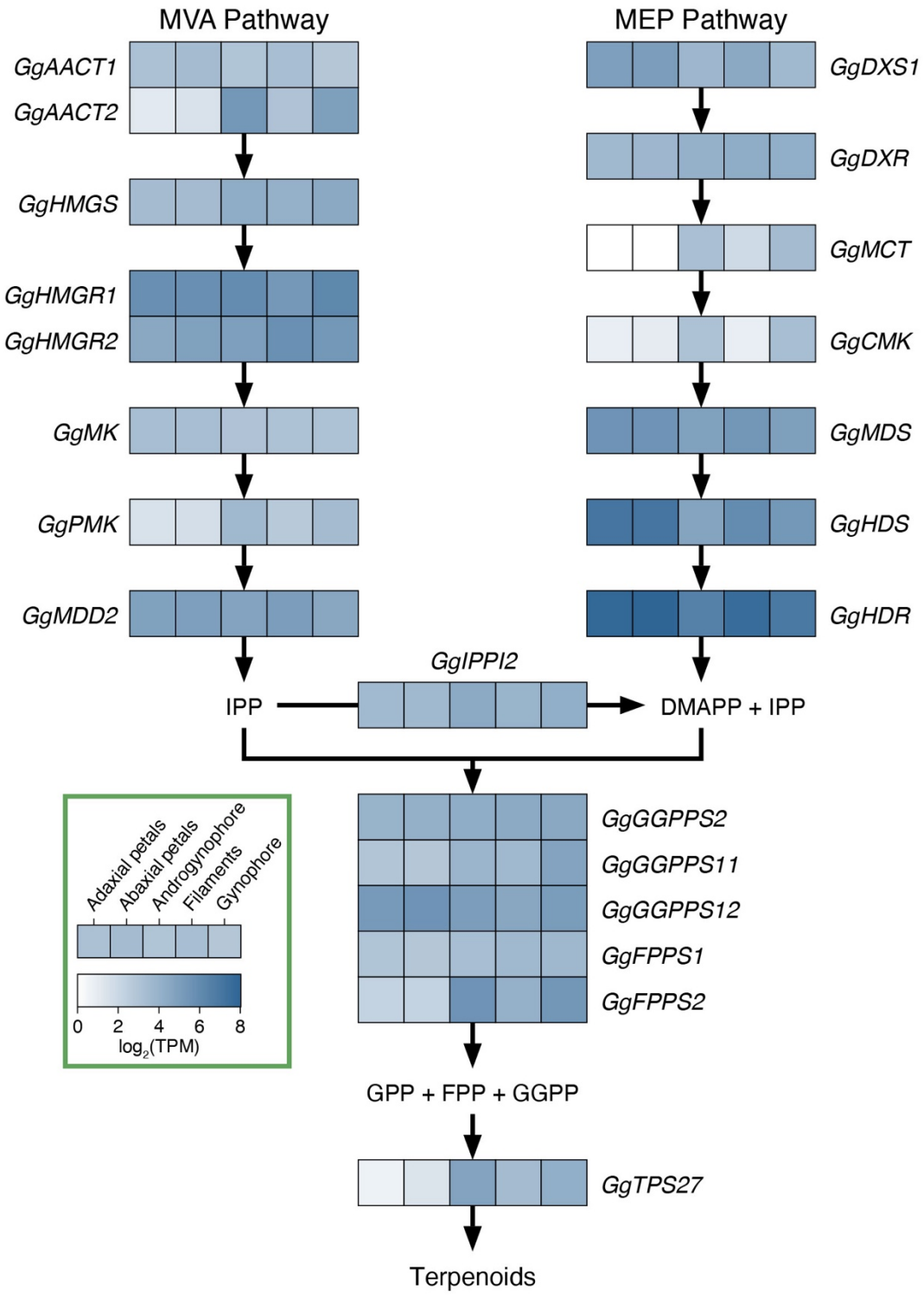

Figure 4.7. Integrated heatmap and terpenoid biosynthetic pathway for *Gynandropsis gynandra* (accession TOT8917 from Malawi) representative transcripts expressed in $\log_2$(TPM). The legend is enclosed in a green box. Genes adjacent to one another (i.e., not separated by an arrow; e.g., *GgAACT1* and *GgAACT2*) are functionally redundant; excluding geranyl diphosphate

synthases (GPPS), geranylgeranyl diphosphate synthases (GGPPS) and farnesyl diphosphate synthases (FPPS) that use different amounts of DMAPP and IPP molecules. Top left, mevalonate (MVA) pathway produces isopentenyl diphosphate (IPP); top right, methylerythritol phosphate (MEP) pathway produces dimethylallyl diphosphate (DMAPP) and IPP; IPP isomerases (IPPI) convert IPP to DMAPP; GPPS, GGPPS, and FPPS use DMAPP and IPP to produce geranyl diphosphate (GPP) and geranylgeranyl diphosphate (GGPP), and farnesyl diphosphate (FPP); terpene synthases (TPS) produce terpenoids from GPP, GGPP, or FPP.

Chapter 5: Developmental and genetic basis of the androgynophore in *Gynandropsis gynandra*[4]

5.1 Introduction

The reproductive success of flowering plants is dependent on pollination. As such, many flowering plants have evolved suites of characteristics to attract and reward pollinators or assist in pollination. Fragrances released by flowers act as an olfactory cue over long distances, flower colour and patterns act as a visual signal over shorter ranges, and the form or position of floral organs can increase the likelihood of pollen transfer or encourage pollinator visitation by providing efficient access to floral rewards (Willmer 2011; Sheehan *et al.* 2012). Elaboration of floral organs, such as changes to shape and size, can have adaptive significance for pollinator interactions. For example, staminodes (sterile stamens) can undergo modifications to attract pollinators, facilitate pollen transfer, and prevent self-pollination (Walker-Larsen and Harder 2000; Botnaru and Schenk 2019). Similarly, some petals have developed nectar spurs (tubular extensions that produce and retain nectar) to provide a convenient reward for certain pollinators (Willmer 2011). Integrating morphological characterizations with genetic analyses has led to significant contributions to our understanding of the mechanisms controlling the development and evolution of such floral features (reviewed by Specht and Howarth 2015; Smyth 2018; Kramer 2019). Expanding research to species that possess characteristics absent in model organisms can provide a more comprehensive picture of the diversification of floral features and the underlying patterns of gene expression (Buzgo *et al.* 2004; Kramer 2007).

A feature presumably involved in pollinator interactions is the androgynophore; a stalk-like structure that supports and elevates the reproductive organs of the flower. Although stalk-like floral structures such as the androgynophore and gynophore (a stalk-like structure supporting the pistil) are commonly mentioned in the dichotomous keys and species descriptions of floras, little is known about their structure, development, and genetics. Further, the type of tissue from which these stalk-like structures are derived is unclear, though an elongated receptacle or basal elongation of the reproductive organs have been speculated (Cronk 2009). The gynophore of *Arachis hypogaea* (peanut) in Fabaceae is an exception as it has been more thoroughly

[4] A version of Chapter 5 has been published in *American Journal of Botany* and is formatted accordingly. The published manuscript can be accessed through the following link: https://doi.org/10.1002/ajb2.16193

researched due to its essential role in underground fruit development (Moctezuma 2003; Xia *et al.* 2013; Zhao *et al.* 2015); however, this gynophore is unique in that its formation is initiated after fertilization. Though androgynophores and gynophores that develop during flowering are often inconspicuous, prominent stalk-like structures are characteristic of Cleomaceae (Iltis *et al.* 2011) and are present in other distantly related species, including the crop plant *Passiflora edulis* (passion fruit) in Passifloraceae.

Gynandropsis gynandra (L.) Briq., a leafy vegetable native to Africa and Asia, is an excellent model to elucidate the developmental and genetic basis of the androgynophore. This species of Cleomaceae has a pronounced androgynophore (Fig. 5.1), though its potential role in pollination has not been thoroughly investigated. In Africa, hawkmoths have been observed visiting *G. gynandra* flowers to feed on nectar droplets on the apical portion of the receptacle (Werth 1942; Martins and Johnson 2013). Although long-tongued hawkmoths act as nectar robbers, short-tongued hawkmoths such as *Hippotion osiris* and *Basiothia medea* (Sphingidae) contact the reproductive organs while feeding (Werth 1942; Martins and Johnson 2013). Thus, the androgynophore of *G. gynandra* may act to raise the reproductive organs to increase the likelihood of pollinator contact. Further research of this potentially ecologically significant feature would be a valuable contribution to our knowledge of *G. gynandra*. As an underutilized crop plant with untapped potential, *G. gynandra* has been studied for its insecticidal activity (Lwande *et al.* 1999; Nyalala *et al.* 2013), medicinal properties (Ajaiyeoba *et al.* 2001; Ghogare *et al.* 2009; Bala *et al.* 2010), and nutrient content (Moyo *et al.* 2018; Sogbohossou *et al.* 2019, 2020). Additionally, *G. gynandra* serves as a model for C_4 photosynthesis studies (van den Bergh *et al.* 2014; Tronconi *et al.* 2020; Huang *et al.* 2021). In summary, investigation of the androgynophore is key to understanding *G. gynandra* reproduction and complements the body of knowledge for this burgeoning model species.

A critical component of the androgynophore is the maintenance of its shape and size to ensure optimal reproductive organ positioning for efficient pollen removal and deposition (Weiss *et al.* 2005). The growth of floral features occurs by two processes: (1) cell proliferation, where an increase in cell mass is coupled with cell division, and (2) cell expansion, accomplished through cell wall loosening and an increase in vacuolar water uptake or endoreduplication (Weiss *et al.* 2005; Bögre *et al.* 2008). Therefore, enlargement of floral structures can be attributed to an increase in cell number and/or cell size (Weiss *et al.* 2005). For example, both

cell division and elongation account for differences in nectar spur length between two *Pelargonium* (Geraniaceae) species (Tsai *et al.* 2018), whereas variation in nectar spur length of *Aquilegia* (Ranunculaceae) species is attributed to cell elongation alone (Puzey *et al.* 2012). In *Passiflora mucronata*, treatment of androgynophores with the plant hormone, auxin, resulted in an increase in androgynophore length (Rocha *et al.* 2015). However, treatment with a polar auxin transport inhibitor resulted in longer cells but shorter androgynophore length, suggesting cell division and elongation contribute to androgynophore lengthening under the influence of plant hormones (Rocha *et al.* 2015).

Plant hormones are synthesized and transported in response to environmental and endogenous changes, and in turn, their signalling coordinates growth and development through the regulation of genetic programs (Weiss *et al.* 2005; Lacombe and Achard 2016). Although plant hormones can act at or near the location of synthesis, the vascular system provides a crucial conduit for their long-distance transport throughout the plant (Santner *et al.* 2009; Lacombe and Achard 2016). For example, basipetal transport of auxin from the anthers contributes to filament elongation in *Tarenaya houtteana* (Cleomaceae; formerly *T. hassleriana*) and androgynophore and gynophore lengthening in *Sieruela rutidosperma* (Cleomaceae) (Koevenig 1973; Koevenig and Sillix 1973; Dattagupta and Datta 1976). Although auxin plays a role in nearly every aspect of growth and development by mediating a complex regulatory network with numerous auxin-responsive genes, organ size and shape is not limited to the influence of this plant hormone alone (Santner *et al.* 2009; Wessinger and Hileman 2020). In *Arabidopsis thaliana*, for instance, filament elongation is regulated by the plant hormones auxin, brassinosteroids, gibberellin, and jasmonic acid (Cecchetti *et al.* 2008; Cheng *et al.* 2009; Ye *et al.* 2010). While the involvement of plant hormones in organ size and shape has been investigated in *A. thaliana*, the expression and function of their associated genes have not been thoroughly studied in other species with novel floral structures.

Here, we investigated androgynophore development and the genetics underlying its growth by addressing the following outstanding questions: (1) What is the rate of androgynophore elongation throughout development and is the elongation due to cell division or expansion? (2) What are the external and internal features of the androgynophore, and do these vary along the length of the androgynophore and throughout development? (3) What are the global gene expression patterns during androgynophore development? (4) Which genes are

putatively involved in androgynophore elongation? Toward these ends, we provide a detailed description of flower and androgynophore growth, establish the predominate mode of androgynophore lengthening, and characterize the vascular anatomy of the androgynophore throughout development. We also explore global gene and floral organ identity gene expression patterns, the putative role of plant hormones in androgynophore development, and identify candidate genes involved in androgynophore elongation.

5.2 Materials and Methods

5.2.1 Plant material

Seeds of *Gynandropsis gynandra* (accession TOT8917 from Malawi) (Sogbohossou *et al.* 2019, 2020) were grown in professional growing mix (Sun Gro Horticulture, Agawam, MA, USA) in a University of Alberta, Department of Biological Sciences growth chamber set to 28°C day/22°C night temperatures with a 12h day/12h night cycle. Voucher specimens were deposited at the University of Alberta Vascular Plant Herbarium (ALTA) (accession 143368 and 143369). Fresh whole and dissected flowers were photographed using an E-520 DSLR camera with a Zuiko Digital ED 50 mm 1:2 macro lens (Olympus, Tokyo, Japan) and an EOS Rebel T7i DSLR camera with an EF-S 18-55 mm STM lens (Canon, Tokyo, Japan). Backgrounds were removed from photographs using the 'Magic Eraser Tool' in Photoshop (Adobe, San Jose, CA, USA).

5.2.2 Floral growth measurements

Fifty buds (five buds from the first inflorescence on 10 plants) were tagged when 0.45 to 0.55 cm long by tying a coloured thread around the pedicel, and flower length was measured daily between 13:00 and 14:00 hours until senescing or fruiting. Measurements were made from the base of the sepals to the apex of the pistil and appearance was noted. Since androgynophore measurements require perianth removal at early stages in floral development, the androgynophore lengths were not measured in conjunction with the aforementioned flower length measurements to avoid potential disturbances to floral growth. Instead, flower and androgynophore lengths were measured for 100 flowers (10 flowers from the first inflorescence on 10 plants) at varying stages of floral development from bud to anthesis. Sepals and petals covering the androgynophore were removed. Androgynophore length was measured from the

apex of the receptacle to the base of the stamens. All measurements were made to the nearest 0.05 cm.

CurveExpert Professional (version 2.6.5) (Hyams Development, Chattanooga, TN, USA) was used to determine the relationship between flower length and androgynophore length. For the 100 flowers measured, androgynophore length was plotted against flower length and the best-fitting non-linear regression model was selected. Using this non-linear regression model, the Hoerl model ($y = ab^x x^c$), androgynophore lengths were calculated for each day for the 50 flowers measured throughout development. These flower length measurements and calculated androgynophore lengths were plotted using the 'ggplot2' R package (version 3.3.1) (Wickham 2016).

5.2.3 Scanning electron microscopy and cell measurements

Flowers from 11 plants were harvested at three developmental stages based on the floral measurements: (1) bud stage (0.5 to 0.7 cm long, with the apex of the pistil level with or exserted slightly above the closed sepals), (2) intermediate stage (1.5 to 1.9 cm long, with the sepals and petals still closed and the pistil exserted above the petals), and (3) anthetic stage (3.6 to 4.5 cm long, with open petals and dehisced anthers) (Fig. 5.2). Specimens were fixed in FAA (50% ethanol, 10% formalin, 5% glacial acetic acid, v/v) on ice under vacuum for 30 min and left at 4°C overnight, dehydrated in an ethanol series, and critical point dried with carbon dioxide using a CPD 030 critical point dryer (Bal-Tec AG, Balzers, Liechtenstein). Dried specimens were dissected and mounted on scanning electron microscopy stubs with conductive carbon tabs, sputter coated with gold using a SEMprep 2 sputter coater (Nanotech, Prestwick, UK) or a Hummer 6.2 sputter coater (Anatech USA, Sparks, NV, USA) and imaged using a ZEISS Sigma 300 VP field emission scanning electron microscope or a ZEISS EVO 10 scanning electron microscope (Carl Zeiss AG, Oberkochen, Germany). Contrast and brightness of the scanning electron micrographs were adjusted using Adobe Photoshop but no other modifications to the images were made.

The length and width of five epidermal cells from 10 images of the distal, middle, and proximal sections of the androgynophore at each developmental stage were measured using ImageJ (version 1.52q) (Schneider *et al.* 2012), for a total of 10 androgynophores and 50 cells for each combination of section and developmental stage. The distal, middle, and proximal

sections were each designated as one third of the androgynophore, with the distal section below the stamens and the proximal section above the receptacle. The cells with the most well-defined edges were selected for measurements. To address whether cell lengths and widths increase as the androgynophore elongates, we compared means between the developmental stages with sections pooled ($N = 150$) for cell length and width measurements. To determine whether cell lengths are uniform throughout the androgynophore, we compared means between the sections of each developmental stage ($N = 50$) for cell length measurements. Levene's test was used to assess for homogeneity of variance between groups using the 'car' R package (version 3.0-8) (Fox and Weisberg 2019). For comparisons of groups with homogeneous variance, ANOVA and Tukey *post hoc* tests were performed using the 'aov' and 'TukeyHSD' R base functions. Groups with heterogeneous variance were compared with Welch's F and Games-Howell *post hoc* tests using 'oneway.test' R base function and 'userfriendlyscience' R package (version 0.7.2) (Peters, 2017). In addition, the number of epidermal cells in a lengthwise file of the androgynophore were estimated for each developmental stage to determine whether cell division contributes to androgynophore elongation. Similar to the Landis *et al.* 2016 cell number estimates, androgynophore lengths were measured from the same specimens used for the aforementioned cell length measurements, and cell number was approximated by dividing the average androgynophore length by the average cell length.

5.2.4 Histological preparations and imaging

Flowers from 11 plants at the three developmental stages were fixed in FAA and dehydrated in an ethanol series as previously mentioned. Samples were then cleared with CitriSolv (Decon Labs, King of Prussia, PA, USA), embedded in Paraplast Plus (Sigma-Aldrich, St. Louis, MO, USA), and stored at 4°C. Samples were sectioned to 8 μm using a Microm HM 325 rotary microtome (Thermo Scientific, Waltham, MA, USA) and mounted on glass slides. Sections were stained with 0.25 mg mL^{-1} Alcian blue and 0.10 mg mL^{-1} safranin O and imaged using a Pixel 5 (Google, Menlo Park, CA, USA) with a NexYZ 3-axis universal smartphone adapter (Celestron, Torrance, CA, USA) attached to an Eclipse 80i light microscope (Nikon, Tokyo, Japan). Sections were cleared with CitriSolv, dehydrated with isopropanol, and air dried. Dried sections were stained with 0.25 mg mL^{-1} Alcian blue and 0.10 mg mL^{-1} safranin O in 0.1 M sodium acetate buffer (prepared from 1 mg mL^{-1} Alcian blue and 1 mg mL^{-1} safranin O in

50% ethanol, v/v stock solutions) (Graham and Trentham, 1998). Stained sections were imaged using a Pixel 5 smartphone (Google, Menlo Park, CA, USA) with a NexYZ 3-axis universal smartphone adapter (Celestron, Torrance, CA, USA) attached to an Eclipse 80i light microscope (Nikon, Tokyo, Japan).

5.2.5 RNA sequencing

Androgynophores at the three aforementioned developmental stages, as well as filaments and gynophores at the anthetic stage, were harvested between 14:00 and 16:00 hours 12- to 36-week-old plants. Filaments and gynophores, other stalk-like floral structures, were collected for comparison to the androgynophore. Bud stage androgynophores were pooled from ten flowers, intermediate stage androgynophores were pooled from six flowers, and anthetic stage androgynophores, filaments, and gynophores were pooled from four flowers. Androgynophores at each stage, and filaments and gynophores at the anthetic stage, were processed from four different plants to achieve a total of four biological replicates each. Excised structures were flash frozen in liquid nitrogen and stored at -80°C. The pooled structures were ground with a pestle while submerged in liquid nitrogen. RNA was extracted from the ground tissue using a RNeasy Micro Kit (Qiagen, Hilden, Germany) with the following modifications to the manufacturer protocol: After vortexing, ground tissue was left in buffer RTL for 5 min to maximize lysis, and after addition of RNase-free water, the RNeasy MinElute spin column was left for 5 min before centrifuging and the resulting eluate was added to the same spin column and centrifuged again to allow maximum RNA yield. RNA was quantified using a NanoDrop 2000 spectrophotometer (Thermo Fisher Scientific, Waltham, MA, USA) and qualified with a 2100 Bioanalyzer (Agilent, Santa Clara, CA, USA). RNA with a minimum RNA Integrity Number (RIN) of 8 was used for successive analyses. Extracted RNA was used to prepare cDNA libraries for androgynophore, filaments, and gynophore samples by poly(A) enrichment using a TruSeq Stranded mRNA Library Prep Kit (cat. no. RS-122-2101; Illumina, San Diego, CA, USA) following the manufacturer low sample protocol. NucleoMag NGS Clean-up and Size Select magnetic beads (Macherey-Nagel, Düren, Germany) were used in place of AMPure XP magnetic beads (Agencourt, Beverly, MA, USA) for sample purification. Androgynophore libraries were normalized, pooled, and sequenced with a HiSeq 2500 System (Illumina, San Diego, CA, USA) by The Centre for Applied Genomics (TCAG) at the Hospital for Sick Children (Toronto,

Ontario, Canada). Filaments and gynophore libraries were normalized, pooled, and sequenced with a HiSeq X System (Illumina) by Canada's Michael Smith Genome Sciences Centre at BC Cancer (Vancouver, British Columbia, Canada). Both the HiSeq 2500 and HiSeq X have low error and variation rates, and error rates tend to be consistent within lab group (Stoler and Nekrutenko 2021).

5.2.6 Transcriptome assembly and analyses

Raw reads were trimmed with Trim Galore! (version 0.6.6) (Krueger, 2012), quality checked with FastQC (version 0.11.9) (Andrews, 2010), and assembled together *de novo* using Trinity (version 2.12.0) (Grabherr *et al.* 2011). A principal component analysis (PCA) was conducted on transcript counts using the 'PtR' script provided with Trinity to ensure no batch effects were introduced by the different sequencing platforms. Benchmarking Universal Single Copy Orthologs (BUSCO) (version 5.1.2) (Simão *et al.* 2015) with the Brassicales library (version 10) (Manni et al., 2021) was used to assess transcriptome assembly completeness. *Gynandropsis gynandra* and *A. thaliana* are housed in the closely related sister families Cleomaceae and Brassicaceae (Brassicales) (Bayat *et al.* 2018). Owing to the recent radiation of these families (Cardinal-McTeague *et al.* 2016), we utilized the wealth of *A. thaliana* genomic data for our transcriptome analyses. As such, the transcriptome was annotated using the Araport11 cDNA database (Cheng *et al.* 2017) and the BLASTn algorithm (version 2.6.0) (Altschul *et al.* 1990) with default parameters. Pairwise differential expression analysis of Trinity transcripts between all combinations of structures and developmental stages was performed using edgeR (version 3.32.1) (Robinson *et al.* 2010). Transcripts with a false discovery rate (FDR) less than 0.001 and fold change greater than ± 4 were classified as significantly differentially expressed; a strict significance threshold was used to reduce the potential of type I errors. *Z*-score heatmaps of transcripts with significant differential expression were generated using the 'analyze_diff_expr.pl' script provided with Trinity and the 'gplots' R package.

Given that the androgynophore is a novel structure, we explored genes for floral organ identity genes and organ development and growth genes. Although gene expression does not provide evidence of homology, it is useful for forming hypotheses. As such, expression of A-class *APETALLA1* and *2* (*AP1*, *AP2*), B-class *APETALLA3* (*AP3*) and *PISTILLATA* (*PI*), C-class *AGAMOUS* (*AG*), and E-class *SEPALLATA1–4* (*SEP1–4*) genes was evaluated. A-class genes

specify sepals, A- and B- class genes specify petals, B- and C- class genes specify stamens, the C-class gene specifies carpels, and E-class genes are required for development of petals, stamens, and carpels (Pelaz *et al.* 2000). In addition, we reviewed the literature for *A. thaliana* genes involved in organ development and growth, including cell division and expansion. Expression heatmaps of floral organ identity genes and candidate androgynophore elongation genes were generated using the 'gplots' R package. Transcripts with the highest bit score and lowest E-value were selected as representatives for the genes of interest. Transcripts with expression below 10 transcripts per millions (TPM), averaged across replicates, for all developmental stages were excluded from further analyses to reduce transcriptional noise. It is possible that potential paralogs were missed by using representative transcripts. However, whole genome analyses between *T. houtteana* and Brassicaceae reveal that overall *T. houtteana* retains single copies of floral organ identity genes with exception of a tandem duplicate B-class *ThAP3* (Cheng *et al.* 2013). Further, *Tarenaya* and *Gynandropsis* share the same genome triplication event (Mabry *et al.* 2020). Candidate androgynophore elongation genes include representative transcripts that are significantly differentially expressed between at least one pairwise comparison of the androgynophore developmental stages. Transcripts were excluded if they are not significantly upregulated in the bud or intermediate stage relative to the anthetic stage (i.e., a transcript that is not upregulated when the androgynophore is lengthening is unlikely to promote elongation).

Filtered fasta files containing transcripts with ≥ 10 TPM, averaged across replicates, were submitted to the Kyoto Encyclopedia of Genes and Genomes (KEGG) Automatic Annotation Server (KAAS) (Moriya *et al.* 2007) to observe transcript expression patterns related to plant hormone biosynthesis and signalling pathways. The single-directional best hit method, with databases for all available Brassicales species (except *Carica papaya*), was used to assign orthologs. *Arabidopsis thaliana*-specific KEGG pathways were summarized using Adobe Illustrator. Additionally, filtered fasta files for all structures and development stages were processed with 'TransDecoder.LongOrfs' and 'TransDecoder.Predict' (Haas *et al.* 2013). These files were submitted to the OrthoVenn2 web platform (Xu *et al.* 2019), using default parameters, for comparison of orthologous gene clusters. As we selected a suitable number of biological replicates (Liu *et al.* 2014), excluded transcripts with low expression from downstream analyses,

and designated a high fold change threshold, qPCR was not performed for our global gene expression investigation (Hughes 2009; Coenye 2021).

5.3 Results

5.3.1 Androgynophore rapidly elongates

We measured flower and androgynophore length throughout development to determine the rate of androgynophore elongation. The flower and androgynophore grow rapidly over 4–5 days (Fig. 5.3). On the first day of measurements, buds from 0.45 to 0.55 cm long were tagged. At this stage, the four petals, six stamens, and pistil are enclosed within the four closed sepals. The petals are partially visible between the sepals, the distal portion of the anthers are exserted above the petals, and the apex of the pistil can be viewed above the anthers, sometimes exserted slightly above the sepals (Fig. 5.4A). The average androgynophore length is 0.05 ± 0.01 cm (SD). On the second day, the bud length ranges from 0.75 to 1.35 cm. The anthers and pistil are partially or entirely exserted above the closed sepals and petals (Fig. 5.4B). The average androgynophore length increased by a factor of 3.6 to 0.18 ± 0.05 cm (SD). On the third day, flower length ranges widely from 1.15 to 3.90 cm and reached one of two stages: (1) sepals and petals remain closed, anthers and pistil are exserted, and gynophore and filaments are partially protruding above the petals (Fig. 5.4C), or, (2) sepals are open, petals are involute with margins rolled inward and are oriented adaxially, stamens are splayed apart and oriented adaxially with undehisced anthers, and the androgynophore is visible (Fig. 5.4D). Again, the average androgynophore length increased by a factor of 3.6 to 0.64 ± 0.19 cm (SD). On the fourth day, the flower length ranges from 3.40 to 4.70 cm. The flower has reached one of two stages, stage 2 mentioned for the third day with involute petals and immature anthers (Fig. 5.4D); or anthesis in which petals are open and anthers have dehisced to reveal pollen (Fig. 5.4E). The rate of androgynophore growth slowed, with the average androgynophore length increasing by a factor of 1.6 to 1.01 ± 0.04 cm (SD). On the final day of measurements, the flower length ranges from 3.80 to 5.25 cm. The flower has reached anthesis or has begun to senesce with petals and stamens beginning to wilt and fall off (Fig. 5.4E). Flowers that displayed signs of senescence were excluded from measurements, as fruit development may have begun to take place, resulting in longer flower lengths. The average androgynophore length remains relatively stable at 1.06 ±

0.02 cm (SD). Overall, the androgynophore rapidly elongates by approximately 1 cm during floral development.

5.3.2 Androgynophore lengthens predominantly via cell elongation

To establish the mode of androgynophore elongation, we measured the length and width of epidermal cells from the distal, middle, and proximal sections of the androgynophore at the three developmental stages. Due to the dramatic increase in cell length, androgynophore lengthening can be primarily attributed to cell elongation rather than cell division. Androgynophore epidermal cells are roughly arranged in files parallel to the direction of elongation (Fig. 5.5A). At the bud stage, androgynophore epidermal cells range from square to rectangular with an average cell length of 15.00 ± 5.03 μm (SD) and width of 8.55 ± 1.67 μm (SD). As the flower develops, androgynophore epidermal cell length and width increase ($F_{(2, 208)}$ = 729.2, $P < 0.05$ and $F_{(2, 262)}$ = 140.9, $P < 0.05$, respectively), with cell length increasing more drastically than cell width resulting in elongated cells at the intermediate and anthetic stages. At the intermediate stage, the average epidermal cell length is 64.80 ± 24.65 μm (SD) and width is 11.49 ± 2.91 μm (SD). From bud to anthetic stage, average epidermal cell length increased by a factor of 9.3 to 139.27 ± 50.26 μm (SD) and width by a factor of 1.7 to 14.10 ± 4.32 μm. All median cell measurements fall within one standard deviation of the mean.

For the bud and intermediate stages, epidermal cells ascend in length from the distal section to the proximal section of the androgynophore ($F_{(2, 95)}$ = 11.0, $P < 0.05$ and $F_{(2, 147)}$ = 40.8, $P <0.05$, respectively), though the Games-Howell *post hoc* test revealed the cell lengths between distal and middle sections of the bud stage are not statistically different (Table 5.1). The epidermal cell lengths of the anthetic stage also differ between sections ($F_{(2, 91)}$ = 35.7, $P < 0.05$), with the middle section having the longest cells rather than the proximal section. This difference in trend may be attributed to misidentification of cell edges at the proximal section of the anthetic stage where it is challenging to discern tapered cells from those that weave below adjacent cells (Fig. 5.6). These woven cells primarily occur at the proximal section of the anthetic stage.

The average androgynophore length and number of epidermal cells in a file along the length of the androgynophore are approximately 0.06 cm with 41.7 cells for the bud stage, 0.34 cm with 53.1 cells for the intermediate stage, and 1.03 cm with 73.5 cells for the anthetic stage.

If the estimated 73.5 cells for the anthetic stage androgynophore remained the same length as in the bud stage and did not elongate throughout development, these cells would account for about 10% of the anthetic stage androgynophore length. Therefore, the expansion of these cells is responsible for the remaining 90% of the anthetic stage androgynophore length, making cell elongation the leading contributor to androgynophore lengthening. Furthermore, the average number of epidermal cells in a file may have been overestimated for the anthetic stage androgynophore due to the previously mentioned woven cells.

The surface of the androgynophore epidermal cells have wrinkles, perhaps cuticular ridges, apparent in the bud and intermediate stages and less prominent in the anthetic stage (Fig. 5.5A). Epidermal cells with a wrinkled surface are also present at the proximal region of the stamens and the apex of the receptacle at the bud and intermediate stages. However, elongated epidermal cells are unique to the androgynophore in comparison to epidermal cells of the adjacent tissue, with rounded cells at the basal area of the stamens and cells with finger-like protrusions at the apical portion of the receptacle (Fig. 5.5B, C). In addition, stomata are common at the base of the stamens but are rarely found on the androgynophore and receptacle apex (Fig. 5.5B).

5.3.3 Androgynophore internal anatomy is uniform

We prepared histological sections of the androgynophore at the bud, intermediate and anthetic stages to characterize its internal anatomy throughout development. In terminology consistent with eudicot stems for ease of description, the androgynophore anatomical organization consists of an epidermis, cortex, vascular cylinder, and pith. The vasculature is unchanging throughout the majority of the androgynophore with a vascular cylinder of closely packed vascular bundles supplying the stamens and gynophore (Fig. 5.7A, B). At the distal section of the androgynophore, below the filaments, the vasculature begins to acropetally diverge, forming a six-lobed flower shape (Fig. 5.7C). Immediately below the filaments, the vascular bundles are separated into an inner ring supplying the gynophore and six outer groups, each consisting of three bundles, supplying the stamens (Fig. 5.7D). The six outer vascular groups depart with the filaments, with three vascular bundles supplying each stamen, leaving the gynophore with a ring of vascular bundles (Fig. 5.7E, F). These vascular patterns are consistent between developmental stages (Appendix 5.1).

5.3.4 Androgynophore transcript expression is dynamic throughout development and is more similar to that of the gynophore than filaments

To explore gene expression patterns throughout androgynophore development and between the androgynophore and other stalk-like floral structures, we performed RNA-sequencing on the androgynophore at bud, intermediate, and anthetic stages and the filaments and gynophore at the anthetic stage. Read depth averaged to 20.9 million paired-end reads for the androgynophore samples and 19.1 million paired-end reads for the filaments and gynophore samples. Median Phred quality scores are minimally 32 per base position for each sample, indicating a base call accuracy of at least 99.9%. The assembled transcriptome has an average contig length of 1263.04, a total transcript count of 246,281 (Appendix 5.2), and 93.9% complete BUSCOs (Appendix 5.3). The PCA of transcript reads reveals defined clustering of replicates for each sample with 38.37% and 10.93% of the variance explained by PC1 and PC2, respectively (Fig. 5.8). There is no obvious trend indicating that sequencing platform is driving clustering.

The complete transcriptome contains 28,320 transcripts that are significantly differentially expressed between at least one pairwise comparison of structures and developmental stages. Differential expression analysis of the complete transcriptome revealed similar expression patterns for the androgynophore at bud and intermediate stages, which are opposite of anthetic stage filament expression (for example, transcripts upregulated in filaments are generally downregulated in the developing androgynophore) (Fig. 5.9A). The anthetic stage androgynophore and gynophore share a mixture of expression with both anthetic stage filaments and the developing androgynophore. Consistent with the *z*-score expression patterns, the anthetic stage androgynophore and gynophore share the most orthologous gene clusters (2309) relative to the anthetic stage androgynophore and filaments (402), and the anthetic stage gynophore and filaments (834) (Fig. 5.10A). In line with its unique *z*-score expression profile, the anthetic stage filaments also have the most unique orthologous clusters (184) relative to the anthetic stage androgynophore (50) and gynophore (29) (Fig. 5.10A). When the androgynophore is examined separately, there are 7062 significantly differentially expressed transcripts for the three developmental stages (Fig. 5.9B). Typically, when a transcript is upregulated in the androgynophore anthetic stage it is downregulated in both the bud and intermediate stages, and vice-versa. However, a cluster of genes are uniquely upregulated in only bud or intermediate stage androgynophores (Fig. 5.9B). The bud and intermediate stage androgynophore share the

greatest orthologous gene clusters (1148), followed by the intermediate and anthetic stage androgynophore (1060) (Fig. 5.10B). Both comparisons contain clusters associated with the gene ontology (GO) biological processes: growth, cell growth, cell division, and cell wall organization. In addition, clusters associated with cell proliferation are shared between the bud and intermediate stage androgynophore but not the intermediate and anthetic stage androgynophore.

5.3.5 Floral organ identity genes and candidate elongation genes are expressed in the developing androgynophore

As the androgynophore is a novel floral structure, we investigated the expression of representative transcripts for floral organ identity genes, throughout development and between adjacent stalk-like structures. Unlike the expression patterns for all significantly differentially expressed transcripts (Fig. 5.9), the expression of floral organ identity genes is more similar between the anthetic stage androgynophore and filaments than the anthetic stage androgynophore and gynophore (Fig. 5.11A). The A-class gene *GgAP1* has less than 10 TPM in all structures except the intermediate stage androgynophore, where expression is slightly higher than the cut-off (11.3 TPM), while *GgAP2* is not expressed in any structure or developmental stage. The B- and C-class genes (*GgAP3*, *GgPI*, and *GgAG*) are significantly differentially expressed with expression lowest in the anthetic stage gynophore. B-class genes (*GgAP3* and *GgPI*) have the highest expression in the developing androgynophore, while the C-class gene (*GgAG*) has the highest expression in the bud stage androgynophore and anthetic stage filaments. Of the E genes (*GgSEP1–4*), which form essential protein tetramers to control floral organ identity (Theißen, 2001), only *GgSEP4* is significantly differentially expressed with expression lowest in the intermediate stage androgynophore and anthetic stage filaments. Altogether, floral organ identity gene expression differs between the androgynophore and the adjacent stalk-like floral structures.

To identify genes putatively involved in androgynophore elongation, we examined the expression of representative transcripts for genes with known functions in *A. thaliana* organ development and growth, throughout androgynophore development. Twelve genes were classified as candidates for the control and regulation of androgynophore elongation (Table 5.2). These genes have the highest expression in the bud or intermediate stage, while the androgynophore is rapidly elongating and lowest expression in the anthetic stage when the

androgynophore is no longer lengthening (Fig. 5.11B). Genes involved in organ growth via cell proliferation (*AN3* and *ER*) (van Zanten *et al.* 2009; Horiguchi *et al.* 2011) are upregulated in the bud stage androgynophore relative to intermediate and anthetic stages. In contrast, genes associated with organ growth via cell expansion (*BDX*, *LNG1*, and *LNG2*) (Lee *et al.* 2018; Salazar-Iribe *et al.* 2018) are upregulated in the intermediate stage androgynophore relative to the bud and anthetic stages. These genes are involved in cell expansion through cell wall loosening (BDX) and increasing vacuolar water uptake (*LNG1* and *LNG2*) (Lee *et al.* 2018; Salazar-Iribe *et al.* 2018).

Other genes that are significantly differentially expressed in the androgynophore and involved in *A. thaliana* structural elongation include *GASA4*, *IAA19*, *MYB21*, and *MYB24* (Chen *et al.* 2007; Cheng *et al.* 2009; Ghelli *et al.* 2018); although their specific effect on cell proliferation versus cell expansion has not been investigated, the expression or function of each is related to plant hormones. *SWEET13* is another gene associated with plant hormones, specifically gibberellin transport (Kanno *et al.* 2016), which has diminishing expression as the androgynophore elongates. As the androgynophore subtends and contains vasculature supplying both stamens and pistil, expression of genes associated with organ fusion was also explored. Although the androgynophore develops as a unit, *DCR* and *HTH*, genes involved in *A. thaliana* post-genital fusion (Krolikowski *et al.* 2003; Panikashvili *et al.* 2009), are significantly differentially upregulated in the developing androgynophore. This expression pattern implies that they may play a role in androgynophore development. Of note, many genes commonly mentioned for their role in *A. thaliana* organ development and growth do not meet our criteria for candidate androgynophore elongation genes including *ANGUSTIFOLIA* (*AN*), *AINTEGUMENTA* (*ANT*), *AINTEGUMENTA-LIKE6/PLETHORA3* (*AIL*/*PLT3*), *AUXIN RESPONSE FACTOR6* and *8* (*ARF6*, *ARF8*), *AUXIN-REGULATED GENE INVOLVED IN ORGAN SIZE* (*ARGOS*), *JAGGED* (*JAG*), and *KLUH* (*KLU*) (Anastasiou and Lenhard 2007; Bögre *et al.* 2008; Cardarelli and Cecchetti 2014) (Appendix 5.4). Even if the conditions are less stringent (FDR > 0.05, FC > 2), these genes would not meet the criteria.

5.3.6 Plant hormones play a role in androgynophore development

To elucidate the potential involvement of plant hormones in androgynophore elongation, we investigated the expression of genes involved in plant hormone biosynthesis and signalling

throughout androgynophore development. Although many questions remain unanswered regarding auxin biosynthetic pathways, genes known to play a role in tryptophan-dependent auxin biosynthesis are expressed when the androgynophore is rapidly elongating at the bud and intermediate stages (Fig. 5.12A). Only genes involved in the first step (*TAA1*, *TAR1*, *TAR2*) of the two-step indole-3-pyruvate (IPA) pathway, the primary auxin biosynthetic pathway in *A. thaliana* (Kasahara 2016; Morffy and Strader 2020), are expressed in the androgynophore. Rather than directly convert IPA to indole-3-acetic acid (IAA/auxin), IPA may be converted to indole-3-acetaldehyde (ALDH) then IAA. However, the gene responsible for converting IPA to ALDH is unknown. In addition, all genes in the auxin signalling pathway are expressed throughout androgynophore development (Fig. 5.12B). The binding of auxin to the auxin receptor TIR1 leads to degradation of the ARF-repressing protein AUX/IAA, allowing for DNA transcription and ultimately resulting in growth (Santner *et al.* 2009).

The genes involved in jasmonic acid biosynthesis are expressed throughout androgynophore development (Fig. 5.12F), whereas not all brassinosteroid and gibberellin biosynthetic pathway genes are expressed at any stage of androgynophore development (Fig. 5.12C, E). Due to the absence of brassinosteroid biosynthesis and the *BIN2* inhibitor BSU1, the brassinosteroid signalling pathway is inactive during androgynophore development (Fig. 5.12D). Despite the inactive brassinosteroid signalling pathway, *TCH4* is expressed in the anthetic stage androgynophore, and *CYCD3* is expressed throughout androgynophore development. However, transcription of these genes is also regulated by other plant hormones (Xu *et al.* 1995; Dewitte *et al.* 2007).

5.4 Discussion

The androgynophore of *G. gynandra* is remarkable as it is pronounced in length and elevation of the reproductive organs. Our study is the first on the developmental and genetic basis of the androgynophore in *G. gynandra*, expanding on previous *G. gynandra* floral morphology work which focused on flower morphs, symmetry, and vasculature (Raghavan 1939; Murty 1953; Karrer 1991; Patchell *et al.* 2011; Zohoungbogbo *et al.* 2018). We showed that *G. gynandra* androgynophore growth is characterized by rapid cell elongation, uniform internal anatomy, and complex gene expression patterns throughout development including differential expression of floral organ identity genes and genes involved in organ development and growth.

5.4.1 Androgynophore structure and elongation

The androgynophore is a relatively uniform structure, which elongates quickly, primarily through cell expansion, during floral development. Androgynophore lengthening via cell expansion is consistent with stalk-like floral structures of other Cleomaceae species. In the ornamental species, *T. houtteana*, filament elongation is due to cell expansion (Koevenig 1973). Likewise, in *S. rutidosperma*, vessel elements extend with the elongating androgynophore and gynophore (Dattagupta and Datta 1976). The androgynophore is a cylindrical structure with elongated cells from base to apex and an epidermis that has no structural indicators of adaxial and abaxial surfaces (Fig. 5.5). Though, the woven cells at the proximal section of the anthetic stage and the vasculature divergence near the filaments in the distal section act as subtle structural references to the proximal-distal axis of the androgynophore. The diverging staminal vasculature has been a point of disagreement in previous histological studies, with Murty (1953, p. 119) asserting Raghavan (1939) finding of three vascular strands supplying each stamen as "obviously incorrect". However, there appears to be three closely grouped vascular bundles for each stamen, particularly noticeable at the apex of the androgynophore (Fig. 5.7D), in agreement with the finding of Raghavan (1939).

The structural uniformity may not contribute to the intrigue of this novel floral feature, yet the fast increase in cell length makes the androgynophore a compelling model for rapid cell elongation. From bud stage to anthetic stage, the androgynophore experiences a 9.3-fold increase in average epidermal cell length (Table 5.1); a drastic expansion in comparison to the 3-fold increase in cell lengths of the *A. thaliana* inflorescence stem during internode elongation (Serrano-Mislata and Sablowski 2018). Although significant progress has been made in identifying factors involved in plant growth (reviewed by Anastasiou and Lenhard 2007; Bögre et al. 2008; Hepworth and Lenhard 2014), many outstanding questions remain. Further research to discover the molecular mechanisms of genetic controls and unravel the intricate genetic networks and complex roles of plant hormones is crucial for advancing our understanding of plant growth. Organs that have been focal for cell division and expansion studies include petals and leaves (reviewed by Irish 2008; Gonzalez *et al.* 2012; Kalve *et al.* 2014; Huang and Irish 2016). However, the distinct adaxial and abaxial surfaces and multiple or intricate cell shapes add to the complexity of petal and leaf cell expansion. For example, *A. thaliana* has petals with conical cells on the adaxial surface and more irregularly shaped cells on the abaxial surface and

leaves with complex jigsaw shaped cells (Irish 2008; Gonzalez *et al.* 2012). In addition, disentangling the factors influencing cell division and expansion is challenging due to the interconnection of these processes in leaf and petal growth (Gonzalez *et al.* 2012; Huang and Irish 2016). Unlike petals and leaves, the androgynophore is radially symmetric and its rapid growth is predominantly due to cell expansion in one axis to produce elongate cells. This reduction in confounding factors elevates the androgynophore as a more tractable model for cell expansion. The hypocotyl of *A. thaliana* is another proposed model for cell elongation as cell division does not contribute to its growth after germination (Boron and Vissenberg 2014). The morphological similarity between the androgynophore and hypocotyl as elongate cylindrical structures, allows for comparisons to uncover unifying factors contributing to cell elongation across structures and taxa.

5.4.2 Genetic mechanisms controlling androgynophore growth

Although androgynophore function in *G. gynandra* has not been investigated, research on other taxa indicates that the androgynophore plays a role in pollinator interactions. Investigation of four *Passiflora* species suggest pollinator-triggered movement of the androgynophore aids in cross-pollination (Scorza and Dornelas 2014). In another species of *Passiflora*, the androgynophore is oriented to facilitate access to nectar, while providing ideal reproductive organ positioning for pollinator contact (Rocha *et al.* 2015). Likewise, in *Emblingia calceoliflora* (Emblingaceae), the androgynophore lifts the reproductive organs near the entrance of the corolla to allow for contact as the pollinator enters to reach the nectary at the base of the androgynophore (Tobe 2015). The likely association with pollinator interactions suggest the androgynophore of *G. gynandra* is under tight regulation to ensure the reproductive organs are elevated appropriately for pollinator contact.

The androgynophore has dynamic transcript expression, not only compared to the other stalk-like floral structures but throughout its development, with many transcripts upregulated during its elongation compared to at anthesis. These upregulated transcripts include representatives for 12 candidate androgynophore elongation genes with known roles in *A. thaliana* organ development and growth (Table 5.2). Candidate androgynophore elongation genes include those that influence the growth of *A. thaliana* leaves (Horiguchi *et al.* 2011; Lee *et al.* 2018) and structures morphologically similar to the androgynophore such as the stem,

filaments, and hypocotyl (Chen *et al.* 2007; van Zanten *et al.* 2009; Cheng *et al.* 2009; Salazar-Iribe *et al.* 2018; Ghelli *et al.* 2018). These candidate genes are homologous to those that effect organ growth in *A. thaliana* through cell proliferation (*GgAN3* and *GgER*) and cell expansion (*GgBDX*, *GgLNG1*, and *GgLNG2*). Other candidate genes (*GgGASA4*, *GgIAA19*, *GgMYB21*, *GgMYB24*, and *GgSWEET13*) require further research into their impact on cell proliferation versus cell expansion in organ growth. In addition, several candidate androgynophore elongation genes (*GgBDX*, *GgGASA4*, *GgIAA19*, *GgMYB21*, *GgMYB24*, and *GgSWEET13*) are homologous to those associated with plant hormones in *A. thaliana* (Table 5.2) and numerous genes involved in plant hormone biosynthesis and signalling are expressed throughout androgynophore development (Fig. 5.12). Though complex interactions of multiple plant hormones play a key role in organ development and growth, their biosynthesis, transport, signalling, and connection to plant growth are still being uncovered (Santner *et al.* 2009; Wessinger and Hileman 2020).

Investigations on Cleomaceae are facilitated by the transfer of knowledge from the well-studied model species *A. thaliana*. Yet, gene function may not be consistent between species as the genomic context differs (Kramer 2015). Several genes often associated with organ development and growth in *A. thaliana*, including *AN*, *ANT*, *AIL/PLT3*, *ARF6*, *ARF8*, *ARGOS*, *JAG*, and *KLU*, did not meet our criteria for candidate androgynophore elongation genes, implying the function of these genes may not be conserved across families and alternative factors may act as key regulators of cell elongation in the androgynophore. These possible deviations from *A. thaliana* emphasize the importance of functional studies to establish the link between genotypic and phenotypic expression in a range of taxa. An advantage to *G. gynandra* research is the established transformation protocol (Newell *et al.* 2010), a prerequisite for the CRISPR/Cas9 gene editing approach to functional studies; though alternative methods of delivering CRISPR-Cas9 gene editing reagents are being explored (Nadakuduti and Enciso-Rodríguez 2021). Another functional study approach is virus-induced gene silencing (VIGS), a post-transcriptional gene silencing technique with an optimized protocol for the closely related *Cleome violacea* (Cleomaceae) (Carey *et al.* 2021). However, the amenability of *G. gynandra* to VIGS has not been investigated. With multiple genes likely contributing to androgynophore development and growth, such is the case with stamens in *A. thaliana* (Cardarelli and Cecchetti 2014) and nectar spurs in *Aquilegia* (Zhang *et al.* 2020; Ballerini *et al.* 2020), the influence of each candidate gene on phenotype could be explored through functional studies. Of the candidate genes, the roles of

GgAN3, *GgIAA19*, *GgMYB21*, *GgMYB24*, and *GgSWEET13* in androgynophore elongation are of particular interest for functional studies as their expression is high in the bud or intermediate stage (60 to 283 TPM) and less than 10 TPM in the anthetic stage (Fig. 5.11B; Appendix 5.4).

5.4.3 What is the androgynophore?

As a uniform cylindrical feature, the androgynophore resembles a stem or inflorescence internode, but differs by its incorporation within the flower. Unlike many other elaborations of floral form (for example, staminodes and nectar spurs), the novel structure of the androgynophore does not appear to be derived from lateral organs. Considering its placement within the flower, floral organ identity genes are expressed in the androgynophore throughout development. With the expression of *GgAP3* and *GgPI* (specifies stamens), *GgAG* (specifies carpels), and *GgSEP1–4* (required for development of stamens and carpels), the androgynophore carries the genetic repertoire for the reproductive organs it subtends, assuming conservation in function of floral organ identity genes. The overall transcript expression pattern is most similar between the androgynophore and gynophore. Both the androgynophore and gynophore appear to be internodes within the flower; whether these features are derived from receptacle or reproductive tissue has had little speculation. We propose that the androgynophore is an elaboration of the receptacle and reproductive structures as it shares attributes with both floral features. The androgynophore appears to be homologous with the receptacle and reproductive structures in the following ways: (1) The androgynophore and receptacle are not lateral floral features, (2) the vasculature arrangement of the androgynophore is consistent with that of other non-lateral structures (for example, eudicot stem internodes) (Fig. 5.7), and (3) B-, C-, and E-class floral organ identity genes, necessary for stamen and carpel development in *A. thaliana*, are expressed throughout androgynophore development. Our study suggests that the receptacle may be overlooked in its contribution to floral diversity as the androgynophore could be modified receptacle. However, additional research on the receptacle is required for comparison; for instance, is the expression of floral organ identity genes also shared between the androgynophore and receptacle?

5.5 Conclusions

Although flowers are a fundamental component of pollination biology, research on *G. gynandra* flower developmental morphology and genetics is lacking. Extensive floral development research established *Aquilegia* as a model system to enrich our understanding of floral diversity and evolution with focus on petaloid sepals, nectar spurs, and staminodes (Kramer 2009). As with *Aquilegia*, *G. gynandra* possesses floral features absent from *A. thaliana*, including the androgynophore and gynophore. Our thorough morphological descriptions and high-quality transcriptome for *G. gynandra* provide the foundation for further androgynophore research to address outstanding questions. With androgynophores seemingly involved in pollination, such is the case with multiple *Passiflora* species (Scorza and Dornelas 2014; Rocha *et al.* 2015), the pronounced androgynophore of *G. gynandra* appears to be a solution for increasing the chance of pollinator and reproductive organ contact. Additional research is needed to identify the factors essential for inducing androgynophore formation and determine if gene co-option plays a role in the development of this novel floral structure.

5.6 Tables

Table 5.1. Mean (± SD) epidermal cell length and width ($N = 50$) at three developmental stages in three sections of the *Gynandropsis gynandra* androgynophore.

Stage	Section	Length (μm)	Width (μm)
Bud	Distal	13.27 ± 4.63	8.47 ± 1.55
	Middle	13.95 ± 3.57	7.97 ± 1.59
	Proximal	17.78 ± 5.54	9.21 ± 1.67
Intermediate	Distal	45.89 ± 21.29	11.04 ± 2.25
	Middle	66.85 ± 19.72	10.41 ± 2.44
	Proximal	81.66 ± 18.62	13.01 ± 3.30
Anthetic	Distal	104.90 ± 29.00	14.07 ± 3.08
	Middle	169.44 ± 49.63	13.27 ± 3.80
	Proximal	144.06 ± 47.76	14.96 ± 5.61

Table 5.2. Summary of the role of candidate *Gynandropsis gynandra* androgynophore elongation genes in *Arabidopsis thaliana* development.

Gene	Abbreviation	Function in *Arabidopsis thaliana*	Reference(s)
ANGUSTIFOLIA3	*AN3*	Leaf blade expansion Cell proliferation	Horiguchi *et al.* 2011
BIIDXI	*BDX*	Hypocotyl cell elongation Cell wall expansion via regulation of pectin methyl esterification Cell expansion via regulation of auxin flux	Salazar-Iribe *et al.* 2018
DEFECTIVE IN CUTICULAR RIDGES	*DCR*	Involved in growth, development, and post-genital organ fusion Cuticle biosynthesis	Panikashvili *et al.* 2009
ERECTA	*ER*	Inflorescence stem and pedicel elongation Cell proliferation via cell cycle regulation	van Zanten *et al.* 2009
GIBBERELLIC ACID-STIMULATED ARABIDOPSIS4	*GASA4*	Hypocotyl elongation May influence gibberellin metabolism	Chen *et al.* 2007
HOTHEAD	*HTH*	Regulates post-genital organ fusion Modulates cuticle properties	Krolikowski *et al.* 2003
INDOLE-3-ACETIC ACID INDUCIBLE19	*IAA19*	Hypocotyl and filament elongation Controlled by auxin levels	Ghelli *et al.* 2018
LONGIFOLIA1, 2	*LNG1*, *LNG2*	Leaf length/longitudinal cell elongation Cell expansion via turgor pressure regulation	Lee *et al.* 2018
MYELOBLASTOSIS21, *24*	*MYB21*, *MYB24*	Filament elongation Acts downstream of gibberellin and jasmonic acid	Cheng *et al.* 2009
SWEET13	*SWEET13*	Regulates seedling and seed development Mediates gibberellin transport	Kanno *et al.* 2016

5.7 Figures

Figure 5.1. *Gynandropsis gynandra* inflorescence. Red arrowhead points to an androgynophore. Scale bar represents 1.0 cm.

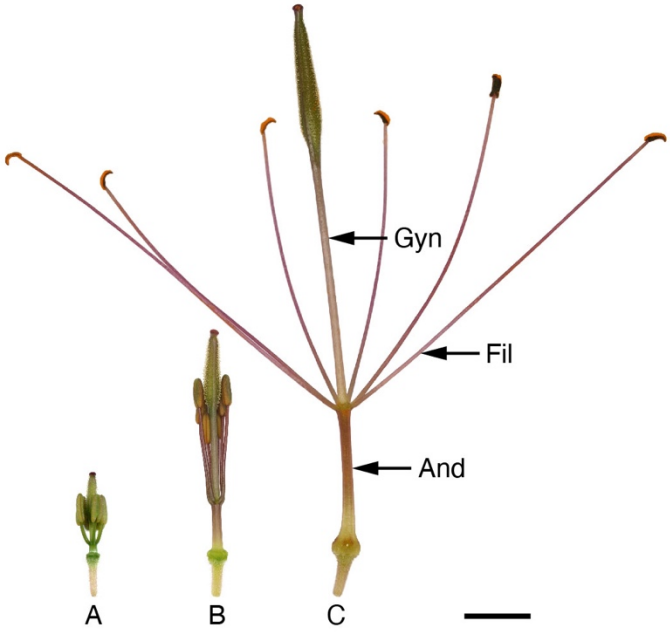

Figure 5.2. Three developmental stages of *Gynandropsis gynandra*. (A) Bud stage. (B) Intermediate stage. (C) Anthetic stage. And: androgynophore; Fil: filaments; Gyn: gynophore. Scale bar represents 0.5 cm.

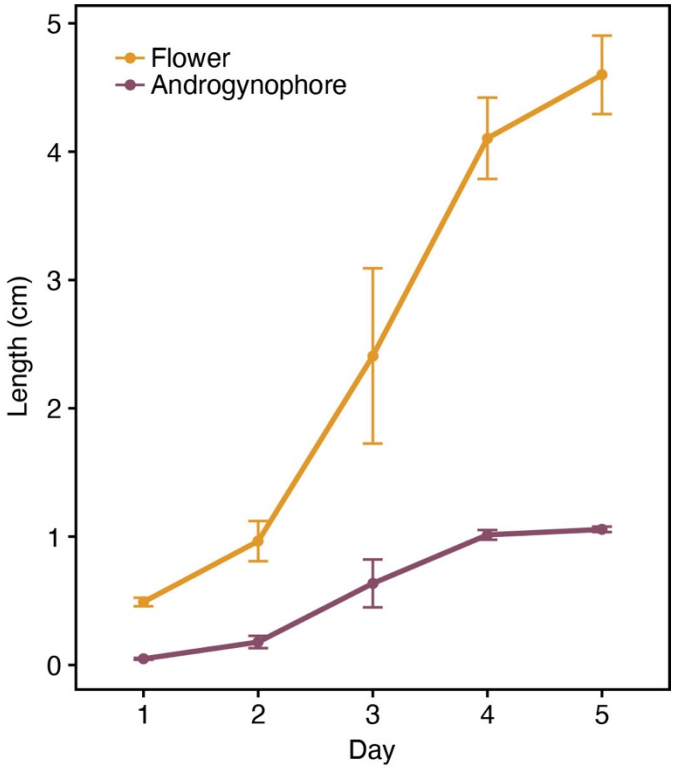

Figure 5.3. Growth curves of *Gynandropsis gynandra* flower and androgynophore length based on daily flower length measurements ($N = 50$) and corresponding calculated androgynophore lengths. Error bars represent standard deviation.

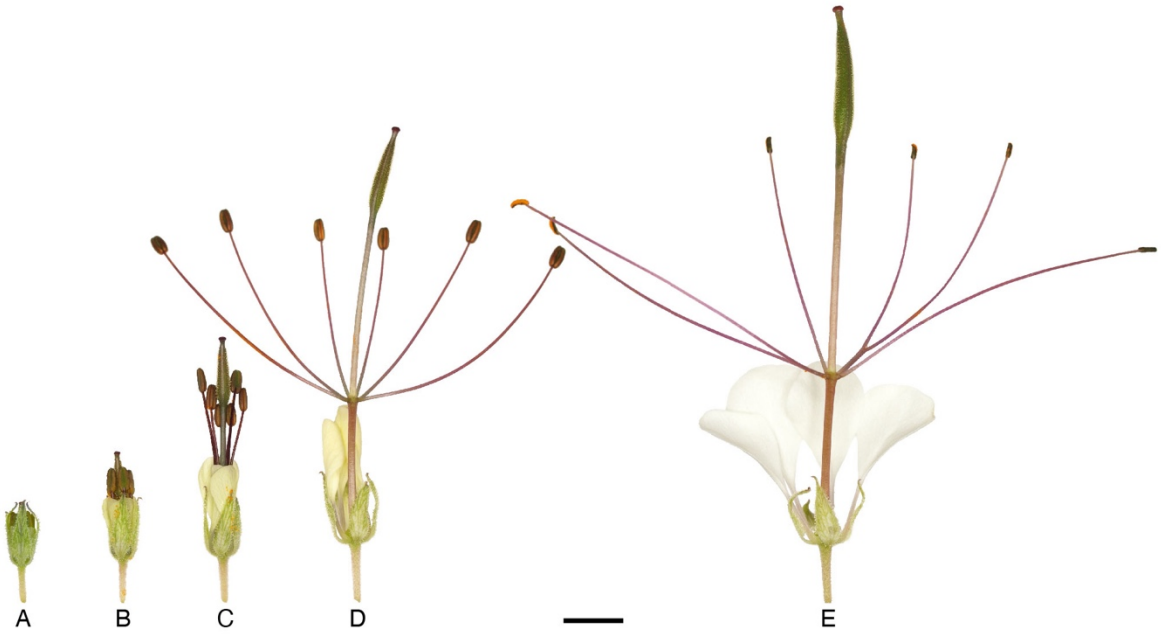

Figure 5.4. *Gynandropsis gynandra* floral development over 5 days. (A) Day 1. (B) Day 2. (C) Day 3. (D) Day 3 or 4. (E) Day 4 or 5. Scale bar represents 0.5 cm.

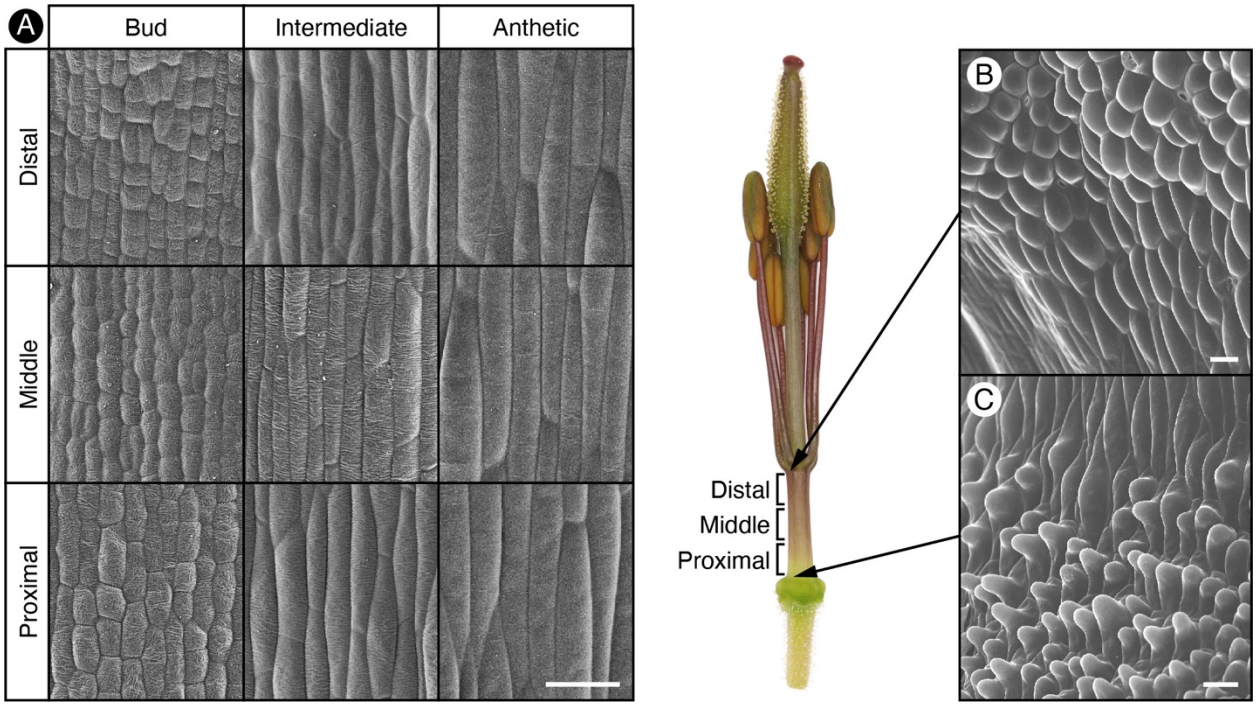

Figure 5.5. Scanning electron micrographs of *Gynandropsis gynandra* androgynophore epidermal cells at three developmental stages. (A) Proximal, middle, and distal androgynophore sections (rows) for bud, intermediate, and anthetic stages (columns). (B) Transition between

androgynophore and stamens at the anthetic stage. (C) Transition between androgynophore and receptacle at the intermediate stage. Scale bars represent 30 μm.

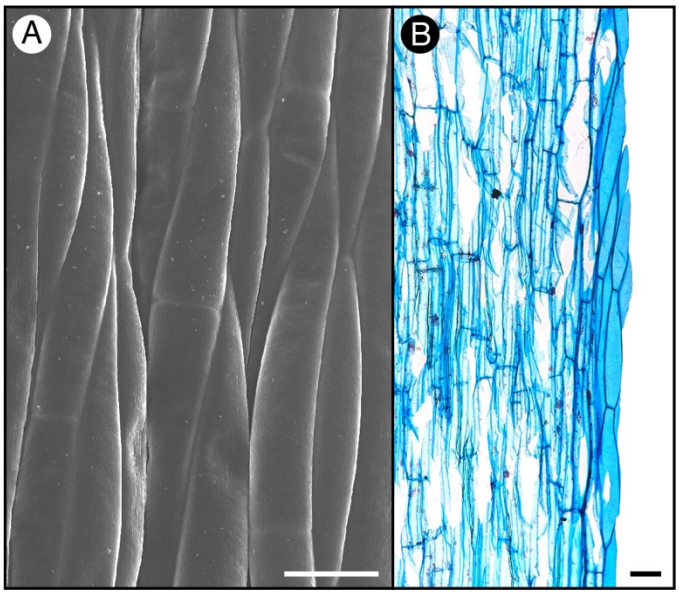

Figure 5.6. Woven epidermal cells of *Gynandropsis gynandra* proximal androgynophore section at the anthetic stage. (A) Scanning electron micrograph. (B) Alcian blue/safranin O-stained section. Scale bars represent 30 μm.

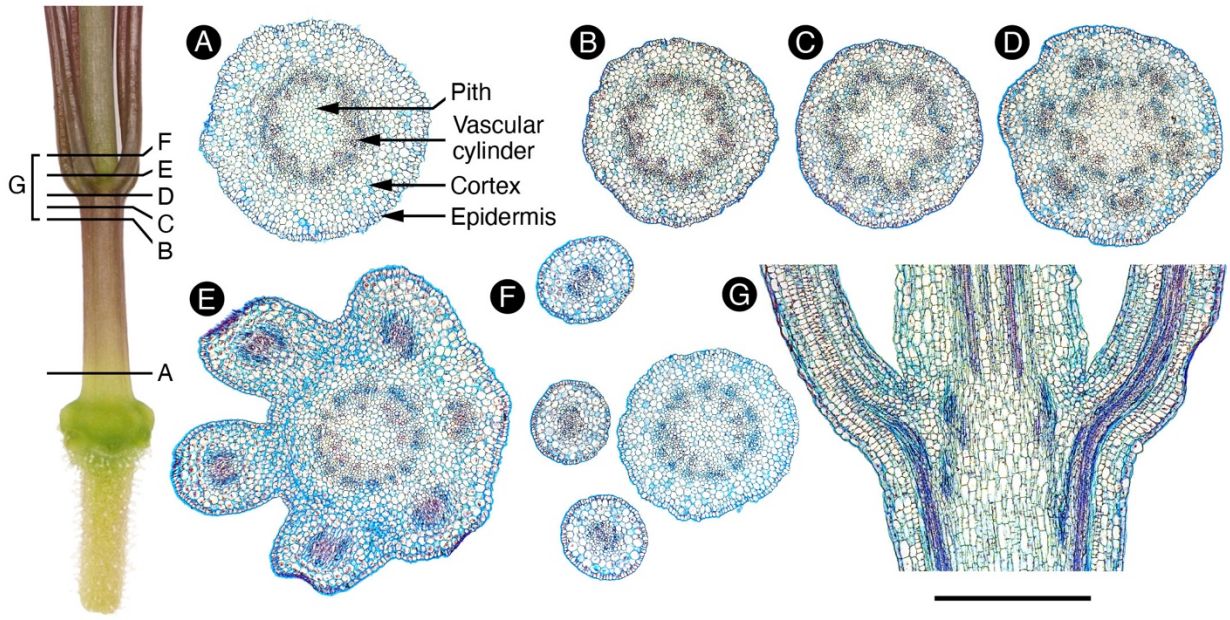

Figure 5.7. Alcian blue/safranin O-stained sections of *Gynandropsis gynandra* androgynophore at the intermediate stage. (A-D) Transverse sections of the androgynophore. (E) Transverse section at the base of the gynophore and filaments. (F) Transverse section of the gynophore and filaments (three filaments are not shown). (G) Longitudinal section of the androgynophore, gynophore, and filaments. Scale bar represents 0.5 mm.

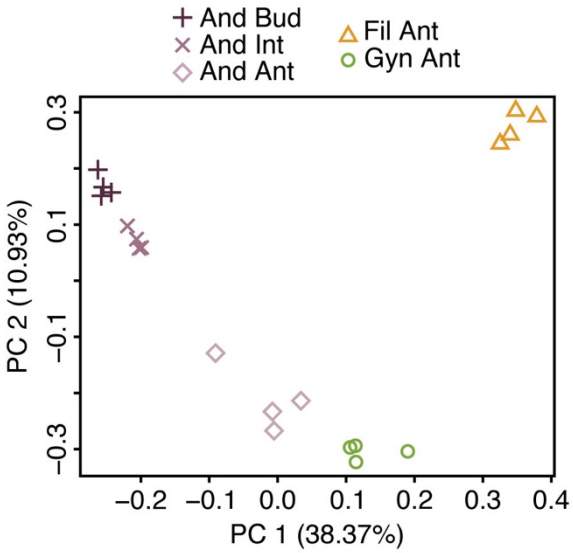

Figure 5.8. Principal component analysis of *Gynandropsis gynandra* transcript counts. And Bud: bud stage androgynophore; And Int: intermediate stage androgynophore; And Ant: anthetic stage androgynophore; Fil Ant: anthetic stage filaments; Gyn Ant: anthetic stage gynophore.

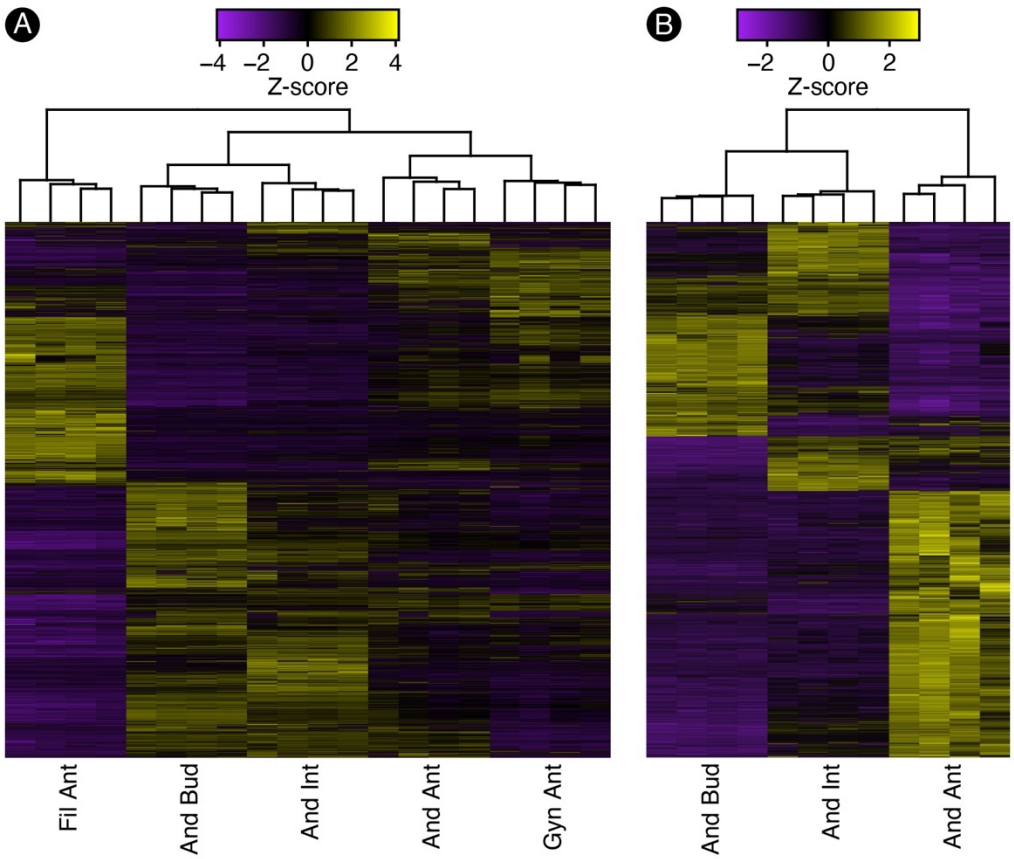

Figure 5.9. Heatmaps of significantly differentially expressed *Gynandropsis gynandra* transcripts expressed as *z*-scores. (A) Filaments and gynophore at the anthetic stage and androgynophore at the bud, intermediate, and anthetic stages ($N = 28{,}320$). (B) Androgynophore at the bud, intermediate, and anthetic stages ($N = 7062$). Columns represent replicates and rows represent transcripts. Fil Ant: anthetic stage filaments; And Bud: bud stage androgynophore; And Int: intermediate stage androgynophore; And Ant: anthetic stage androgynophore; Gyn Ant: anthetic stage gynophore.

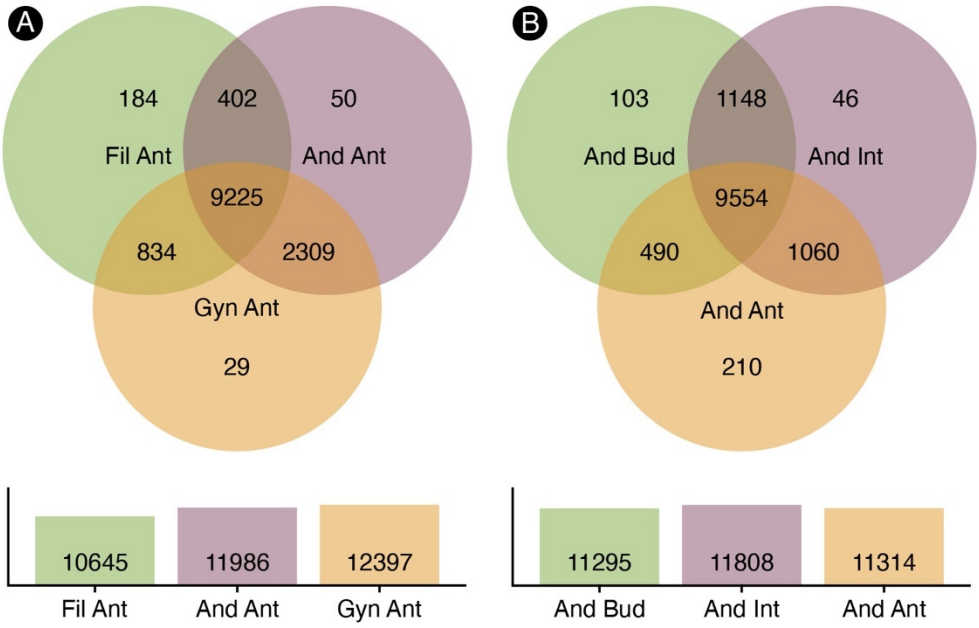

Figure 5.10. Venn diagrams of *Gynandropsis gynandra* orthologous gene clusters. (A) Filament, androgynophore, and gynophore at the anthetic stage. (B) Androgynophore at the bud, intermediate, and anthetic stages. And Bud: bud stage androgynophore; And Int: intermediate stage androgynophore; And Ant: anthetic stage androgynophore; Fil Ant: anthetic stage filaments; Gyn Ant: anthetic stage gynophore.

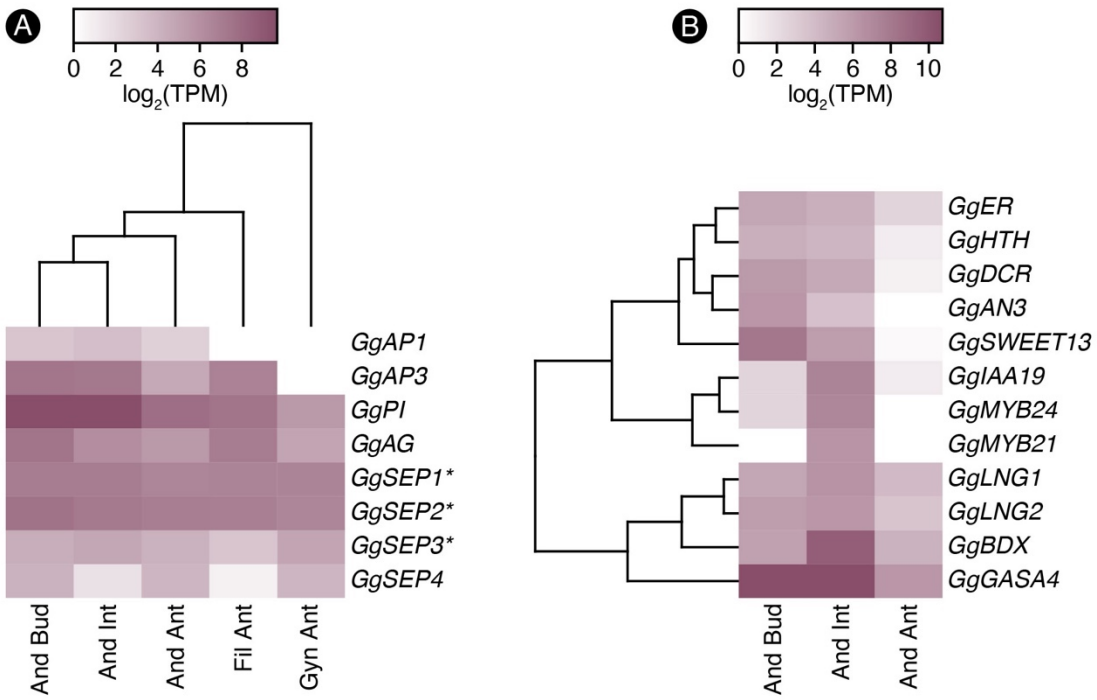

Figure 5.11. Heatmaps of *Gynandropsis gynandra* representative transcripts expressed in log_2(TPM). (A) Floral organ identity genes comparing androgynophore, filament, and gynophore. (B) Candidate androgynophore elongation genes across developmental stages. Transcripts are significantly differentially expressed between at least one pairwise comparison unless indicated otherwise by an asterisk; an asterisk represents no significant differential expression. And Bud: bud stage androgynophore; And Int: intermediate stage androgynophore; And Ant: anthetic stage androgynophore; Fil Ant: anthetic stage filaments; Gyn Ant: anthetic stage gynophore.

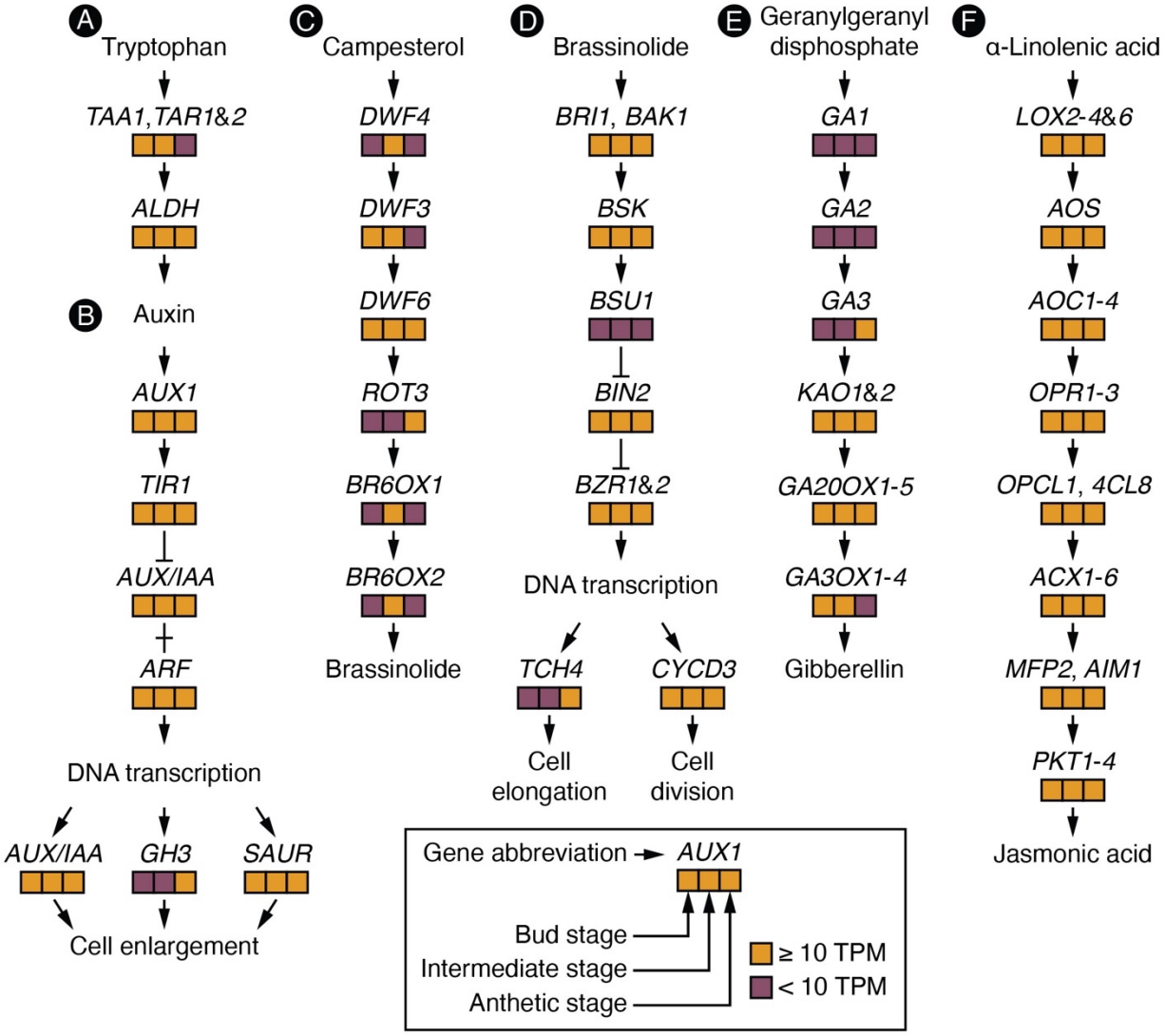

Figure 5.12. Expression of *Gynandropsis gynandra* androgynophore transcripts in *Arabidopsis thaliana*-specific KEGG pathways. (A) Auxin biosynthesis. (B) Auxin signalling. (C) Brassinosteroid biosynthesis. (D) Brassinosteroid signalling. (E) Gibberellin biosynthesis. (F) Jasmonic acid biosynthesis. Each pathway begins with the precursor molecule and ends with the synthesized molecule or outcome. Functionally redundant genes are included for biosynthetic pathways; representative genes are shown in signalling pathways.

Chapter 6: Conclusion

The development of new model organisms and systems is essential for addressing fundamental questions in evo-devo (e.g., what are the mechanisms underlying morphological diversity?). Although work on model organisms like *A. thaliana* and *A. majus* has significantly advanced our knowledge of floral development and genetics, focusing on few taxa limits our understanding of diversification as it provides a narrow representation of floral variation (Kramer 2009; Damerval and Becker 2017). As such, many floral features that are involved or presumably involved in pollinator interactions are poorly understood (Marshall and Johnsen 2017; Liao *et al.* 2021). Cleomaceae is an ideal addition for floral evo-devo investigations as its flowers exhibit substantial morphological diversity (i.e., nectary shape and position, novel floral organs, petal colour and patterns) (Bayat *et al.* 2018). However, much of its floral diversity has not been described in detail. In this thesis, I contribute to the development of Cleomaceae as a model clade and our knowledge of floral traits associated with pollination biology by: examining the morphological and anatomical diversity of nectaries across Cleomaceae (**Chapter 2**); providing the first *in vivo* colour images of UV-fluorescent nectar for several Cleomaceae species (**Chapter 3**); characterizing the floral fragrances of *G. gynandra* and describing its cell morphology and volatile biosynthesis gene expression patterns across floral structures (**Chapter 4**); and investigating the morphological and genetic basis of the androgynophore of *G. gynandra* throughout development (**Chapter 5**).

6.1 Floral nectary and nectar studies in Cleomaceae

Floral nectaries have evolved multiple times and rapidly diversified with the adaptive radiation of animal pollinators (Nicolson *et al.* 2007; Liao *et al.* 2021). The nectar they secrete is crucial for maintaining the reproductive success of many flowering plants (Nicolson *et al.* 2007; Liao *et al.* 2021). Despite ties to pollinator interactions, floral nectaries have often been overlooked in floral development and phylogenetic studies, and we are only beginning to recognize the diversity of nectary forms and complexity of the nectar they secrete (Nicolson *et al.* 2007; Liao *et al.* 2021). Cleomaceae is optimal for broadening our knowledge on floral nectaries and nectar because of its significant variation in floral nectary morphology and vibrantly fluorescent nectar. In **Chapter 2**, I present the first detailed comparative morphological investigation of floral nectaries across Cleomaceae, complementing previous brief comparisons

(Stoudt 1941; Iltis 1958; Karrer 1991). Though Cleomaceae floral nectaries share some characteristics (i.e., commonly receptacular, located between the perianth and stamens, supplied by vasculature, and secrete nectar via nectarostomata), they display dramatic diversity in form, ranging from adaxial protrusions or concavities to annular disks. With the substantive variation in floral nectary morphology described in **Chapter 2** as a starting point, Cleomaceae represents an ideal model clade to elucidate the mechanisms underlying floral nectary position (e.g., adaxial vs. annular), size, and shape (e.g., protrusions vs. concavities), as genetic analyses have primarily focused on floral nectary initiation.

Apart from cotton (*Gossypium*, Malvaceae), *CRABS CLAW* (*CRC*) is essential for nectary initiation across the core eudicots (Bowman and Smyth 1999; Lee, Baum, Oh, *et al.* 2005; Fourquin *et al.* 2014; Morel *et al.* 2018; Pei *et al.* 2021). *CRC* is expressed in both floral and extrafloral nectaries in many taxa (Lee, Baum, Oh, *et al.* 2005) and the role of promoting nectary initiation is supported by functional data in legumes, *Arabidopsis*, and *Petunia* (Bowman and Smyth 1999; Fourquin *et al.* 2014; Morel *et al.* 2018). Additionally, in *Arabidopsis* and *Petunia, AGAMOUS* (*AG*) and *SHATTERPROOF* (*SHP*) act redundantly to promote *CRC* (Lee, Baum, Alvarez, *et al.* 2005; Morel *et al.* 2018). In Cleomaceae, *CRC* is expressed in the floral nectaries of both *Cleomella sparsifolia* and *Cleome violacea* (Lee, Baum, Oh, *et al.* 2005; Carey *et al.* 2023). Further, the roles of *CvCRC, CvAG*, and *CvSHP* in promoting nectary initiation are conserved in *Cleome violacea* (Carey *et al.* 2023). Despite the variation in floral nectary morphology described in **Chapter 2**, I predict that *CRC* is responsible for nectary initiation across Cleomaceae. Gene expression analyses combined with functional studies of additional Cleomaceae taxa would inform on this hypothesis. *Gynandropsis gynandra* and *T. houtteana* would be ideal species to begin with as they have published genomes, established transformation protocols, and a different floral nectary form than *Cleome violacea* (i.e., annular vs. adaxial) (Newell *et al.* 2010; Tsai *et al.* 2012; Cheng *et al.* 2013; Hoang *et al.* 2023).

While shared *CRC* expression and functional studies suggest a conserved role in nectary formation across core eudicots (Slavković *et al.* 2021; Liao *et al.* 2021), less is known about the genetic controls underlying the diversity in floral nectary morphology. Unlike nectary initiation, the genes involved in floral nectary size do not appear to be conserved in *Arabidopsis* and *Petunia*, with *BLADE ON PETIOLE 1* and *2* (*BOP1, BOP2*) promoting growth in *Arabidopsis* (McKim *et al.* 2008) and *BLIND ENHANCER* (*BEN*) and *REPRESSOR OF B-FUNCTION*

(*ROB*) negatively regulating size in *Petunia* (Morel *et al.* 2018). In *Cleome violacea*, a *BOP2* homolog is expressed throughout nectary development, yet additional experiments are required to identify its contribution to floral nectary size (Carey *et al.* 2023). Aside from floral nectary size controls, information on the regulators of position and shape is lacking.

Transcriptome analyses are useful in these studies for identifying differentially expressed genes but additional experimental approaches are required to elucidate gene function and interactions (Eamens *et al.* 2008; Becker and Lange 2010). The link between genotype and phenotype can be established by varying the expression of a candidate gene identified through transcriptomics. Approaches to functional studies in plants include virus-induced gene silencing (VIGS) and transformation, both of which can silence the genes of interest to evaluate their function (Purkayastha and Dasgupta 2009; Krenek *et al.* 2015). *Cleome violacea* has an established VIGS protocol, which was used to collect the aforementioned floral nectary initiation functional data (Carey *et al.* 2021, 2023); the amenability of other Cleomaceae species to this protocol requires testing. As previously mentioned, *G. gynandra* and *T. houtteana* have established transformation procedures (Newell *et al.* 2010; Tsai *et al.* 2012). Together, these methods could be used to address questions regarding the basis of floral nectary position, size, and shape. For instance: (1) How do global gene expression patterns differ between annular vs. adaxial and protruding vs. concave floral nectaries?; and (2) Is *BOP2* a regulator of floral nectary size across Cleomaceae?.

In addition to providing the thorough morphological descriptions essential for genetic investigations on Cleomaceae floral nectaries, I provide a modified fast green and safranin O staining protocol to yield vibrantly coloured histological sections. The commonly cited protocols for fast green and safranin O staining involve a few highly hazardous chemicals (Johansen 1940; Ruzin 1999). For example, picric acid is acutely toxic and a powerful explosive, requiring special handling for disposal (Sigma-Aldrich 2021b). Replacing these chemicals with less hazardous alternatives provides a safer methodology for plant tissue staining. In particular, this modified protocol could be used to expand our knowledge on floral nectary anatomy across flowering plants, as it results in brightly red-stained nectary parenchyma.

As with floral nectaries, there is much to learn about the nectar of Cleomaceae taxa. Previous studies have primarily focused on simple quantifications including nectar volume and sugar concentration (Krupnick *et al.* 1999; Martins and Johnson 2013; Higuera-Díaz *et al.* 2015;

Raju and Rani 2016; Domingos-Melo *et al.* 2020; Carey *et al.* 2023). Though nectar sugar concentration does not appear to be correlated with pollinator types, flowers pollinated by birds, bats, or hawkmoths tend to secrete larger volumes of nectar than flowers pollinated by other insects (Nicolson *et al.* 2007; Willmer 2011). Interestingly, in a study on hawkmoth pollinated flowering plants in East Africa, *G. gynandra* had one of the lowest nectar volumes (0.5 ± 0.18 μL) but the highest nectar sugar concentration (48.7 ± 3.74%) of the 25 species examined (Martins and Johnson 2013). The nectar volume of *G. gynandra* is similar to that of generalist pollinated species, *Cleomella serrulata* (0.85 ± 0.96 μL) and *P. dodecandra* (0.63 ± 0.32 μL) (Higuera-Díaz *et al.* 2015). In contrast, the flowers of bat pollinated *Tarenaya longicarpa* (32.63 ± 11.47 μL) and hummingbird pollinated *Cleomella arborea* (14.95 ± 1.45 μL) hold larger volumes of nectar (Krupnick *et al.* 1999; Domingos-Melo *et al.* 2020). Further, there may be a positive correlation between nectar parenchyma abundance and nectar volume (Pacini *et al.* 2003; Nicolson *et al.* 2007). A combination of Cleomaceae floral nectary anatomy (**Chapter 2**), nectar measurements, and pollination studies would be informative towards these trends. This research could be expanded with additional pollination studies; for example, *Cleome violacea*, one of the most extensively studied Cleomaceae species, is missing pollinator data.

Though important data, volume and sugar concentration measurements do not capture the numerous constituents of nectar (e.g., amino acids, proteins, microbes) (Nicolson *et al.* 2007). While Carey *et al*. (2023) provided evidence for yeast and bacteria inhabiting *Cleome violacea* nectar, there is much to be learned about the chemical composition of Cleomaceae nectar. In **Chapter 3**, I present the first *in vivo* colour images of the striking UV-fluorescent nectar for several Cleomaceae species. However, many questions regarding nectar fluorescence remain, for example: (1) Is this phenomenon ubiquitous across Cleomaceae taxa?; (2) What fluorophores are responsible for the vibrant blue fluorescence?; and (3) Does fluorescence contribute to pollinator attraction?. Beyond investigating UV-fluorescence of additional taxa, metabolomic analyses of Cleomaceae nectar (e.g., chemical separation and characterization coupled with fluorescence detection) could be used for fluorophore identification. Mori *et al.* (2018) used metabolomic analyses to identify pollen fluorophores for several species across flowering plants, then performed a two-choice behavioural assay by exposing honeybees to sugar water and filter paper with and without one of the identified fluorescent compounds. However, the relevance of UV-fluorescence amongst the array of other visual signals (i.e., human-visible colour, UV-

reflectance) has been questioned (Kevan 1976; Iriel and Lagorio 2010). Though knowledge on the genetic mechanism of fluorophore biosynthesis would be required, functional silencing would offer an alternative behavioural assay approach to determine if UV-fluorescent nectar contributes to the suite of signals for pollinator attraction.

6.2 *Gynandropsis gynandra*, a model organism for evo devo studies

Nectar and colour do not act alone in pollinator attraction; rather, flowers present an assortment of signals (e.g., UV-reflectance/absorbance, scent, arrangement of flowers and floral structures) to appeal to the sensory preferences of pollinators (Willmer 2011; Junker and Parachnowitsch 2015). Though suites of floral characteristics can have synergistic effects toward plant-pollinator interactions, multiple features are often only extensively studied in taxa with specialized pollination systems or model organisms, some of which are self-pollinated (i.e., *A. thaliana*) or wind pollinated (*Zea mays*; Poaceae) (Tang *et al.* 2007; Strable and Scanlon 2009; Dellinger 2020). Many investigations are limited to a narrow set of visible floral traits (e.g., colour, shape, and rewards), resulting in an oversimplification of pollination syndromes (Junker and Parachnowitsch 2015; Dellinger 2020). Integration of more intricate floral characteristics, such as scent and nectar composition, cell shapes and textures, and UV-reflectance and -absorbance, provides a more comprehensive understanding of the mechanisms driving plant-pollinator interactions (Dellinger 2020).

As a leafy vegetable and medicinal plant, much of *G. gynandra* research has focused on its vegetative characteristics and validation of traditional knowledge (Chataika *et al.* 2021; Mashamaite *et al.* 2022; Moyo and Aremu 2022). *Gynandropsis gynandra* is also used as a model for C_4 photosynthesis with studies facilitated by comparisons to the closely related C_3 model species, *A. thaliana* (Aubry *et al.* 2016; Williams *et al.* 2016; Huang *et al.* 2021; Hoang *et al.* 2023). Despite the interest in developing minor crop plants for domestication and the importance of pollination in assuring seed set, *G. gynandra* flowers have not been thoroughly investigated (Sogbohossou *et al.* 2018). With *G. gynandra* as a focal species in the preceding chapters, I establish a more holistic picture of its flower by exploring the morphology, chemistry, and genetics of floral traits associated with pollinator interactions including the floral nectary, floral fragrance, and androgynophore. This information could be used toward the research and development of improved *G. gynandra* cultivars, which would not only benefit rural African

communities that rely on *G. gynandra* as a source of nutrition and income but improve global crop diversity and food security amidst a changing climate (Sogbohossou *et al.* 2018; Henkhaus *et al.* 2020).

Reviewed in **Chapter 4**, the pollinators of *G. gynandra* vary geographically with bee and butterfly pollination in Asia and hawkmoth pollination in Africa. Hawkmoth pollinated flowers tend to open at dusk or night and have bright white petals (Willmer 2011; Stöckl and Kelber 2019). Due to the long proboscis and high metabolic requirements of hawkmoths, the petals of hawkmoth pollinated flowers are commonly tubular or spurred with a copious amount of nectar at their base (Willmer 2011; Stöckl and Kelber 2019). In addition, these flowers typically have a strong fragrance dominated by nitrogen-containing compounds, oxygenated terpenoids, and benzenoid esters (Willmer 2011; Stöckl and Kelber 2019; Pichersky and Dudareva 2020). When considering visual cues alone, *G. gynandra* does not have the typical assemblage of floral characteristics associated with hawkmoth pollination (Martins and Johnson 2013). Martins and Johnson (2013) also note that *G. gynandra* flowers are not as strongly scented as other hawkmoth pollinated flowers in East Africa. However, the detailed characterization of floral fragrance in **Chapter 4** reveals nitrogen-containing compounds as the main component of the floral scent profile for an African accession of *G. gynandra*; thus, demonstrating the importance of establishing a holistic view of the flower for understanding pollinator interactions. In addition, the floral scent of the African accession contains a greater abundance of nitrogen-containing compounds than the Asian accession. These differing floral scent profiles combined with variation in morphology, phenology, foliar phytochemistry, and pollinators (Wu *et al.* 2018; Sogbohossou *et al.* 2019, 2020; Blalogoe *et al.* 2020; Houdegbe *et al.* 2022) support the recognition of geographically separated *G. gynandra* subspecies.

Though *G. gynandra* does not have tubular or spurred petals, other novel floral structures may be involved in hawkmoth pollination. As discussed in **Chapter 5**, the androgynophore and gynophore elevate the reproductive organs of the flower, presumably to facilitate pollen transfer with hovering hawkmoths. The comprehensive examination of morphology, anatomy, and gene expression patterns of the androgynophore throughout development (**Chapter 5**) could be mirrored for the gynophore, as this novel floral structure has not been extensively studied outside of *Arachis hypogaea* (Fabaceae; peanut) (Moctezuma 2003; Xia *et al.* 2013; Zhao *et al.* 2015). Further, functional studies could be used to directly test the roles of the candidate

androgynophore elongation genes identified in **Chapter 5**. Though the established transformation protocol for *G. gynandra* has been successfully applied to photosynthesis research (Newell *et al.* 2010; Williams *et al.* 2016), transformation techniques are time and labour intensive (Burch-Smith *et al.* 2004; Carey *et al.* 2021). Development of a VIGS protocol for *G. gynandra* would be a valuable resource for evaluating gene function as it does not require transformation (Burch-Smith *et al.* 2004; Carey *et al.* 2021). These protocols could be used not only to verify candidate gene function but to address outstanding questions including: (1) Are the genetic controls of androgynophore elongation consistent across *G. gynandra* African and Asian accessions?; and (2) does the genetic mechanism controlling androgynophore lengthening influence the elongation of other stalk-like floral structures (i.e., filaments and gynophore)?. Altogether, I provide a more comprehensive understanding of floral features associated with pollinator interactions across Cleomaceae, with emphasis on *G. gynandra*, and offer the basis for additional research on these and other intriguing floral features.

Bibliography

Achigan-Dako EG, Sogbohossou DEO, Houdegbe CA, *et al.* 2021. Ten years of *Gynandropsis gynandra* research for improvement of nutrient-rich leaf consumption: lessons learnt and way forwards. *Annual Plant Reviews* **4**: 767–812.

Ajaiyeoba EO, Onocha PA, Olarenwaju OT. **2001**. *In vitro* anthelmintic properties of *Buchholzia coriaceae* and *Gynandropsis gynandra* extracts. *Pharmaceutical Biology* **39**: 217–220.

Almeida OJG, Cota-Sánchez JH, Paoli AAS. **2013**. The systematic significance of floral morphology, nectaries, and nectar concentration in epiphytic cacti of tribes Hylocereeae and Rhipsalideae (Cactaceae). *Perspectives in Plant Ecology, Evolution and Systematics* **15**: 255–268.

Altschul SF, Gish W, Miller W, Myers EW, Lipman DJ. **1990**. Basic local alignment search tool. *Journal of Molecular Biology* **215**: 403–410.

Anastasiou E, Lenhard M. **2007**. Growing up to one's standard. *Current Opinion in Plant Biology* **10**: 63–69.

Andersson S, Nilsson LA, Grooth I, Bergström G. **2002**. Floral scents in butterfly-pollinated plants: possible convergence in chemical composition. *Botanical Journal of the Linnean Society* **140**: 129–153.

Andrews S. **2010**. FastQC: a quality control tool for high throughput sequence data [online]. Website http://www.bioinformatics.babraham.ac.uk/projects/fastqc/ [accessed 13 June 2023].

Anich PS, Anthony S, Carlson M, *et al.* 2021. Biofluorescence in the platypus (*Ornithorhynchus anatinus*). *Mammalia* **85**: 179–181.

Antoń S, Kamińska M. **2015**. Comparative floral spur anatomy and nectar secretion in four representatives of Ranunculaceae. *Protoplasma* **252**: 1587–1601.

Armbruster WS. **2017**. The specialization continuum in pollination systems: diversity of concepts and implications for ecology, evolution and conservation. *Functional Ecology* **31**: 88–100.

Arnold KE, Owens IPF, Marshall NJ. **2002**. Fluorescent signaling in parrots. *Science* **295**: 92.

Aubourg S, Lecharny A, Bohlmann J. **2002**. Genomic analysis of the terpenoid synthase (*AtTPS*) gene family of *Arabidopsis thaliana*. *Molecular Genetics and Genomics* **267**: 730–745.

Aubry S, Aresheva O, Reyna-Llorens I, Smith-Unna R, Hibberd JM, Genty B. **2016**. A specific transcriptome signature for guard cells from the C4 plant *Gynandropsis gynandra*. *Plant Physiology* **170**: 1345–1357.

Bala A, Kar B, Haldar PK, Mazumder UK, Bera S. **2010**. Evaluation of anticancer activity of *Cleome gynandra* on Ehrlich's ascites carcinoma treated mice. *Journal of Ethnopharmacology* **129**: 131–134.

Ballerini ES, Min Y, Edwards MB, Kramer EM, Hodges SA. **2020**. *POPOVICH*, encoding a C2H2 zinc-finger transcription factor, plays a central role in the development of a key innovation, floral nectar spurs, in *Aquilegia*. *Proceedings of the National Academy of Sciences of the United States of America* **117**: 22552–22560.

Bayat S, Schranz ME, Roalson EH, Hall JC. **2018**. Lessons from Cleomaceae, the sister of crucifers. *Trends in Plant Science* **23**: 808–821.

Becker A, Lange M. **2010**. VIGS – genomics goes functional. *Trends in Plant Science* **15**: 1–4.

van den Bergh E, Hofberger JA, Schranz ME. **2016**. Flower power and the mustard bomb: comparative analysis of gene and genome duplications in glucosinolate biosynthetic pathway evolution in Cleomaceae and Brassicaceae. *American Journal of Botany* **103**: 1212–1222.

van den Bergh E, Külahoglu C, Bräutigam A, *et al.* 2014. Gene and genome duplications and the origin of C4 photosynthesis: birth of a trait in the Cleomaceae. *Current Plant Biology* **1**: 2–9.

Bernhard A. **1999**. Flower structure, development, and systematics in Passifloraceae and in *Abatia* (Flacourtiaceae). *International Journal of Plant Sciences* **160**: 135–150.

Blalogoe JS, Odindo AO, Sogbohossou EOD, Sibiya J, Achigan-Dako EG. **2020**. Origin-dependence of variation in seed morphology, mineral composition and germination percentage in *Gynandropsis gynandra* (L.) Briq. accessions from Africa and Asia. *BMC Plant Biology* **20**: 168.

Bögre L, Magyar Z, López-Juez E. **2008**. New clues to organ size control in plants. *Genome Biology* **9**: 226.

Boron AK, Vissenberg K. **2014**. The *Arabidopsis thaliana* hypocotyl, a model to identify and study control mechanisms of cellular expansion. *Plant Cell Reports* **33**: 697–706.

Botnaru L, Schenk JJ. **2019**. Staminode evolution in *Mentzelia* section *Bartonia* (Loasaceae) and its impact on insect visitation rates. *Botanical Journal of the Linnean Society* **190**: 151–164.

Bouchard A, Hofland GW, Witkamp G-J. **2007**. Properties of sugar, polyol, and polysaccharide water-ethanol solutions. *Journal of Chemical & Engineering Data* **52**: 1838–1842.

Bower CC. **2006**. Specific pollinators reveal a cryptic taxon in the bird orchid, *Chiloglottis valida sensu lato* (Orchidaceae) in south-eastern Australia. *Australian Journal of Botany* **54**: 53–64.

Bowman JL, Smyth DR. **1999**. *CRABS CLAW*, a gene that regulates carpel and nectary development in *Arabidopsis*, encodes a novel protein with zinc finger and helix-loop-helix domains. *Development* **126**: 2387–2396.

Burch-Smith TM, Anderson JC, Martin GB, Dinesh-Kumar SP. **2004**. Applications and advantages of virus-induced gene silencing for gene function studies in plants. *The Plant Journal* **39**: 734–746.

Burkill IH. **1916**. Notes on the pollination of flowers in India—note no. 8, miscellanea. *Journal of the Asiatic Society of Bengal* **12**: 239–265.

Buzgo M, Soltis DE, Soltis PS, Ma H. **2004**. Towards a comprehensive integration of morphological and genetic studies of floral development. *Trends in Plant Science* **9**: 164–173.

Cane JH. **2008**. Breeding biologies, seed production and species-rich bee guilds of *Cleome lutea* and *Cleome serrulata* (Cleomaceae). *Plant Species Biology* **23**: 152–158.

Cardarelli M, Cecchetti V. **2014**. Auxin polar transport in stamen formation and development: how many actors? *Frontiers in Plant Science* **5**: 333.

Cardinal-McTeague WM, Sytsma KJ, Hall JC. **2016**. Biogeography and diversification of Brassicales: a 103 million year tale. *Molecular Phylogenetics and Evolution* **99**: 204–224.

Carey S, Higuera-Díaz M, Mankowski P, Rocca A, Hall JC. **2021**. Virus-induced gene silencing as a tool for functional studies in *Cleome violacea*. *Applications in Plant Sciences* **9**: e11435.

Carey S, Zenchyzen B, Deneka AJ, Hall JC. **2023**. Nectary development in *Cleome violacea*. *Frontiers in Plant Science* **13**: 1085900.

Cecchetti V, Altamura MM, Falasca G, Costantino P, Cardarelli M. **2008**. Auxin regulates *Arabidopsis* anther dehiscence, pollen maturation, and filament elongation. *The Plant Cell* **20**: 1760–1774.

Chandra P, Kunuku V, Janga R, Rani D, Rao S, Aluri JSR. **2013**. A study on interactions of insects with herbaceous plants in Visakhapatnam. *Advances in Pollen Spore Research* **31**: 69–79.

Chataika BY, Akundabweni LS-M, Houdegbe AC, Achigan-Dako EG, Sibiya J, Masamba K. **2021**. Dietary phytochemical screening of spider plant (*Gynandropsis gynandra* (L.) Briq.) accessions from Africa and Asia to identify genotypes for use in nutraceutical breeding. *Frontiers in Sustainable Food Systems* **5**: 733909.

Chen I-C, Lee S-C, Pan S-M, Hsieh H-L. **2007**. *GASA4*, a GA-stimulated gene, participates in light signaling in *Arabidopsis*. *Plant Science* **172**: 1062–1071.

Chen F, Ro D-K, Petri J, *et al.* 2004. Characterization of a root-specific *Arabidopsis* terpene synthase responsible for the formation of the volatile monoterpene 1,8-cineole. *Plant Physiology* **135**: 1956–1966.

Cheng S, van den Bergh E, Zeng P, *et al.* 2013. The *Tarenaya hassleriana* genome provides insight into reproductive trait and genome evolution of crucifers. *The Plant Cell* **25**: 2813–2830.

Cheng C-Y, Krishnakumar V, Chan AP, Thibaud-Nissen F, Schobel S, Town CD. **2017**. Araport11: a complete reannotation of the *Arabidopsis thaliana* reference genome. *The Plant Journal* **89**: 789–804.

Cheng H, Song S, Xiao L, *et al.* 2009. Gibberellin acts through jasmonate to control the expression of *MYB21*, *MYB24*, and *MYB57* to promote stamen filament growth in *Arabidopsis*. *PLOS Genetics* **5**: e1000440.

Chess SKR, Raguso RA, LeBuhn G. **2008**. Geographic divergence in floral morphology and scent in *Linanthus dichotomus* (Polemoniaceae). *American Journal of Botany* **95**: 1652–1659.

Coenye T. **2021**. Do results obtained with RNA-sequencing require independent verification? *Biofilm* **3**: 100043.

Cronk Q. **2009**. *The Molecular Organography of Plants*. Oxford, United Kingdom: Oxford University Press.

Bentley B, Elias TS. **1983**. *The Biology of Nectaries*. New York, New York, USA: Columbia University Press.

Dafni A, Lehrer M, Kevan PG. **1997**. Spatial flower parameters and insect spatial vision. *Biological Reviews* **72**: 239–282.

Damerval C, Becker A. **2017**. Genetics of flower development in Ranunculales – a new, basal eudicot model order for studying flower evolution. *New Phytologist* **216**: 361–366.

Das B, Roy S, Kalita S, Boro KK, Nath M, Nath N. **2022**. Comparative foliar morphological and palynological studies of Cleomaceae of Assam, India. *Biodiversitas Journal of Biological Diversity* **23**: 2920–2934.

Dattagupta S, Datta PC. **1976**. Some aspects of androgynophore development in *Cleome rutidosperma*. *Phytomorphology* **26**: 102–108.

Davis AR, Gunning BES. **1992**. The modified stomata of the floral nectary of *Vicia faba* L. 1. development, anatomy and ultrastructure. *Protoplasma* **166**: 134–152.

Davis AR, Gunning BES. **1993**. The modified stomata of the floral nectary of *Vicia faba* L. 3. physiological aspects, including comparisons with foliar stomata. *Botanica Acta* **106**: 241–253.

Degenhardt J, Köllner TG, Gershenzon J. **2009**. Monoterpene and sesquiterpene synthases and the origin of terpene skeletal diversity in plants. *Phytochemistry* **70**: 1621–1637.

Delaux P-M, Hetherington AJ, Coudert Y, *et al.* 2019. Reconstructing trait evolution in plant evo-devo studies. *Current Biology* **29**: R1110–R1118.

Dellinger AS. **2020**. Pollination syndromes in the 21st century: where do we stand and where may we go? *New Phytologist* **228**: 1193–1213.

Dewitte W, Scofield S, Alcasabas AA, *et al.* 2007. *Arabidopsis* CYCD3 D-type cyclins link cell proliferation and endocycles and are rate-limiting for cytokinin responses. *Proceedings of the National Academy of Sciences* **104**: 14537–14542.

Dimandja J-MD. **2020**. Chapter 1 - Introduction and historical background: the “inside” story of comprehensive two-dimensional gas chromatography. *Separation Science and Technology* **12**: 1–40.

Dobson HEM, Bergström G. **2000**. The ecology and evolution of pollen odors. *Plant Systematics and Evolution* **222**: 63–87.

Domingos-Melo A, Diniz UM, Chalegre SL, Machado IC. **2020**. "Sweet rain" from bat-pollinated flowers: how does sugar concentration modulate nectar retention? *International Journal of Plant Sciences* **182**: 71–77.

Dudareva N, Klempien A, Muhlemann JK, Kaplan I. **2013**. Biosynthesis, function and metabolic engineering of plant volatile organic compounds. *New Phytologist* **198**: 16–32.

Dudareva N, Pichersky E. **2006**. *Biology of Floral Scent*. Boca Raton, Florida, United States: CRC Press.

Dyer AG, Neumeyer C. **2005**. Simultaneous and successive colour discrimination in the honeybee (*Apis mellifera*). *Journal of Comparative Physiology A* **191**: 547–557.

Eamens A, Wang M-B, Smith NA, Waterhouse PM. **2008**. RNA silencing in plants: yesterday, today, and tomorrow. *Plant Physiology* **147**: 456–468.

Edger PP, Heidel-Fischer HM, Bekaert M, *et al.* 2015. The butterfly plant arms-race escalated by gene and genome duplications. *Proceedings of the National Academy of Sciences* **112**: 8362–8366.

Effmert U, Große J, Röse USR, Ehrig F, Kägi R, Piechulla B. **2005**. Volatile composition, emission pattern, and localization of floral scent emission in *Mirabilis jalapa* (Nyctaginaceae). *American Journal of Botany* **92**: 2–12.

Endress PK. **1984**. The role of inner staminodes in the floral display of some relic Magnoliales. *Plant Systematics and Evolution* **146**: 269–282.

Endress PK. **2006**. Angiosperm floral evolution: morphological developmental framework. *Advances in Botanical Research*. **44**: 1–61.

Endress PK, Matthews ML. **2006**. Elaborate petals and staminodes in eudicots: diversity, function, and evolution. *Organisms Diversity & Evolution* **6**: 257–293.

Erbar C, Leins P. **1997**. Studies on the early floral development in Cleomoideae (Capparaceae) with emphasis on the androecial development. *Plant Systematics and Evolution* **206**: 119–132.

Farré-Armengol G, Fernández-Martínez M, Filella I, Junker RR, Peñuelas J. **2020**. Deciphering the biotic and climatic factors that influence floral scents: a systematic review of floral volatile emissions. *Frontiers in Plant Science* **11**: 1154.

Farré-Armengol G, Filella I, Llusià J, Peñuelas J. **2017**. β-Ocimene, a key floral and foliar volatile involved in multiple interactions between plants and other organisms. *Molecules* **22**: 1148.

Fleming TH, Geiselman C, Kress WJ. **2009**. The evolution of bat pollination: a phylogenetic perspective. *Annals of Botany* **104**: 1017–1043.

Forterre Y, Skotheim JM, Dumais J, Mahadevan L. **2005**. How the Venus flytrap snaps. *Nature* **433**: 421–425.

Fourquin C, Primo A, Martínez-Fernández I, Huet-Trujillo E, Ferrándiz C. **2014**. The *CRC* orthologue from *Pisum sativum* shows conserved functions in carpel morphogenesis and vascular development. *Annals of Botany* **114**: 1535–1544.

Fox J, Weisberg S. **2019**. *An R Companion to Applied Regression*. Thousand Oaks, California, USA: SAGE Publishing.

García Y, Friberg M, Parachnowitsch AL. **2021**. Spatial variation in scent emission within flowers. *Nordic Journal of Botany* **39**: e03014.

Ghelli R, Brunetti P, Napoli N, *et al.* 2018. A newly identified flower-specific splice variant of *AUXIN RESPONSE FACTOR8* regulates stamen elongation and endothecium lignification in *Arabidopsis*. *The Plant Cell* **30**: 620–637.

Ghogare UR, Nirmal SA, Patil RY, Kharya MD. **2009**. Antinociceptive activity of *Gynandropsis gynandra* leaves. *Natural Product Research* **23**: 327–333.

Giurfa M, Núñez J, Chittka L, Menzel R. **1995**. Colour preferences of flower-naive honeybees. *Journal of Comparative Physiology A* **177**: 247–259.

Gonçalves-Souza P, Schlindwein C, Dötterl S, Paiva EAS. **2017**. Unveiling the osmophores of *Philodendron adamantinum* (Araceae) as a means to understanding interactions with pollinators. *Annals of Botany* **119**: 533–543.

Gonzalez N, Vanhaeren H, Inzé D. **2012**. Leaf size control: complex coordination of cell division and expansion. *Trends in Plant Science* **17**: 332–340.

Gotelli MM, Galati BG, Medan D. **2017**. Morphological and ultrastructural studies of floral nectaries in Rhamnaceae. *The Journal of the Torrey Botanical Society* **144**: 63–73.

Gotelli MM, Galati BG, Zarlavsky G, Nicolau M, Reposi S. **2020**. Localization, morphology, anatomy and ultrastructure of osmophores in species of Rhamnaceae. *Protoplasma* **257**: 1109–1121.

Grabherr MG, Haas BJ, Yassour M, *et al.* 2011. Trinity: reconstructing a full-length transcriptome without a genome from RNA-Seq data. *Nature biotechnology* **29**: 644–652.

Graham ET, Trentham WR. **1998**. Staining paraffin extracted, alcohol rinsed and air dried plant tissue with an aqueous mixture of three dyes. *Biotechnic & Histochemistry*. 73: 178–185.

Haas BJ, Papanicolaou A, Yassour M, *et al.* 2013. *De novo* transcript sequence reconstruction from RNA-seq using the Trinity platform for reference generation and analysis. *Nature Protocols* **8**: 1494–1512.

Hansen DM, Beer K, Müller CB. **2006**. Mauritian coloured nectar no longer a mystery: a visual signal for lizard pollinators. *Biology Letters* **2**: 165–168.

Hansen DM, Olesen JM, Mione T, Johnson SD, Müller CB. **2007**. Coloured nectar: distribution, ecology, and evolution of an enigmatic floral trait. *Biological Reviews* **82**: 83–111.

Harris PJ, Trethewey JAK. **2010**. The distribution of ester-linked ferulic acid in the cell walls of angiosperms. *Phytochemistry Reviews* **9**: 19–33.

Henkhaus N, Bartlett M, Gang D, *et al.* 2020. Plant science decadal vision 2020–2030: reimagining the potential of plants for a healthy and sustainable future. *Plant Direct* **4**: e00252.

Hepworth J, Lenhard M. **2014**. Regulation of plant lateral-organ growth by modulating cell number and size. *Current opinion in plant biology* **17**: 36–42.

Higuera-Díaz M, Manson JS, Hall JC. **2015**. Pollination biology of *Cleomella serrulata* and *Polanisia dodecandra* in a protected natural prairie in southern Alberta, Canada. *Botany* **93**: 745–757.

Hileman LC. **2014**. Trends in flower symmetry evolution revealed through phylogenetic and developmental genetic advances. *Philosophical Transactions of the Royal Society B: Biological Sciences* **369**: 20130348.

Hoang N V, Sogbohossou EOD, Xiong W, *et al.* 2023. The *Gynandropsis gynandra* genome provides insights into whole-genome duplications and the evolution of C4 photosynthesis in Cleomaceae. *The Plant Cell* **35**: 1334–1359.

Horiguchi G, Nakayama H, Ishikawa N, *et al.* 2011. *ANGUSTIFOLIA3* plays roles in adaxial/abaxial patterning and growth in leaf morphogenesis. *Plant and Cell Physiology* **52**: 112–124.

Houdegbe AC, Achigan-Dako EG, Sogbohossou EOD, Schranz ME, Odindo AO, Sibiya J. **2022**. Phenotypic variation in biomass and related traits among four generations advanced lines of *Cleome* (*Gynandropsis gynandra* L. (Briq.)). *PLOS ONE* **17**: e0275829.

Huang T, Irish VF. **2016**. Gene networks controlling petal organogenesis. *Journal of Experimental Botany* **67**: 61–68.

Huang C-F, Liu W-Y, Lu M-YJ, Chen Y-H, Ku MSB, Li W-H. **2021**. Whole-genome duplication facilitated the evolution of C4 photosynthesis in *Gynandropsis gynandra*. *Molecular Biology and Evolution* **38**: 4715–4731.

Hughes TR. **2009**. "Validation" in genome-scale research. *Journal of Biology* **8**: 3.

Iltis HH. **1958**. Studies in the Capparidaceae-IV. *Polanisia* Raf. *Brittonia* **10**: 33–58.

Iltis HH, Hall JC, Cochrane TS, Sytsma KJ. **2011**. Studies in the Cleomaceae I. on the separate recognition of Capparaceae, Cleomaceae, and Brassicaceae. *Annals of the Missouri Botanical Garden* **98**: 28–36.

Iriel A, Lagorio MG. **2010**. Is the flower fluorescence relevant in biocommunication? *Naturwissenschaften* **97**: 915–924.

Irish VF. **2008**. The *Arabidopsis* petal: a model for plant organogenesis. *Trends in Plant Science* **13**: 430–436.

Johansen DA. **1940**. *Plant microtechnique*. New York, New York, USA: McGraw-Hill Book Company, Inc.

Junker RR, Parachnowitsch AL. **2015**. Working towards a holistic view on flower traits—how floral scents mediate plant-animal interactions in concert with other floral characters. *Journal of the Indian Institute of Science* **95**: 43–68.

Kalve S, De Vos D, Beemster GTS. **2014**. Leaf development: a cellular perspective. *Frontiers in Plant Science* **5**: 362.

Kanehisa M, Furumichi M, Sato Y, Kawashima M, Ishiguro-Watanabe M. **2023**. KEGG for taxonomy-based analysis of pathways and genomes. *Nucleic Acids Research* **51**: D587–D592.

Kanno Y, Oikawa T, Chiba Y, *et al.* 2016. AtSWEET13 and AtSWEET14 regulate gibberellin-mediated physiological processes. *Nature Communications* **7**: 13245.

Karrer AB. **1991**. *Blütenentwicklung und systematische Stellung der Papaveraceae und Capparaceae*. PhD Thesis, University of Zürich, Switzerland.

Kasahara H. **2016**. Current aspects of auxin biosynthesis in plants. *Bioscience, Biotechnology, and Biochemistry* **80**: 34–42.

Keefover-Ring K. **2022**. The chemical biogeography of a widespread aromatic plant species shows both spatial and temporal variation. *Ecology and Evolution* **12**: e9265.

Kettler BA, Solís SM, Ferrucci MS. **2019**. Comparative survey of secretory structures and floral anatomy of *Cohniella cepula* and *Cohniella jonesiana* (Orchidaceae: Oncidiinae). New evidences of nectaries and osmophores in the genus. *Protoplasma* **256**: 703–720.

Kevan PG. **1976**. Fluorescent nectar. *Science* **194**: 341–342.

Knudsen JT, Tollsten L. **1993**. Trends in floral scent chemistry in pollination syndromes: floral scent composition in moth-pollinated taxa. *Botanical Journal of the Linnean Society* **113**: 263–284.

Knudsen JT, Tollsten L, Bergström LG. **1993**. Floral scents—a checklist of volatile compounds isolated by head-space techniques. *Phytochemistry* **33**: 253–280.

Koevenig JL. **1973**. Floral development and stamen filament elongation in *Cleome hassleriana*. *American Journal of Botany* **60**: 122–129.

Koevenig JL, Sillix D. **1973**. Movement of IAA in sections from spider flower (*Cleome hassleriana*) stamen filaments. *American Journal of Botany* **60**: 231–235.

Kohler AM, Olson ER, Martin JG, Anich PS. **2019**. Ultraviolet fluorescence discovered in New World flying squirrels (*Glaucomys*). *Journal of Mammalogy* **100**: 21–30.

Konarska A. **2020**. Microstructure of floral nectaries in *Robinia viscosa* var. *hartwigii* (Papilionoideae, Fabaceae)—a valuable but little-known melliferous plant. *Protoplasma* **257**: 421–437.

Koski MH, Ashman T-L. **2014**. Dissecting pollinator responses to a ubiquitous ultraviolet floral pattern in the wild. *Functional Ecology* **28**: 868–877.

Krakos KN, Fabricant SA. **2014**. Generalist versus specialist pollination systems in 26 *Oenothera* (Onagraceae). *Journal of Pollination Ecology* **14**: 235–243.

Kramer EM. **2007**. Understanding the genetic basis of floral diversity. *Bioscience* **57**: 479–487.

Kramer EM. **2009**. *Aquilegia*: a new model for plant development, ecology, and evolution. *Annual Review of Plant Biology* **60**: 261–277.

Kramer E. **2015**. A stranger in a strange land: the utility and interpretation of heterologous expression. *Frontiers in Plant Science* **6**: 734.

Kramer EM. **2019**. Plus ça change, plus c'est la même chose: the developmental evolution of flowers. *Current Topics in Developmental Biology* **131**: 211–238.

Kramer EM, Hodges SA. **2010**. *Aquilegia* as a model system for the evolution and ecology of petals. *Philosophical Transactions of the Royal Society B: Biological Sciences* **365**: 477–490.

Krenek P, Samajova O, Luptovciak I, Doskocilova A, Komis G, Samaj J. **2015**. Transient plant transformation mediated by *Agrobacterium tumefaciens*: principles, methods and applications. *Biotechnology Advances* **33**: 1024–1042.

Krolikowski KA, Victor JL, Wagler TN, Lolle SJ, Pruitt RE. **2003**. Isolation and characterization of the *Arabidopsis* organ fusion gene *HOTHEAD*. *The Plant Journal* **35**: 501–511.

Krueger F. **2012**. Trim galore: A wrapper tool around Cutadapt and FastQC to consistently apply quality and adapter trimming to FastQ files, with some extra functionality for MspI-digested RRBS-type (Reduced Representation Bisufite-Seq) libraries [online]. Website https://www.bioinformatics.babraham.ac.uk/projects/trim_galore/ [accessed 12 June 2023].

Krupnick GA, Weis AE, Campbell DR. **1999**. The consequences of floral herbivory for pollinator service to *Isomeris arborea*. *Ecology* **80**: 125–134.

Kurup R, Johnson AJ, Sankar S, Hussain AA, Kumar CS, Sabulal B. **2013**. Fluorescent prey traps in carnivorous plants. *Plant Biology* **15**: 611–615.

De la Barrera E, Nobel PS. **2004**. Nectar: properties, floral aspects, and speculations on origin. *Trends in Plant Science* **9**: 65–69.

Lacombe B, Achard P. **2016**. Long-distance transport of phytohormones through the plant vascular system. *Current opinion in plant biology* **34**: 1–8.

Lamb JY, Davis MP. **2020**. Salamanders and other amphibians are aglow with biofluorescence. *Scientific Reports* **10**: 2821.

Landis JB, O'Toole RD, Ventura KL, *et al.* 2016. The phenotypic and genetic underpinnings of flower size in Polemoniaceae. *Frontiers in Plant Science* **6**: 1144.

Lee J-Y, Baum SF, Alvarez J, Patel A, Chitwood DH, Bowman JL. **2005**. Activation of *CRABS CLAW* in the nectaries and carpels of *Arabidopsis*. *The Plant Cell* **17**: 25–36.

Lee J-Y, Baum SF, Oh S-H, Jiang C-Z, Chen J-C, Bowman JL. **2005**. Recruitment of CRABS CLAW to promote nectary development within the eudicot clade. *Development* **132**: 5021–5032.

Lee YK, Rhee JY, Lee SH, *et al.* 2018. Functionally redundant *LNG3* and *LNG4* genes regulate turgor-driven polar cell elongation through activation of *XTH17* and *XTH24*. *Plant Molecular Biology* **97**: 23–36.

Liao IT, Hileman LC, Roy R. **2021**. On the horizon for nectar-related research. *American Journal of Botany* **108**: 2326–2330.

Lim MLM, Land MF, Li D. **2007**. Sex-specific UV and fluorescence signals in jumping spiders. *Science* **315**: 481.

Litt A, Kramer EM. **2010**. The ABC model and the diversification of floral organ identity. *Seminars in Cell & Developmental Biology* **21**: 129–137.

Liu Y, Zhou J, White KP. **2014**. RNA-seq differential expression studies: more sequence or more replication? *Bioinformatics* **30**: 301–304.

Lunau K, Ren Z-X, Fan X-Q, Trunschke J, Pyke GH, Wang H. **2020**. Nectar mimicry: a new phenomenon. *Scientific Reports* **10**: 7039.

de Luna-Valdez L, Chenge-Espinosa M, Hernández-Muñoz A, *et al.* 2021. Reassessing the evolution of the 1-deoxy-D-xylulose 5-phosphate synthase family suggests a possible novel function for the DXS class 3 proteins. *Plant Science* **310**: 110960.

Lwande W, Ndakala AJ, Hassanali A, *et al.* 1999. *Gynandropsis gynandra* essential oil and its constituents as tick (*Rhipicephalus appendiculatus*) repellents. *Phytochemistry* **50**: 401–405.

Mabry ME, Brose JM, Blischak PD, *et al.* 2020. Phylogeny and multiple independent whole-genome duplication events in the Brassicales. *American Journal of Botany* **107**: 1148–1164.

Machado I, Cristina Lopes A, Valentina Leite A, Virgíniade Brito Neves C. **2006**. *Cleome spinosa* (Capparaceae): polygamodioecy and pollination by bats in urban and Caatinga

areas, northeastern Brazil. *Botanische Jahrbücher für Systematik, Pflanzengeschichte und Pflanzengeographie* **127**: 69–82.

Maiti S, Mitra A. **2017**. Morphological, physiological and ultrastructural changes in flowers explain the spatio-temporal emission of scent volatiles in *Polianthes tuberosa* L. *Plant and Cell Physiology* **58**: 2095–2111.

Manni M, Berkeley MR, Seppey M, Simão FA, Zdobnov EM. **2021**. BUSCO update: novel and streamlined workflows along with broader and deeper phylogenetic coverage for scoring of eukaryotic, prokaryotic, and viral genomes. *Molecular Biology and Evolution* **38**: 4647–4654.

Marshall J, Johnsen S. **2017**. Fluorescence as a means of colour signal enhancement. *Philosophical Transactions of the Royal Society B: Biological Sciences* **372**: 20160335.

Martins DJ, Johnson SD. **2013**. Interactions between hawkmoths and flowering plants in East Africa: polyphagy and evolutionary specialization in an ecological context. *Biological Journal of the Linnean Society* **110**: 199–213.

Mashamaite CV, Manyevere A, Chakauya E. **2022**. *Cleome gynandra*: a wonder climate-smart plant for nutritional security for millions in semi-arid areas. *Frontiers in Plant Science* **13**: 1003080.

Masierowska ML. **2003**. Floral nectaries and nectar production in brown mustard (*Brassica juncea*) and white mustard (*Sinapis alba*) (Brassicaceae). *Plant Systematics and Evolution* **238**: 97–107.

Mazel CH, Cronin TW, Caldwell RL, Marshall NJ. **2004**. Fluorescent enhancement of signaling in a mantis shrimp. *Science* **303**: 51.

McCallum KP, McDougall FO, Seymour RS. **2013**. A review of the energetics of pollination biology. *Journal of Comparative Physiology B* **183**: 867–876.

McKim SM, Stenvik G-E, Butenko MA, *et al.* 2008. The *BLADE-ON-PETIOLE* genes are essential for abscission zone formation in *Arabidopsis*. *Development* **135**: 1537–1546.

Meaders C, Min Y, Freedberg KJ, Kramer E. **2020**. Developmental and molecular characterization of novel staminodes in *Aquilegia*. *Annals of Botany* **126**: 231–243.

Mercadante-Simões MO, Paiva EAS. **2016**. Anatomy and ultrastructure of the floral nectary of *Tontelea micrantha* (Celastraceae: Salacioideae). *Plant Species Biology* **31**: 117–124.

Mitchell RJ, Irwin RE, Flanagan RJ, Karron JD. **2009**. Ecology and evolution of plant-pollinator interactions. *Annals of Botany* **103**: 1355–1363.

Moctezuma E. **2003**. The peanut gynophore: a developmental and physiological perspective. *Canadian Journal of Botany* **81**: 183–190.

Monteiro JJ. **1875**. *Angola and the River Congo*. New York, New York, USA: Macmillan.

Morel P, Heijmans K, Ament K, *et al.* 2018. The floral C-lineage genes trigger nectary development in *Petunia* and *Arabidopsis*. *The Plant Cell* **30**: 2020–2037.

Morffy N, Strader LC. **2020**. Old town roads: routes of auxin biosynthesis across kingdoms. *Current Opinion in Plant Biology* **55**: 21–27.

Mori S, Fukui H, Oishi M, *et al.* 2018. Biocommunication between plants and pollinating insects through fluorescence of pollen and anthers. *Journal of Chemical Ecology* **44**: 591–600.

Moriya Y, Itoh M, Okuda S, Yoshizawa AC, Kanehisa M. **2007**. KAAS: an automatic genome annotation and pathway reconstruction server. *Nucleic Acids Research* **35**: W182–W185.

Moyo M, Amoo SO, Aremu AO, *et al.* 2018. Determination of mineral constituents, phytochemicals and antioxidant qualities of *Cleome gynandra*, compared to *Brassica oleracea* and *Beta vulgaris*. *Frontiers in Chemistry* **5**: 128.

Moyo M, Aremu AO. **2022**. Nutritional, phytochemical and diverse health-promoting qualities of *Cleome gynandra*. *Critical Reviews in Food Science and Nutrition* **62**: 3535–3552.

Moyroud E, Glover BJ. **2017**. The physics of pollinator attraction. *New Phytologist* **216**: 350–354.

Moyroud E, Wenzel T, Middleton R, *et al.* 2017. Disorder in convergent floral nanostructures enhances signalling to bees. *Nature* **550**: 469–474.

Muhlemann JK, Klempien A, Dudareva N. **2014**. Floral volatiles: from biosynthesis to function. *Plant, Cell & Environment* **37**: 1936–1949.

Murty YS. **1953**. A contribution to the anatomy and morphology of normal and some abnormal flowers of *Gynandropsis gynandra* (L.) Briq. *Journal of Indian Botanical Society* **32**: 108–122.

Nadakuduti SS, Enciso-Rodríguez F. **2021**. Advances in genome editing with CRISPR systems and transformation technologies for plant DNA manipulation. *Frontiers in Plant Science* **11**: 637159.

Neto RLS, Thomas WW, Roalson EH, Barbosa MR de V. **2022**. Taxonomic revision of *Tarenaya* (Cleomaceae). *Annals of the Missouri Botanical Garden* **107**: 250–313.

Newell CA, Brown NJ, Liu Z, *et al.* 2010. *Agrobacterium tumefaciens*-mediated transformation of *Cleome gynandra* L., a C4 dicotyledon that is closely related to *Arabidopsis thaliana*. *Journal of Experimental Botany* **61**: 1311–1319.

Nicolson SW, Nepi M, Pacini E. **2007**. *Nectaries and Nectar*. Dordrecht, Netherlands: Springer.

Nikolov LA. **2019**. Brassicaceae flowers: diversity amid uniformity. *Journal of Experimental Botany* **70**: 2623–2635.

Nozzolillo C, Amiguet VT, Bily AC, *et al.* 2010. Novel aspects of the flowers and floral pigmentation of two *Cleome species* (Cleomaceae), *C. hassleriana* and *C. serrulata*. *Biochemical Systematics and Ecology* **38**: 361–369.

Nyalala SO, Petersen MA, Grout BWW. **2013**. Volatile compounds from leaves of the African spider plant (*Gynandropsis gynandra*) with bioactivity against spider mite (*Tetranychus urticae*). *Annals of Applied Biology* **162**: 290–298.

Ollerton J, Winfree R, Tarrant S. **2011**. How many flowering plants are pollinated by animals? *Oikos* **120**: 321–326.

Olson ER, Carlson MR, Ramanujam VM, *et al.* 2021. Vivid biofluorescence discovered in the nocturnal Springhare (Pedetidae). *Scientific Reports* **11**: 1–8.

Onyango CM, Kunyanga CN, Ontita EG, Narla RD, Kimenju JW. **2013**. Current status on production and utilization of spider plant (*Cleome gynandra* L.) an underutilized leafy vegetable in Kenya. *Genetic Resources and Crop Evolution* **60**: 2183–2189.

Oronje ML, Kraemer M, Hagen M, Gikungu M, Kasina M. **2012**. Pollination needs and seed production of spider plant (*Cleome gynandra* L.: Cleomaceae) in Kenya. *Heritage Management for Sustainable Development: Proceedings of the 3rd National Museums of Kenya Biennial Scientific Conference* **1**: 14–25.

Pacini E, Nepi M, Vesprini JL. **2003**. Nectar biodiversity: a short review. *Plant Systematics and Evolution* **238**: 7–21.

Pamarthi RK, Nagaraju S, Pandey A, Semwal DP, Bhatt KC, Ahlawat SP. **2022**. "Kukkavaminta" [*Arivela viscosa* (L.) Raf. (Cleomaceae)]: a less-known "seasoning spice" from West Godavari district of Andhra Pradesh, India. *Genetic Resources and Crop Evolution* **69**: 2919–2928.

Panikashvili D, Shi JX, Schreiber L, Aharoni A. **2009**. The *Arabidopsis DCR* encoding a soluble BAHD acyltransferase is required for cutin polyester formation and seed hydration properties. *Plant Physiology* **151**: 1773–1789.

Parachnowitsch AL, Manson JS, Sletvold N. **2019**. Evolutionary ecology of nectar. *Annals of Botany* **123**: 247–261.

Patchell MJ, Bolton MC, Mankowski P, Hall JC. **2011**. Comparative floral development in Cleomaceae reveals two distinct pathways leading to monosymmetry. *International Journal of Plant Sciences* **172**: 352–365.

Patchell MJ, Roalson EH, Hall JC. **2014**. Resolved phylogeny of Cleomaceae based on all three genomes. *Taxon* **63**: 315–328.

Pei Y, Zhang J, Wu P, *et al.* 2021. *GoNe* encoding a class VIIIb *AP2/ERF* is required for both extrafloral and floral nectary development in *Gossypium*. *The Plant Journal* **106**: 1116–1127.

Pelaz S, Ditta GS, Baumann E, Wisman E, Yanofsky MF. **2000**. B and C floral organ identity functions require *SEPALLATA* MADS-box genes. *Nature* **405**: 200–203.

Peters G. **2017**. Diamond plots: a tutorial to introduce a visualisation tool that facilitates interpretation and comparison of multiple sample estimates while respecting their inaccuracy. *PsyArXiv*.

Phillips MA, D'Auria JC, Gershenzon J, Pichersky E. **2008**. The *Arabidopsis thaliana* type I isopentenyl diphosphate isomerases are targeted to multiple subcellular compartments and have overlapping functions in isoprenoid biosynthesis. *The Plant Cell* **20**: 677–696.

Pichersky E, Dudareva N. **2020**. *Biology of Plant Volatiles*. Boca Raton, Florida, United States: CRC Press.

Prötzel D, Heß M, Scherz MD, Schwager M, Padje A van't, Glaw F. **2018**. Widespread bone-based fluorescence in chameleons. *Scientific Reports* **8**: 698.

Purkayastha A, Dasgupta I. **2009**. Virus-induced gene silencing: a versatile tool for discovery of gene functions in plants. *Plant Physiology and Biochemistry* **47**: 967–976.

Puzey JR, Gerbode SJ, Hodges SA, Kramer EM, Mahadevan L. **2012**. Evolution of spur-length diversity in *Aquilegia* petals is achieved solely through cell-shape anisotropy. *Proceedings of the Royal Society B: Biological Sciences* **279**: 1640–1645.

Raghavan TS. **1939**. Studies in the Capparidaceae.—II. floral anatomy and some structural features of the Capparidaceous flower. *Journal of the Linnean Society of London, Botany* **52**: 239–257.

Raguso RA. **2004**. Why are some floral nectars scented? *Ecology* **85**: 1486–1494.

Raguso RA. **2008**. Wake up and smell the roses: the ecology and evolution of floral scent. *Annual Review of Ecology, Evolution, and Systematics* **39**: 549–569.

Raguso RA, Levin RA, Foose SE, Holmberg MW, McDade LA. **2003**. Fragrance chemistry, nocturnal rhythms and pollination "syndromes" in *Nicotiana*. *Phytochemistry* **63**: 265–284.

Raguso RA, Pellmyr O. **1998**. Dynamic headspace analysis of floral volatiles: a comparison of methods. *Oikos* **81**: 238–254.

Raju AJS, Rani DS. **2016**. Reproductive ecology of *Cleome gynandra* and *Cleome viscosa* (Capparaceae). *Phytologia Balcanica* **22**: 15–28.

Rausher MD. **2008**. Evolutionary transitions in floral color. *International Journal of Plant Sciences* **169**: 7–21.

Razem FA, Davis AR. **1999**. Anatomical and ultrastructural changes of the floral nectary of *Pisum sativum* L. during flower development. *Protoplasma* **206**: 57–72.

Ren G, Healy RA, Klyne AM, Horner HT, James MG, Thornburg RW. **2007**. Transient starch metabolism in ornamental tobacco floral nectaries regulates nectar composition and release. *Plant Science* **173**: 277–290.

Riffell JA, Lei H, Abrell L, Hildebrand JG. **2013**. Neural basis of a pollinator's buffet: olfactory specialization and learning in *Manduca sexta*. *Science* **339**: 200–204.

Robinson MD, McCarthy DJ, Smyth GK. **2010**. edgeR: a Bioconductor package for differential expression analysis of digital gene expression data. *Bioinformatics* **26**: 139–140.

Rocha DI, Monte Bello CC, Sobol S, Samach A, Dornelas MC. **2015**. Auxin and physical constraint exerted by the perianth promote androgynophore bending in *Passiflora mucronata* L. (Passifloraceae). *Plant Biology* **17**: 639–646.

Rosin FM, Kramer EM. **2009**. Old dogs, new tricks: regulatory evolution in conserved genetic modules leads to novel morphologies in plants. *Developmental Biology* **332**: 25–35.

Roy R, Schmitt AJ, Thomas JB, Carter CJ. **2017**. Review: nectar biology: from molecules to ecosystems. *Plant Science* **262**: 148–164.

Ruzin SE. **1999**. *Plant Microtechnique and Microscopy*. Oxford, United Kingdom: Oxford University Press.

Salazar-Iribe A, Cruz-Valderrama JE, Jímenez-Durán K, Gómez-Maqueo X, Gamboa-deBuen A. **2018**. BIIDXI, a DUF642 cell wall protein, is involved in hypocotyl growth via auxin efflux. *Journal of Plant Physiology* **231**: 105–109.

Santner A, Calderon-Villalobos L, Estelle M. **2009**. Plant hormones are versatile chemical regulators of plant growth. *Nature Chemical Biology* **5**: 301–307.

Saroop S, Kaul V. **2019**. Tritrophism in mellitophylic *Cleome viscosa* L. *Genetic Resources and Crop Evolution* **66**: 1367–1370.

Schneider CA, Rasband WS, Eliceiri KW. **2012**. NIH Image to ImageJ: 25 years of image analysis. *Nature Methods* **9**: 671–675.

Schrager-Lavelle A, Klein H, Fisher A, Bartlett M. **2017**. Grass flowers: An untapped resource for floral evo-devo. *Journal of Systematics and Evolution* **55**: 525–541.

Schuurink R, Tissier A. **2020**. Glandular trichomes: micro-organs with model status? *New Phytologist* **225**: 2251–2266.

Scogin R. **1979a**. 5, 7-Dimethoxy-4'-hydroxyisoflavone from *Fremontia* (Sterculiaceae) nectar. *Aliso: A Journal of Systematic and Floristic Botany* **9**: 479–480.

Scogin R. **1979b**. Nectar constituents in the genus *Fremontia* (Sterculiaceae): sugars, flavonoids, and proteins. *Botanical Gazette* **140**: 29–31.

Scorza LCT, Dornelas MC. **2014**. Rapid touch-stimulated movement in the androgynophore of Passiflora flowers (subgen. *Decaloba*; Sect. *Xerogona*): an adaptation to enhance cross-pollination? *Plant Signaling & Behavior* **9**: e27932.

Senior RJ. **1951**. The use of "cellosolve" as a dehydrating agent in microtechnique. *Proceedings of the Pennsylvania Academy of Science* **25**: 26–28.

Serrano-Mislata A, Sablowski R. **2018**. The pillars of land plants: new insights into stem development. *Current opinion in plant biology* **45**: 11–17.

Sharma B, Yant L, Hodges SA, Kramer EM. **2014**. Understanding the development and evolution of novel floral form in *Aquilegia*. *Current Opinion in Plant Biology* **17**: 22–27.

Shaver TN, Lingren PD, Marshall HF. **1997**. Nighttime variation in volatile content of flowers of the night blooming plant *Gaura drummondii*. *Journal of Chemical Ecology* **23**: 2673–2682.

Sheehan H, Hermann K, Kuhlemeier C. **2012**. Color and scent: how single genes influence pollinator attraction. *Cold Spring Harbor Symposia on Quantitative Biology* **77**: 117–133.

Shi H, Li W, Xu X. **2016**. Learning the comparing and converting method of sequence Phred quality score. *Proceedings of the 2016 6th International Conference on Management, Education, Information and Control (MEICI 2016)* **1**: 260–263.

Sigma-Aldrich. **2021a**. Xylenes safety data sheet 534056 [online]. Website https://www.sigmaaldrich.com/CA/en/sds/sigald/534056 [accessed 08 August 2022].

Sigma-Aldrich. **2021b**. Picric acid safety data sheet 197378 [online]. Website https://www.sigmaaldrich.com/CA/en/sds/aldrich/197378 [accessed 08 August 2022].

Sigma-Aldrich. **2021c**. 2-methoxyethanol safety data sheet 284467 [online]. Website https://www.sigmaaldrich.com/CA/en/sds/sial/284467 [accessed 08 August 2022].

Simão FA, Waterhouse RM, Ioannidis P, Kriventseva E V, Zdobnov EM. **2015**. BUSCO: assessing genome assembly and annotation completeness with single-copy orthologs. *Bioinformatics* **31**: 3210–3212.

Slavković F, Dogimont C, Morin H, Boualem A, Bendahmane A. **2021**. The genetic control of nectary development. *Trends in Plant Science* **26**: 260–271.

Smith SD. **2010**. Using phylogenetics to detect pollinator-mediated floral evolution. *New Phytologist* **188**: 354–363.

Smyth DR. **2018**. Evolution and genetic control of the floral ground plan. *New Phytologist* **220**: 70–86.

Sobel J, Streisfeld M. **2013**. Flower color as a model system for studies of plant evo-devo. *Frontiers in Plant Science* **4**: 321.

Sogbohossou EOD, Achigan-Dako E, Maundu P, *et al.* 2018. A roadmap for breeding orphan leafy vegetable species: a case study of *Gynandropsis gynandra* (Cleomaceae). *Horticulture Research* **5**: 2.

Sogbohossou EOD, Achigan-Dako EG, Mumm R, de Vos RCH, Schranz ME. **2020**. Natural variation in specialised metabolites production in the leafy vegetable spider plant (*Gynandropsis gynandra* L. (Briq.)) in Africa and Asia. *Phytochemistry* **178**: 112468.

Sogbohossou EOD, Kortekaas D, Achigan-Dako E, *et al.* 2019. Association between vitamin content, plant morphology and geographical origin in a worldwide collection of the orphan crop *Gynandropsis gynandra* (Cleomaceae). *Planta* **250**: 933–947.

Soltis PS, Soltis DE. **2014**. Flower diversity and angiosperm diversification. *Flower Development: Methods and Protocols* **1110**: 85–102.

Specht CD, Howarth DG. **2015**. Adaptation in flower form: a comparative evodevo approach. *New Phytologist* **206**: 74–90.

Stöckl AL, Kelber A. **2019**. Fuelling on the wing: sensory ecology of hawkmoth foraging. *Journal of Comparative Physiology A* **205**: 399–413.

Stoler N, Nekrutenko A. **2021**. Sequencing error profiles of Illumina sequencing instruments. *NAR Genomics and Bioinformatics* **3**: lqab019.

Stoudt HN. **1941**. The floral morphology of some of the Capparidaceae. *American Journal of Botany* **28**: 664–675.

Strable J, Scanlon MJ. **2009**. Maize (*Zea mays*): a model organism for basic and applied research in plant biology. *Cold Spring Harbor Protocols* **4**: pdb-emo132.

Tang C, Toomajian C, Sherman-Broyles S, *et al.* 2007. The evolution of selfing in *Arabidopsis thaliana*. *Science* **317**: 1070–1072.

Teranishi R, Buttery RG, Kint S, *et al.* 1991. Chemical composition of *Gaura drummondii* flower volatiles. *Journal of Essential Oil Research* **3**: 287–288.

Tholl D. **2006**. Terpene synthases and the regulation, diversity and biological roles of terpene metabolism. *Current Opinion in Plant Biology* **9**: 297–304.

Tholl D, Boland W, Hansel A, Loreto F, Röse USR, Schnitzler J-P. **2006**. Practical approaches to plant volatile analysis. *The Plant Journal* **45**: 540–560.

Tholl D, Lee S. **2011**. Terpene specialized metabolism in *Arabidopsis thaliana*. *The Arabidopsis Book* **9**: e0143.

Thorp RW, Briggs DL, Estes JR, Erickson EH. **1975**. Nectar fluorescence under ultraviolet irradiation. *Science* **189**: 476–478.

Thulin M, Roalson EH. **2017**. Resurrection of the genus *Rorida* (Cleomaceae), a distinctive Old World segregate of *Cleome*. *Systematic Botany* **42**: 569–577.

Tobe H. **2015**. Floral morphology and structure of *Emblingia calceoliflora* (Emblingiaceae, Brassicales): questions and answers. *Journal of Plant Research* **128**: 481–495.

Tronconi MA, Hüdig M, Schranz ME, Maurino VG. **2020**. Independent recruitment of duplicated β-subunit-coding NAD-ME genes aided the evolution of C4 photosynthesis in Cleomaceae. *Frontiers in Plant Science* **11**: 572080.

Tsai Y-T, Chen P-Y, To K-Y. **2012**. Plant regeneration and stable transformation in the floricultural plant *Cleome spinosa*, a C3 plant closely related to the C4 plant *C. gynandra*. *Plant Cell Reports* **31**: 1189–1198.

Tsai T, Diggle PK, Frye HA, Jones CS. **2018**. Contrasting lengths of *Pelargonium* floral nectar tubes result from late differences in rate and duration of growth. *Annals of Botany* **121**: 549–560.

Tucker GC, Vanderpool SS. **2010**. Cleomaceae. In: Flora of North America Editorial Committee, eds. *Flora of North America.* Oxford, United Kingdom: Oxford University Press.

Vogel S, Hadacek F. **2004**. Contributions to the functional anatomy and biology of *Nelumbo nucifera* (Nelumbonaceae) III. An ecological reappraisal of floral organs. *Plant Systematics and Evolution* **249**: 173–189.

Vogel S, Renner SS. **1990**. *The Role of Scent Glands in Pollination: On the Structure and Function of Osmophores*. Washington, DC, USA: Smithsonian Institution Libraries and National Science Foundation.

Volkov AG, Foster JC, Ashby TA, Walker RK, Johnson JA, Markin VS. **2010**. *Mimosa pudica*: electrical and mechanical stimulation of plant movements. *Plant, Cell & Environment* **33**: 163–173.

Vranová E, Coman D, Gruissem W. **2013**. Network analysis of the MVA and MEP pathways for isoprenoid synthesis. *Annual Review of Plant Biology* **64**: 665–700.

Walker-Larsen J, Harder LD. **2000**. The evolution of staminodes in angiosperms: patterns of stamen reduction, loss, and functional re-invention. *American Journal of Botany* **87**: 1367–1384.

Wang G, Dixon RA. **2009**. Heterodimeric geranyl(geranyl)diphosphate synthase from hop (*Humulus lupulus*) and the evolution of monoterpene biosynthesis. *Proceedings of the National Academy of Sciences* **106**: 9914–9919.

Weiss J, Delgado L, Egea-Cortines M. **2005**. Genetic control of floral size and proportions. *The International Journal of Developmental Biology* **49**: 513–525.

Werth E. **1942**. Über einige umstrittene oder weniger bekannte bestäubungseinrichtungen tropischer blumen. *Berichte der Deutschen Botanischen Gesellschaft* **60**: 473–494.

Weryszko-Chmielewska E, Sulborska A. **2011**. Morphological characters of the flowers and the structure of the nectaries of *Acer platanoides* L. *Acta Agrobotanica* **64**: 19–28.

Wessinger CA, Hileman LC. **2020**. Parallelism in flower evolution and development. *Annual Review of Ecology, Evolution, and Systematics* **51**: 387–408.

Whitney HM, Bennett KMV, Dorling M, *et al.* 2011. Why do so many petals have conical epidermal cells? *Annals of Botany* **108**: 609–616.

Wickham H. **2016**. ggplot2: elegant graphics for data analysis [online]. Website https://ggplot2.tidyverse.org [accessed 23 May 2023].

Widhalm JR, Jaini R, Morgan JA, Dudareva N. **2015**. Rethinking how volatiles are released from plant cells. *Trends in Plant Science* **20**: 545–550.

Widhiono I, Sudiana E. **2015**. Peran tumbuhan liar dalam konservasi keragaman serangga penyerbuk ordo Hymenoptera. *Prosiding Seminar Nasional Masyarakat Biodiversitas Indonesia* **1**: 1586–1590.

Williams BP, Burgess SJ, Reyna-Llorens I, *et al.* 2016. An untranslated cis-element regulates the accumulation of multiple C4 enzymes in *Gynandropsis gynandra* mesophyll cells. *The Plant Cell* **28**: 454–465.

Willmer P. **2011**. *Pollination and Floral Ecology*. Princeton, New Jersey, USA: Princeton University Press.

Winter Y, López J, von Helversen O. **2003**. Ultraviolet vision in a bat. *Nature* **425**: 612–614.

Wu T, Solberg SO, Yndgaard F, Chou Y-Y. **2018**. Morphological patterns in a world collection of *Cleome gynandra*. *Genetic Resources and Crop Evolution* **65**: 271–283.

Xia H, Zhao C, Hou L, *et al.* 2013. Transcriptome profiling of peanut gynophores revealed global reprogramming of gene expression during early pod development in darkness. *BMC Genomics* **14**: 517.

Xu L, Dong Z, Fang L, *et al.* 2019. OrthoVenn2: a web server for whole-genome comparison and annotation of orthologous clusters across multiple species. *Nucleic Acids Research* **47**: W52–W58.

Xu W, Purugganan MM, Polisensky DH, Antosiewicz DM, Fry SC, Braam J. **1995**. *Arabidopsis* TCH4, regulated by hormones and the environment, encodes a xyloglucan endotransglycosylase. *The Plant Cell* **7**: 1555–1567.

Ye Q, Zhu W, Li L, *et al.* 2010. Brassinosteroids control male fertility by regulating the expression of key genes involved in *Arabidopsis* anther and pollen development. *Proceedings of the National Academy of Sciences* **107**: 6100–6105.

van Zanten M, Snoek LB, Proveniers MCG, Peeters AJM. **2009**. The many functions of ERECTA. *Trends in Plant Science* **14**: 214–218.

Zenchyzen B, Weissner S, Martin J, *et al.* 2023. Comparative nectary morphology across Cleomaceae (Brassicales). *Plants* **12**: 1263.

Zhang F-P, Cai X-H, Wang H, Ren Z-X, Larson-Rabin Z, Li D-Z. **2012**. Dark purple nectar as a foraging signal in a bird-pollinated Himalayan plant. *New Phytologist* **193**: 188–195.

Zhang R, Min Y, Holappa LD, *et al.* 2020. A role for the auxin response factors *ARF6* and *ARF8* homologs in petal spur elongation and nectary maturation in *Aquilegia*. *New Phytologist* **227**: 1392–1405.

Zhang X, Zhao L. **2018**. Morphology, structure and ultrastructure of staminal nectary in *Lamprocapnos* (Fumarioideae, Papaveraceae). *Flora* **242**: 128–136.

Zhao C, Zhao S, Hou L, *et al.* 2015. Proteomics analysis reveals differentially activated pathways that operate in peanut gynophores at different developmental stages. *BMC Plant Biology* **15**: 188.

Zohoungbogbo HPF, Houdegbe CA, Sogbohossou DEO, *et al.* 2018. Andromonoecy in *Gynandropsis gynandra* (L.) Briq. (Cleomaceae) and effects on fruit and seed production. *Genetic Resources and Crop Evolution* **65**: 2231–2239.

Appendices

Appendix 2.1. Accession numbers for the nine Cleomaceae species voucher specimens. All voucher specimens were collected by B.Z. or B.Z. and S.W. and deposited in the University of Alberta Vascular Plant Herbarium (ALTA).

Species	ALTA Accession Number
Arivela viscosa	143371
Cleome amblyocarpa	144822
Cleome violacea	144828
Gynandropsis gynandra	143369
Melidiscus giganteus	144833
Polanisia dodecandra	144836
Sieruela hirta	143370
Sieruela rutidosperma	144838
Tarenaya houtteana	144840

Appendix 2.2. Brief descriptions of the flowers at the three developmental stages for the nine Cleomaceae species.

Species	Stage	Description
Arivela viscosa	Bud	Sepals closed with petals inserted; 0.4–0.6 cm from base of sepals to apex of sepals
	Intermediate	Sepals closed with petals exserted; 0.7–0.9 cm from base of sepals to apex of petals
	Anthesis	Anthesis; sepals and petals open, anthers dehisced
Cleome amblyocarpa	Bud	Sepals closed with petals inserted; 0.2 cm from base of sepals to apex of sepals
	Intermediate	Sepals closed with petals exserted; 0.5–0.6 cm from base of sepals to apex of petals
	Anthesis	Anthesis; sepals and petals open, anthers dehisced
Cleome violacea	Bud	Sepals closed with petals exserted; 0.1–0.4 cm in length from base of sepals to apex of petals
	Intermediate	Petals beginning to open
	Anthesis	Anthesis; sepals and petals open, anthers dehisced
Gynandropsis gynandra	Bud	Sepals closed with petals inserted, apex of pistil level with sepals or exserted; 0.5–0.7 cm from base of sepals to apex of pistil
	Intermediate	Sepals closed with petals exserted, pistil elevated above petals; 1.5–1.9 cm from base of sepals to apex of pistil
	Anthesis	Anthesis; sepals and petals open, anthers dehisced
Melidiscus giganteus	Bud	Sepals closed with abaxial sepal apex extending beyond closed petals; 1.5–2.5 cm from base of sepals to apex of petals
	Intermediate	Sepals open, filaments and gynophore exserted and incurved with anthers and pistil enclosed in petals
	Anthesis	Anthesis; sepals and petals open, anthers and pistil released from petals
Polanisia dodecandra	Bud	Sepals closed with petals inserted, beak of pistil exserted; 0.5–0.7 cm from base of sepals to apex of pistil
	Intermediate	Sepals and petals opening, filaments not fully elongated; 1.0–1.2 cm from base of sepals to apex of pistil
	Anthesis	Anthesis; sepals and petals open, anthers dehisced
Sieruela hirta	Bud	Sepals closed with petals inserted; 0.4–0.9 cm from base of sepals to apex of sepals
	Intermediate	Sepals closed with petals exserted; 1.0–1.5 cm from base of sepals to apex of petals
	Flower	Anthesis; sepals and petals open, anthers dehisced
Sieruela rutidosperma	Bud	Sepals closed with petals exserted; 0.3–0.5 cm from base of sepals to apex of petals
	Intermediate	Sepals closed with petals exserted; 0.6–0.7 cm from base of sepals to apex of petals
	Anthesis	Anthesis; sepals and petals open, anthers dehisced
Tarenaya houtteana	Bud	Sepals closed with petals exserted; 0.7–1.9 cm from base of sepals to apex of petals
	Intermediate	Sepals open, filaments and gynophore exserted and incurved with anthers and pistil enclosed in petals
	Anthesis	Anthesis; sepals and petals open, anthers and pistil released from petals

Appendix 4.1. Statistics for *de novo* assembly of *Gynandropsis gynandra* transcriptome. Results for paired-end reads based on all transcripts, with those based only on the longest isoform per gene in parentheses.

N50	2082 (1479)
Median contig length	720 (379)
Average contig length	1201.31 (761.02)
Total assembled bases	266672603 (86529024)
Total Trinity genes	113702
Total Trinity transcripts	221985
GC%	41.65

Appendix 4.2. BUSCO assessment results for *Gynandropsis gynandra* transcriptome.

Complete BUSCOs	4302 (93.6%)
Complete and single-copy BUSCOs	1441 (31.4%)
Complete and duplicated BUSCOs	2861 (62.2%)
Fragmented BUSCOs	65 (1.4%)
Missing BUSCOs	229 (5.0%)
Total BUSCO groups searched	4596

Appendix 5.1. Alcian blue/safranin O-stained transverse sections of *Gynandropsis gynandra* throughout development. Bud, intermediate, and anthetic stages (columns) of the gynophore and filaments (only two filaments shown), distal section of the androgynophore, and proximal or middle section of the androgynophore (rows). Scale bar represents 0.2 mm for all sections.

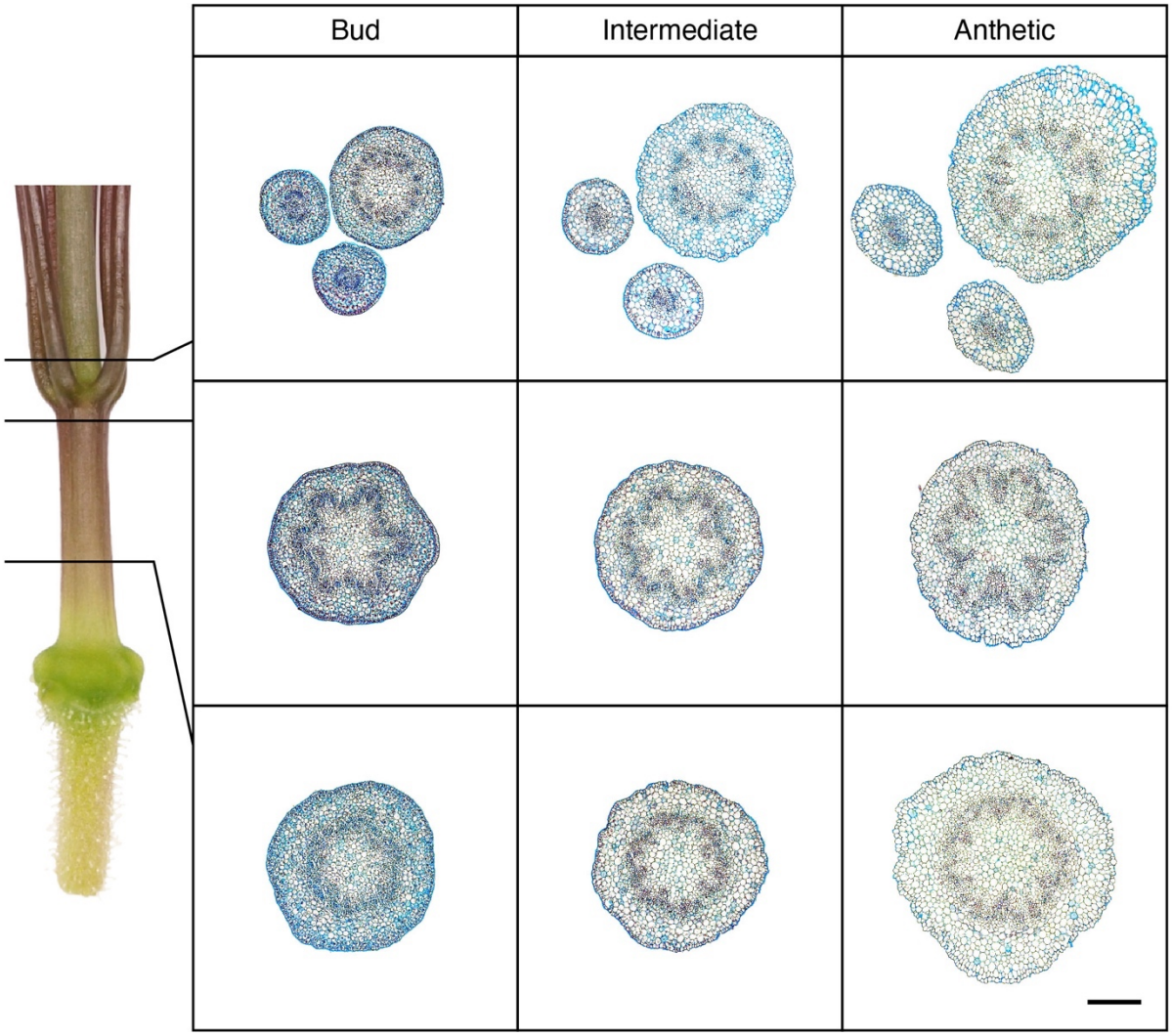

Appendix 5.2. Statistics for *de novo* assembly of *Gynandropsis gynandra* transcriptome. Results for paired-end reads based on all transcripts, with those based only on the longest isoform per gene in parentheses.

N50	2198 (1418)
Median contig length	769 (362)
Average contig length	1263.04 (729.63)
Total assembled bases	311063027 (87415815)
Total Trinity genes	119808
Total Trinity transcripts	246281
GC%	41.76

Appendix 5.3. BUSCO assessment results for *Gynandropsis gynandra* transcriptome.

	All transcripts	Transdecoder filtered transcripts
Complete BUSCOs	4311 (93.8%)	4040 (87.9%)
Complete and single-copy BUSCOs	636 (13.8%)	2281 (49.6%)
Complete and duplicated BUSCOs	3675 (80.0%)	1759 (38.3%)
Fragmented BUSCOs	66 (1.4%)	126 (2.7%)
Missing BUSCOs	219 (4.8%)	430 (9.4%)
Total BUSCO groups searched	4596	4596

Appendix 5.4. Expression and significance of *Gynandropsis gynandra* representative transcripts for genes involved in *Arabidopsis thaliana* organ development and growth.

		Transcripts per million (TPM)			Fold change (FC)			False discovery rate (FDR)			
Gene	Gene ID	Bud	Int	Ant	Bud vs. Int	Bud vs. Ant	Int vs. Ant	Bud vs. Int	Bud vs. Ant	Int vs. Ant	Reference
ABCB1	AT2G36910	65.9	128.2	119.7	1.93	1.83	1.09	7.2E-05	1.7E-03	9.3E-01	Cardarelli, M., *et al.* 2014. *Front. Plant Sci.* 5: 333.
ABCB19	AT3G28860	76.3	90.7	88.3	1.18	1.17	1.04	7.0E-01	6.0E-01	1.0E+00	Cardarelli, M., *et al.* 2014. *Front. Plant Sci.* 5: 333.
ACL5	AT5G19530	93.8	109.2	53.1	1.15	1.75	2.08	7.9E-01	1.7E-02	3.8E-04	Hanzawa, Y., *et al.* 2000. *EMBO J.* 19: 4248-4256.
AFB1	AT4G03190	14.6	13.5	7.9	1.08	1.84	1.74	9.6E-01	3.9E-02	8.9E-02	Cardarelli, M., *et al.* 2014. *Front. Plant Sci.* 5: 333.
AFB2	AT3G26810	2.5	1.7	2.2	1.45	1.11	1.27	7.0E-01	9.5E-01	8.9E-01	Cardarelli, M., *et al.* 2014. *Front. Plant Sci.* 5: 333.
AFB3	AT1G12820	15.1	11.2	15.6	1.36	1.04	1.37	2.6E-01	9.9E-01	2.6E-01	Cardarelli, M., *et al.* 2014. *Front. Plant Sci.* 5: 333.
AIL6/PLT3	AT5G10510	-	-	-	-	-	-	-	-	-	Krizek, B. A., *et al.* 2009. *Plant Physiol.* 150: 1916-1929.
AN	AT1G01510	5.0	3.8	7.5	1.32	1.53	1.97	7.3E-01	3.0E-01	1.1E-01	Kim, G.-T., *et al.* 2002. *EMBO J.* 21: 1267-1279.
AN3	AT5G28640	76.2	13.0	0.7	5.89	100.68	17.62	1.3E-16	1.1E-38	5.3E-11	Horiguchi, G., *et al.* 2011. *Plant Cell Physiol.* 52: 112–124.
ANT	AT4G37750	10.5	1.0	6.4	10.86	1.63	6.48	1.4E-13	1.1E-01	2.3E-06	Bögre, B., *et al.* 2008. *Genome Biol.* 226.
ARF1	AT1G59750	18.3	10.6	20.5	1.74	1.13	1.91	8.0E-02	8.5E-01	4.9E-02	Cardarelli, M., *et al.* 2014. *Front. Plant Sci.* 5: 333.
ARF2	AT5G62000	36.9	11.6	35.8	3.22	1.02	3.06	5.9E-11	1.0E+00	5.3E-07	Cardarelli, M., *et al.* 2014. *Front. Plant Sci.* 5: 333.
ARF6	AT1G30330	45.3	46.9	24.9	1.03	1.81	1.91	1.0E+00	2.7E-04	2.0E-04	Cardarelli, M., *et al.* 2014. *Front. Plant Sci.* 5: 333.
ARF8	AT5G37020	44.4	48.6	30.1	1.09	1.46	1.63	9.5E-01	6.1E-02	9.5E-03	Cardarelli, M., *et al.* 2014. *Front. Plant Sci.* 5: 333.
ARGOS	AT3G59900	11.5	12.7	38.2	1.10	3.34	2.96	1.0E+00	1.0E-03	3.0E-03	Bögre, B., *et al.* 2008. *Genome Biol.* 226.
ARL	AT2G44080	8.4	12.5	31.9	1.47	3.80	2.52	4.8E-01	4.0E-03	8.1E-02	Xu, R., *et al.* 2011. *Development* 138: 4545-4554.
BB	AT3G63530	11.0	5.1	4.8	2.16	2.26	1.07	9.2E-03	1.4E-02	1.0E+00	Hepworth, J., *et al.* 2014. *Curr. Opin. Plant Biol.* 17: 36-42.
BDX	AT4G32460	51.4	835.6	24.5	16.13	2.10	34.90	1.8E-31	4.4E-02	1.1E-36	Salazar-Iribe, A., *et al.* 2018. *J. Plant Physiol.* 231: 105–109.
bHLH	AT1G03040	-	-	-	-	-	-	-	-	-	Hepworth, J., *et al.* 2014. *Curr. Opin. Plant Biol.* 17: 36-42.
BPEp	AT1G59640.2	0.1	0.8	0.2	7.35	-	5.57	2.2E-01	2.2E-01	8.9E-02	Ghelli, R., *et al.* 2018. *Plant Cell* 30: 620-637.
COI1	AT2G39940	4.8	8.1	10.7	1.68	2.25	1.30	4.1E-02	4.4E-04	4.5E-01	Huang, H., *et al.* 2020. *BMC Plant Biol.* 20: 64.
CUC2	AT5G53950	-	-	-	-	-	-	-	-	-	Bögre, B., *et al.* 2008. *Genome Biol.* 226.
DA1	AT1G19270	3.3	2.7	4.0	1.22	1.21	1.44	9.7E-01	8.8E-01	6.8E-01	Hepworth, J., *et al.* 2014. *Curr. Opin. Plant Biol.* 17: 36-42.

DAD1	AT2G44810	-	-	-	-	-	-	-	-	-	Cheng, H., *et al.* 2009. *PLOS Genet.* 5: e1000440.
DCR	AT5G23940	65.5	34.9	1.8	1.89	35.20	19.12	1.3E-02	1.2E-48	3.5E-24	Panikashvili, D., *et al.* 2009. *Plant Physiol.* 151: 1773-1789.
DWF4	AT3G50660	4.8	21.1	7.6	4.36	1.59	2.82	6.1E-10	2.5E-01	3.1E-05	Bögre, B., *et al.* 2008. *Genome Biol.* 226.
E2FA	AT2G36010	-	-	-	-	-	-	-	-	-	Bögre, B., *et al.* 2008. *Genome Biol.* 226.
E2FB	AT5G22220	-	-	-	-	-	-	-	-	-	Bögre, B., *et al.* 2008. *Genome Biol.* 226.
E2FC	AT1G47870	10.6	6.0	5.1	1.78	2.05	1.19	2.1E-02	6.9E-02	9.2E-01	Bögre, B., *et al.* 2008. *Genome Biol.* 226.
EBP1	AT3G51800	26.0	11.5	11.0	2.31	2.39	1.08	1.0E+00	9.4E-01	1.0E+00	Bögre, B., *et al.* 2008. *Genome Biol.* 226.
ELI1	AT5G05170	25.7	46.4	36.2	1.79	1.42	1.30	3.7E-04	1.7E-01	4.2E-01	Weiss, J., *et al.* 2005. *Int. J. of Dev. Biol.* 49: 513-525.
ER	AT2G26330	39.3	26.6	5.7	1.49	6.81	4.69	3.8E-02	1.3E-21	1.3E-15	van Zanten, M., *et al.* 2009. *Trends Plant Sci.* 14: 214–218.
EXPA10	AT1G26770	130.9	217.4	82.2	1.65	1.59	2.70	5.1E-02	5.4E-01	9.8E-02	Xu, R., *et al.* 2011. *Development* 138: 4545-4554.
FAS1	AT1G65470	12.1	4.9	5.9	2.50	2.04	1.19	7.1E-01	2.9E-01	1.0E+00	Hepworth, J., *et al.* 2014. *Curr. Opini. Plant Biol.* 17: 36-42.
FIL	AT2G45190	-	-	-	-	-	-	-	-	-	Weiss, J., *et al.* 2005. *Int. J. of Dev. Biol.* 49: 513-525.
FRA2	AT1G80350	24.0	18.6	15.9	1.30	1.50	1.18	3.4E-01	1.3E-01	7.4E-01	Weiss, J., *et al.* 2005. *Int. J. of Dev. Biol.* 49: 513-525.
GAI	AT1G14920	76.1	74.8	54.7	1.03	1.38	1.39	1.0E+00	1.6E-01	2.0E-01	Cheng, H., *et al.* 2009. *PLOS Genet.* 5: e1000440.
GASA4	AT5G15230	1681.4	1606.3	77.0	1.05	21.81	21.30	1.0E+00	7.4E-43	3.5E-42	Chen, I.-C., *et al.* 2007. *Plant Sci.* 172: 1062–1071.
HTH	AT1G72970	25.8	20.7	2.3	1.25	10.96	8.99	7.2E-01	8.9E-25	4.3E-15	Krolikowski, K. A., *et al.* 2003. *Plant J.* 35: 501-511.
IAA19	AT3G15540	5.8	171.6	2.3	29.38	2.46	74.18	1.3E-19	1.0E-01	4.4E-44	Ghelli, R., *et al.* 2018. *Plant Cell* 30: 620-637.
IDD14	AT1G68130	8.9	21.2	20.6	2.36	2.33	1.04	2.5E-05	7.1E-05	1.0E+00	Cardarelli, M., *et al.* 2014. *Front. Plant Sci.* 5: 333.
IDD15	AT2G01940	22.7	22.7	13.4	1.01	1.68	1.72	1.0E+00	2.2E-01	2.3E-01	Cardarelli, M., *et al.* 2014. *Front. Plant Sci.* 5: 333.
IDD16	AT1G25250	-	-	-	-	-	-	-	-	-	Cardarelli, M., *et al.* 2014. *Front. Plant Sci.* 5: 333.
JAG	AT1G68480	-	-	-	-	-	-	-	-	-	Bögre, B., *et al.* 2008. *Genome Biol.* 226.
JAZ1	AT1G19180	115.2	103.2	63.0	1.12	1.81	1.66	9.2E-01	2.6E-02	1.4E-01	Huang, H., *et al.* 2020. *BMC Plant Biol.* 20: 64.
KLU	AT1G13710	-	-	-	-	-	-	-	-	-	Bögre, B., *et al.* 2008. *Genome Biol.* 226.
KOR	AT5G49720	56.8	93.4	82.8	1.63	1.47	1.14	7.6E-03	7.4E-02	7.7E-01	Hanzawa, Y., *et al.* 2000. *EMBO J.* 19: 4248-4256.
KRP1	AT2G23430	0.3	0.9	4.6	-	0.00	0.00	-	1.3E+01	4.9E+00	Bögre, B., *et al.* 2008. *Genome Biol.* 226.
KRP2	AT3G50630	37.2	67.8	32.0	1.81	1.16	2.15	7.8E-05	7.2E-01	1.5E-04	Cheng, Y., *et al.,* 2015. *Front. Plant Sci.* 6: 825.
KRP3	AT5G48820	3.5	2.0	5.4	1.78	1.55	2.68	2.3E-01	3.8E-01	1.7E-02	Cheng, Y., *et al.,* 2015. *Front. Plant Sci.* 6: 825.
KRP4	AT2G32710	24.9	16.6	17.7	1.51	1.40	1.05	1.4E-01	2.3E-01	1.0E+00	Bögre, B., *et al.* 2008. *Genome Biol.* 226.
KRP5	AT3G24810	-	-	-	-	-	-	-	-	-	Wen, B., *et al.* 2013. *J. Exp. Bot.* 64: 1-13.

KRP6	AT3G19150	-	-	-	-	-	-	-	-	-	Sizani, B., *et al.* 2018. *New Phytol.* 221: 1345-1358.
KRP7	AT1G49620	-	-	-	-	-	-	-	-	-	Cheng, Y., *et al.,* 2015. *Front. Plant Sci.* 6: 825.
LHP1	AT5G17690	11.8	6.7	7.4	1.79	1.60	1.09	4.2E-03	3.6E-02	9.5E-01	Larsson, A. S., *et al.* 1998. *Genetics* 149: 597-605.
LNG1	AT5G15580	38.7	89.5	18.1	2.29	2.12	5.00	7.7E-07	3.1E-05	6.5E-21	Lee, Y. K., *et al.* 2018. *Plant Mol. Biol.* 97: 23–36.
LNG2	AT3G02170	60.8	73.9	11.5	1.21	5.24	6.51	5.9E-01	1.4E-17	1.3E-21	Lee, Y. K., *et al.* 2018. *Plant Mol. Biol.* 97: 23–36.
LNG3	AT1G74160	21.9	19.2	8.1	1.15	2.68	2.40	8.3E-01	3.3E-04	2.4E-03	Lee, Y. K., *et al.* 2018. *Plant Mol. Biol.* 97: 23–36.
LNG4	AT1G18620	-	-	-	-	-	-	-	-	-	Lee, Y. K., *et al.* 2018. *Plant Mol. Biol.* 97: 23–36.
LOX1	AT1G55020	38.0	41.2	60.5	1.08	1.61	1.45	9.8E-01	5.9E-02	2.2E-01	Cheng, H., *et al.* 2009. *PLOS Genet.* 5: e1000440.
LOX2	AT3G45140	-	-	-	-	-	-	-	-	-	Hepworth, J., *et al.* 2014. *Curr. Opin. Plant Biol.* 17: 36-42.
MED14	AT3G04740	-	-	-	-	-	-	-	-	-	Hepworth, J., *et al.* 2014. *Curr. Opin. Plant Biol.* 17: 36-42.
MED25	AT1G25540	17.3	19.6	26.2	1.12	1.52	1.32	9.2E-01	5.2E-02	3.7E-01	Hepworth, J., *et al.* 2014. *Curr. Opin. Plant Biol.* 17: 36-42.
MED8	AT2G03070	15.9	13.2	11.4	1.22	1.38	1.16	8.1E-01	2.8E-01	8.9E-01	Hepworth, J., *et al.* 2014. *Curr. Opin. Plant Biol.* 17: 36-42.
MYB21	AT3G27810	0.2	87.0	0.0	375.94	-	5179.06	7.8E-105	-	2.0E-99	Cheng, H., *et al.* 2009. *PLOS Genet.* 5: e1000440.
MYB24	AT5G40350	6.0	147.1	0.3	24.33	-	423.19	1.7E-29	-	2.9E-33	Cheng, H., *et al.* 2009. *PLOS Genet.* 5: e1000440.
MYB57	AT3G01530	-	-	-	-	-	-	-	-	-	Cheng, H., *et al.* 2009. *PLOS Genet.* 5: e1000440.
NUB/CUC1	AT1G13400	-	-	-	-	-	-	-	-	-	Bögre, B., *et al.* 2008. *Genome Biol.* 226.
OLI5/PGY3	AT3G25520	572.2	327.1	172.5	1.76	3.30	1.93	2.7E-04	1.1E-05	3.4E-02	Bögre, B., *et al.* 2008. *Genome Biol.* 226.
OLI7	AT5G39740	642.3	320.8	237.3	2.02	2.69	1.38	3.0E-05	3.9E-05	4.0E-01	Fujikura, U., *et al.* 2009. *Plant J.* 59: 499–508.
OPR3	AT2G06050	22.1	41.6	15.6	1.87	1.40	2.70	3.3E-04	3.5E-01	1.1E-04	Huang, H., *et al.* 2020. *BMC Plant Biol.* 20: 64.
OSR1	AT2G41230	-	-	-	-	-	-	-	-	-	Feng, G., *et al.* 2011. *New Phytol.* 191: 635-646.
PAPS1	AT1G17980	11.0	13.1	14.8	1.18	1.35	1.12	7.1E-01	2.4E-01	8.8E-01	Hepworth, J., *et al.* 2014. *Curr. Opin. Plant Biol.* 17: 36-42.
PGX1	AT3G26610	-	-	-	-	-	-	-	-	-	Xiao, C., *et al.* 2014. *Plant Cell* 26: 1018-1035.
PGY1	AT2G27530	0.0	0.0	0.2	-	-	-	-	-	-	Bögre, B., *et al.* 2008. *Genome Biol.* 226.
PGY2	AT1G33140	619.3	352.4	243.8	1.77	2.52	1.47	1.7E-04	2.2E-04	2.6E-01	Bögre, B., *et al.* 2008. *Genome Biol.* 226.
PIN2	AT5G57090	31.1	17.7	29.9	1.77	1.04	1.66	5.6E-02	1.0E+00	7.4E-02	Cardarelli, M., *et al.* 2014. *Front. Plant Sci.* 5: 333.
PLT1	AT3G20840	-	-	-	-	-	-	-	-	-	Bögre, B., *et al.* 2008. *Genome Biol.* 226.
PLT2	AT1G51190	-	-	-	-	-	-	-	-	-	Bögre, B., *et al.* 2008. *Genome Biol.* 226.
PLT4	AT5G17430	-	-	-	-	-	-	-	-	-	Bögre, B., *et al.* 2008. *Genome Biol.* 226.
PLT5	AT5G57390	-	-	-	-	-	-	-	-	-	Bögre, B., *et al.* 2008. *Genome Biol.* 226.

PLT7	AT5G65510	-	-	-	-	-	-	-	-	-	Bögre, B., *et al.* 2008. *Genome Biol.* 226.
PPD1	AT4G14713	13.5	3.6	5.3	3.77	2.52	1.45	1.3E-06	1.3E-03	5.3E-01	Xu, R., *et al.* 2011. *Development* 138: 4545-4554.
PPD2	AT4G14720	-	-	-	-	-	-	-	-	-	Xu, R., *et al.* 2011. *Development* 138: 4545-4554.
RBR1	AT3G12280	10.9	8.8	12.0	1.26	1.10	1.35	6.2E-01	8.7E-01	3.5E-01	Bögre, B., *et al.* 2008. *Genome Biol.* 226.
REV	AT5G60690	3.6	4.0	5.6	1.11	1.57	1.38	1.0E+00	1.8E-01	6.3E-01	Weiss, J., *et al.* 2005. *Int. J. of Dev. Biol.* 49: 513-525.
RGA1	AT2G01570	-	-	-	-	-	-	-	-	-	Cheng, H., *et al.* 2009. *PLOS Genet.* 5: e1000440.
RGL1	AT1G66350	76.7	61.8	72.1	1.25	1.06	1.15	4.5E-01	9.3E-01	7.8E-01	Cheng, H., *et al.* 2009. *PLOS Genet.* 5: e1000440.
RGL2	AT3G03450	-	-	-	-	-	-	-	-	-	Cheng, H., *et al.* 2009. *PLOS Genet.* 5: e1000440.
RGL3	AT5G17490	-	-	-	-	-	-	-	-	-	Cheng, H., *et al.* 2009. *PLOS Genet.* 5: e1000440.
ROT3	AT4G36380	0.1	2.9	6.7	36.83	86.43	2.30	9.0E-09	3.4E-15	2.2E-02	Xu, R., *et al.* 2011. *Development* 138: 4545-4554.
RPT2a	AT2G20140	86.1	88.3	64.2	1.02	1.33	1.40	1.0E+00	2.5E-01	1.4E-01	Xu, R., *et al.* 2011. *Development* 138: 4545-4554.
SAUR63	AT1G29440	-	-	-	-	-	-	-	-	-	Chae, K., *et al.* 2012. *Plant J.* 71: 684-697.
SIM	AT5G04470	-	-	-	-	-	-	-	-	-	Hepworth, J., *et al.* 2014. *Curr. Opin. Plant Biol.* 17: 36-42.
SMR1	AT3G10525	-	-	-	-	-	-	-	-	-	Hepworth, J., *et al.* 2014. *Curr. Opin. Plant Biol.* 17: 36-42.
SPY	AT3G11540	17.3	11.7	12.9	1.49	1.34	1.08	6.8E-01	6.8E-01	9.9E-01	Hepworth, J., *et al.* 2014. *Curr. Opin. Plant Biol.* 17: 36-42.
SWEET13	AT5G50800	283.0	60.0	1.3	4.75	208.43	45.60	7.1E-12	5.4E-05	3.4E-03	Kanno, Y., *et al.* 2016. *Nat. Commun.* 7: 13245.
SWEET14	AT4G25010	-	-	-	-	-	-	-	-	-	Kanno, Y., *et al.* 2016. *Nat. Commun.* 7: 13245.
TCP14	AT3G47620	12.9	5.9	14.0	2.21	1.09	2.35	7.1E-03	9.7E-01	8.1E-02	Kieffer, M., *et al.* 2011. *Plant J.* 68: 147-158.
TCP15	AT1G69690	24.2	27.6	19.3	1.13	1.25	1.45	8.9E-01	5.6E-01	1.9E-01	Kieffer, M., *et al.* 2011. *Plant J.* 68: 147-158.
TCP24	AT1G30210	12.1	10.8	11.2	1.13	1.07	1.03	9.2E-01	9.6E-01	1.0E+00	Bögre, B., *et al.* 2008. *Genome Biol.* 226.
TIR1	AT3G62980	12.6	17.6	16.1	1.39	1.28	1.11	1.9E-01	4.5E-01	9.2E-01	Cardarelli, M., *et al.* 2014. *Front. Plant Sci.* 5: 333.
TMK1	AT1G66150	23.6	41.9	11.6	1.76	2.02	3.67	8.6E-03	4.1E-04	2.8E-09	Hepworth, J., *et al.* 2014. *Curr. Opin. Plant Biol.* 17: 36-42.
TOR	AT1G50030	11.2	10.8	15.0	1.04	1.35	1.37	1.0E+00	2.8E-01	3.6E-01	Hepworth, J., *et al.* 2014. *Curr. Opin. Plant Biol.* 17: 36-42.
WOX1	AT3G18010	-	-	-	-	-	-	-	-	-	Hepworth, J., *et al.* 2014. *Curr. Opin. Plant Biol.* 17: 36-42.
WOX3	AT2G28610	-	-	-	-	-	-	-	-	-	Hepworth, J., *et al.* 2014. *Curr. Opin. Plant Biol.* 17: 36-42.
WOX9	AT2G33880	-	-	-	-	-	-	-	-	-	Bögre, B., *et al.* 2008. *Genome Biol.* 226.
XTH17	AT1G65310	-	-	-	-	-	-	-	-	-	Lee, Y. K., *et al.* 2018. *Plant Mol. Biol.* 97: 23–36.
XTH24	AT4G30270	0.1	0.2	138.1	-	1976.36	748.44	-	3.7E-11	8.5E-14	Lee, Y. K., *et al.* 2018. *Plant Mol. Biol.* 97: 23–36.
XTH9	AT4G03210	86.7	29.8	22.7	2.93	3.80	1.34	4.4E-06	8.9E-11	5.1E-01	Hyodo, H., *et al.* 2003. *Plant Mol. Biol.* 52: 473-482.

YAB3	AT4G00180	-	-	-	-	-	-	-	-	-	Weiss, J., *et al.* 2005. *Int. J. of Dev. Biol.* 49: 513-525.
YUC2	AT4G13260	-	-	-	-	-	-	-	-	-	Cardarelli, M., *et al.* 2014. *Front. Plant Sci.* 5: 333.
YUC6	AT5G25620	-	-	-	-	-	-	-	-	-	Cardarelli, M., *et al.* 2014. *Front. Plant Sci.* 5: 333.